Analysis of the relationship between glycogen turnover and cell size in *Escherichia coli*

by
Felix van der Walt

Thesis presented in partial fulfilment of the requirements for the degree of Master of Science in the Faculty AgriSciences at Stellenbosch University

The financial assistance of the National Research Foundation (NRF) towards this research is hereby acknowledged. Opinions expressed and conclusions arrived at, are those of the author and are not necessarily to be attributed to the NRF.

Supervisor: Prof James R Lloyd

March 2020

Declaration

By submitting this thesis electronically, I declare that the entirety of the work contained therein is my own, original work, that I am the sole author thereof (save to the extent explicitly otherwise stated), that reproduction and publication thereof by Stellenbosch University will not infringe any third party rights and that I have not previously in its entirety or in part submitted it for obtaining any qualification.

March 2020

Abstract

Glycogen represents an important carbon energy store in organisms across all domains of life. Under permissible conditions, excess environmental glucose is incorporated into glycogen by the Gram-negative bacterium *Escherichia coli* to provide the cell with an endogenous carbon store. This can rapidly be mobilized to provide the cell with energy for sustained viability when nutritional conditions deteriorate. Extracellular nutrient availability positively impacts cell size and growth rate in a variety of organisms. Bacteria cultured in nutrient-rich media display significant increases in growth rate and cell size, compared to their slow-growing counterparts in nutrient-deprived conditions. Such nutrient-dependent increases in size and growth are accompanied by equally dramatic elevations in the rates of macromolecular biosynthesis (DNA/RNA/protein). How bacteria respond to environmental cues through their ability to sense size and correct random fluctuations that would deviate it from 'normal' has been the subject of substantial investigations over the last few decades. This is unsurprising as cell size control and homeostasis are fundamental to cell biology and, of course, to the survival of unicellular bacteria like *E. coli*. Research has historically focused on cell size and progression of the bacterial cell cycle within the context of extracellular nutrient availability, yet little is known about how endogenous metabolism affects these aspects of bacterial physiology.

This investigation aimed to elucidate how glycogen turnover impacts cell size and progression of cell cycle events using *E. coli* mutants affecting three glycogen catabolic enzymes, glycogen phosphorylase (GlgP), glycogen debranching enzyme (GlgX) and maltodextrin phosphorylase (MalP). Disruption of *malP* resulted in a profound effect on cell size as Δ*malP* mutants are unable to properly coordinate cell cycle progression during exponential growth, leading to substantial heterogeneity in size. This manifests as subpopulations of elongated and filamentous cells. Whilst such mutants do not necessarily form fewer Z-rings per cell, they clearly delay division and grow into filaments and the underlying reason for this appears to be a malfunction of DNA replication. Mutations in either *glgP* or *glgX* differently impact DNA replication and cell size and mutants with a lesion in the latter allele contain coinciding glycogen and protein inclusion bodies, particularly noticeable during exponential growth.

The nature of the flaws to cell size control and DNA replication observed in Δ*malP* mutant strains, specifically the Δ*malP*/Δ*glgP*/Δ*glgX* triple mutant, was further scrutinized by introducing lesions to genes involved in several interacting processes. Mutating genes associated with glycogen accumulation, pyruvate kinase activity, and SOS-mediated or UDP-glucose-dependent division inhibition led to the formation of mutant cells either smaller or equal in size to the wild type. Partial suppressions to the size defects of the triple mutant were observed in quadruple mutant strains with disruptions to genes involved in amino acid metabolism, ppGpp biosynthesis, UDP-glucose generation, DNA replication and nucleoid structuring. DNA replication is clearly coordinated with diverse physiological processes acting in concert to link duplication of the genome with cell size, growth rate and environmental conditions.

Uittreksel

Glikogeen verteenwoordig ’n belangrike voorraad van koolstofenergie in organismes van alle lewensdomeine. Onder toelaatbare omstandighede word oortollige glukose van die omgewing deur die Gram-negatiewe bakterium *Escherichia coli* omgeskakel na glikogeen om die sel met ’n endogene koolstofvoorraad te voorsien. Dit kan spoedig gemobiliseer word om die sel met energie vir onafgebroke lewensvatbaarheid te voorsien, wanneer voedingstoestande agteruit gaan. Die beskikbaarheid van ekstrasellulêre voedingstowwe het ’n positiewe impak op selgrootte en groeikoers in verskeie organismes. Bakterieë wat in voedingsryke middele gekweek word, wys beduidende verhogings in groeikoers en selgrootte, in vergelyking met stadig-groeiende bakterieë wat onder voedingstofarm omstandighede gekweek word. Sulke voedingstof-afhanklike verhogings in grootte en groei word vergesel deur ewe drastiese versnellings in die tempo van makromolekulêre biosintese (DNA/RNA/proteïen). Hoe bakterieë op sekere omgewingskodes reageer deur hul grootte waar te neem en om ewekansige fluktuasies wat van ‘normaal’ afwyk, reg te stel was die onderwerp van beduidende ondersoeke oor die afgelope dekades. Dit is nie verbasend nie aangesien die beheer en homeostase van selgrootte fundamenteel is vir selbiologie en, natuurlik, die oorlewing van eensellige bakterieë soos *E. coli*. Navorsing het tot dusver op selgrootte en die verloop van die bakteriële selsiklus binne die konteks van die beskikbaarheid van ekstrasellulêre voedingstowwe gefokus, terwyl daar min inligting bestaan oor die impak van endogene metabolisme op hierdie aspekte van bakteriële fisiologie.

Die doel van hierdie ondersoek was om te verduidelik hoe glikogeenomset selgrootte en vordering van sekere stappe van die selsiklus beïnvloed deur gebruik te maak van ’n reeks *E. coli* mutante wat kombinasies van drie glikogeenkataboliese ensieme kortkom, naamlik glikogeenfosforilase (GlgP), glikogeen-onvertakkingsensiem (GlgX) en maltodekstrien-fosforilase (MalP). Ontwrigting van *malP* het ’n diepgaande effek op selgrootte omdat Δ*malP*-mutante blykbaar nie die selsiklusprogressie tydens eksponensiële groei korrek kan koördineer nie en dit lei tot aansienlike heterogeniteit in selgrootte. Dit manifesteer as subpopulasies van langwerpige en filamentagtige selle. Terwyl sulke mutante nie noodwendig minder Z-ringe per sel vorm nie, word selverdeling duidelik vertraag, en die onderliggende rede dat selle filamente vorm, blyk ’n abnormale werking van DNA-replikasie te wees. Mutasies in óf *glgP* óf *glgX* affekteer DNA-replikasie en selgrootte op verskillende maniere en mutante met ’n letsel in die laasgenoemde alleel bevat saamvallende glikogeen-en proteïen-insluitingsliggame, veral merkbaar tydens eksponensiële groei.

Die aard van die gebrekke in selgroottebeheer en DNA-replikasie in Δ*malP*-mutante, veral die Δ*malP*/Δ*glgP*/Δ*glgX* trippel-mutant, is verder bestudeer deur gene te verwyder wat by verskeie interaktiewe prosesse betrokke is. Mutasies in gene wat geassosieer is met glikogeenakkumulasie, pirovaatkinase-aktiwiteit, en SOS-bemiddelde of UDP-glukose-afhanklike vertraging van verdeling het gelei tot die vorming van mutante selle wat óf kleiner óf dieselfde grootte soos die wilde tipe is. Gedeeltelike onderdrukkings van die groottedefekte van die trippel-mutant is waargeneem by

viervoudige mutante met addisionele uitwissings in gene wat betrokke is by aminosuurmetabolisme, ppGpp-biosintese, UDP-glukose-voortbrenging, DNA-replikasie en nukleoïed-strukturering. DNA-replikasie word duidelik met verskeie fisiologiese prosesse gekoördineer wat gesamentlik werk om duplisering van die genoom aan selgrootte, groeikoers en omgewingstoestande te koppel.

Acknowledgements

The completion of this thesis relied on the aid and involvement of several people and institutes.

How will I ever be able to thank my family for their love and support throughout the course of this degree?

Although I steadily stumbled over several obstacles, I thank my family, friends and supervisor for never giving up on me even if, at times, I felt like giving up on myself.

Naming all the friends I've made along the way would make for a lengthy list, so I'd like to thank all those friends who have graced me with their light, shared their wisdom and saved me from insanity.

Knowledgeable and passionate teachers I met at school, varsity and throughout my life deserve a huge thanks for igniting within me the desire to learn, investigate and grow as a scientist.

Yielding the article on cell size would have been impossible had it not been for the invaluable input and expertise of the staff at CAF and our collaborators in Zürich, who I'd like so sincerely thank.

Opportunities to complete such exciting work don't come around often, so I'd like to thank the NRF, the director of the IPB and a dynamic supervisor for financing this tremendous learning opportunity.

Undertaking this endeavour would have been impossible without that guiding Light and Love from Above, so thank you God for giving me the chance to exist and make a difference on Earth.

"What is true for *E. coli* is true for the elephant."

- Jacques Monod

Table of Contents

List of Figures

List of Tables

List of Acronyms, Abbreviations, Initialisms and non-SI units

AA	Amino acid
ADP	Adenosine diphosphate
ADPG	Adenosine diphosphate glucose
AMP	Adenosine monophosphate
ATP	Adenosine triphosphate
BCIP/NBT	5-Bromo-4-chloro-3-indolyl phosphate/nitro blue tetrazolium
bp	base pair
BSA	Bovine serum albumin
cAMP	cyclic AMP
CCM	Central carbon metabolism
CFU	Colony-forming unit
CRP	cAMP receptor protein
CsrA	Carbon storage regulator A
CyaA	Adenylate cyclase
DAPI	4',6-diamidino-2-phenylindole
DNA	Deoxyribonucleic acid
DnaA	Chromosomal replication initiator protein
dNTP	deoxyribonucleotide triphosphate
EDTA	Ethylenediaminetetraacetic acid
EM	Electron microscopy
FA	Fatty acid
FITC	Fluorescein isothiocyanate
FtsZ	Cell division protein
g	Gram
G1P	Glucose 1-phosphate
G6P	Glucose 6-phosphate
GalU	UTP: glucose 1-phosphate uridylyltransferase
GFP	Green fluorescent protein
GlgA	Glycogen synthase
GlgB	Glycogen branching enzyme
GlgC	ADPG pyrophosphorylase
GlgP	Glycogen phosphorylase
GlgX	Glycogen debranching enzyme
Glk	Glucokinase
GTE	Glucose-Tris-EDTA
GTP	Guanosine triphosphate
hrs	Hours
HU	Histone-like DNA-binding protein (HupA and HupB heterodimer)
kDa	kilo Dalton
LB	Lysogeny broth
M	Molar
MalP	Maltodextrin phosphorylase
MalQ	Amylomaltase
MalZ	Amyloglucosidase
Mg^{2+}	Magnesium divalent cation
mins	Minutes

mL	Millilitres
mM	Millimolar
mRNA	messenger RNA
NAP	Nucleoid associated protein
$NaPO_4$	Sodium phosphate
nm	Nanometre
NO	Nucleoid occlusion
OD_{450}	Optical density at 450 nm
PAGE	Polyacrylamide gel electrophoresis
PAS	Periodic acid-Schiff
PBS	Phosphate-buffered saline
PBS-E	Phosphate-buffered saline-EDTA
PCR	Polymerase chain reaction
PDH^c	Pyruvate dehydrogenase complex
PEB	Protein extraction buffer
PEP	Phosphoenolpyruvate
PG	Peptidoglycan
Pgm	Phosphoglucomutase
PMSF	Phenylmethylsulfonyl fluoride
ppGpp	Guanosine tetraphosphate and guanosine pentaphosphate collectively
PTS	Phosphotransferase system
PVDF	Polyvinylidene fluoride
RIDA	Regulatory inactivation of DnaA
RNA	Ribonucleic acid
RNAP	RNA polymerase
RPM	Revolutions per minute
rRNA	ribosomal RNA
SBS	SlmA binding site
SD	Standard deviation
SDS	Sodium dodecyl sulphate
SEM	Standard error of the mean
TBS	Tris-buffered saline
TCA	Tricarboxylic acid
TE	Tris-EDTA
Tris-HCl	Trisaminomethane hydrochloride
tRNA	transfer RNA
UDPG	Uridine diphosphate glucose
v/v	Volume per volume
w/v	Weight per volume
WT	Wild type
x g	Relative centrifugal force
°C	Degrees Celsius
α	Alpha
β	Beta
µg	Micrograms
µL	Microliters
µm	Micrometres

1. Chapter 1 – General introduction

1. Glycogen as a carbon energy store

Glycogen is a highly branched homopolysaccharide which mainly consists of α-1,4-linked glucose units with numerous α-1,6 branches. Diverse organisms including animals, yeast and most bacteria can synthesize this polymer in response to changing environmental conditions[1,2], and then degrade it for energy production. Glycogen is an effective cytosolic glucose store that accumulates without markedly affecting cell osmolarity[3,4].

The first report of glycogen granules in the model Gram-negative bacterium, *Escherichia coli* was presented in the late 1950s[5]. Upon examination of ultrathin bacterial sections by electron microscopy (EM), the researchers observed large “holes” in the cytosol of stationary-phase bacteria and occasionally smaller “holes” were seen in exponential cells. They appeared along the cell periphery and substantial polar “holes” were observed in some stationary phase bacteria. Their sizes were comparable to those reported for glycogen granules and it was concluded that they represent glycogen deposits that were dissolved upon treatment (with ethanol) of ultrathin slices for EM analysis. Over the last two decades, various research groups have identified glycogen granules at the cell periphery within *E. coli* cells using mostly EM examination of diverse bacterial strains under various growth conditions[2,6–13].

Much is known about the conditions that lead to glycogen accumulation in this organism. *E. coli* glycogen synthesis appears to be prompted when extracellular carbon is abundant but the lack of other nutrients, such as nitrogen, impairs rapid proliferation[2,5]. Though glycogen is not essential for survival[14] it has long been thought to aid in long-term persistence by providing endogenous energy which may be used for maintenance when carbon supplies are depleted[15–18]. Glycogen stores have also been shown to aid in metabolic adaptation[19], with glycogen breakdown supplying energy to fuel rapid restart of metabolic processes in growth arrested cells when conditions become favorable. This offers a competitive advantage for colonization of specific environments, like the mammalian gut[18]. There is also a developmental switch in glycogen accumulation, with cells in the exponential phase containing less glycogen than those in stationary phase.

2. Glycogen metabolism

Glycogen biosynthesis in *E. coli* is mediated by the protein products of *glgC* (ADP-glucose pyrophosphorylase), *glgA* (glycogen synthase) and *glgB* (glycogen branching enzyme); its degradation is facilitated by the actions of glycogen phosphorylase, encoded by *glgP*, and glycogen debranching enzyme, encoded by *glgX*. These five genes are found within a single transcriptional unit, arranged in the order *glgBXCAP*. Recent RT-PCR analyses suggest that transcription of all *glg* genes is under the control of a main promoter located upstream of *glgB*, whilst a secondary, internal promoter, located within the *glgC* locus, drives expression of *glgA* and *glgP*[20,21].

2.1. Glucose-dependent glycogen biosynthesis

Glucose enters *E. coli* cells via the glucose phosphotransferase system (PTS), which uses phosphoenolpyruvate (PEP) as a phosphate donor to synthesize glucose 6-phosphate (G6P). This system energizes sugar transport by facilitating a series of phosphoryl transfer reactions between several protein partners[22]. The state of phosphorylation of these proteins reflects the availability of carbon and energy in the cell and allows integration of this information with diverse metabolic processes[23]. Intracellular G6P has several important fates but under specific conditions may be channelled into glycogen synthesis (Figure 1.1) after being converted into glucose 1-phosphate (G1P) by phosphoglucomutase[24] (Pgm; EC 5.4.2.2) and combined with Mg^2-bound ATP by ADP-glucose pyrophosphorylase[25] (GlgC; EC 2.7.7.27) to form ADP-glucose (ADPG).

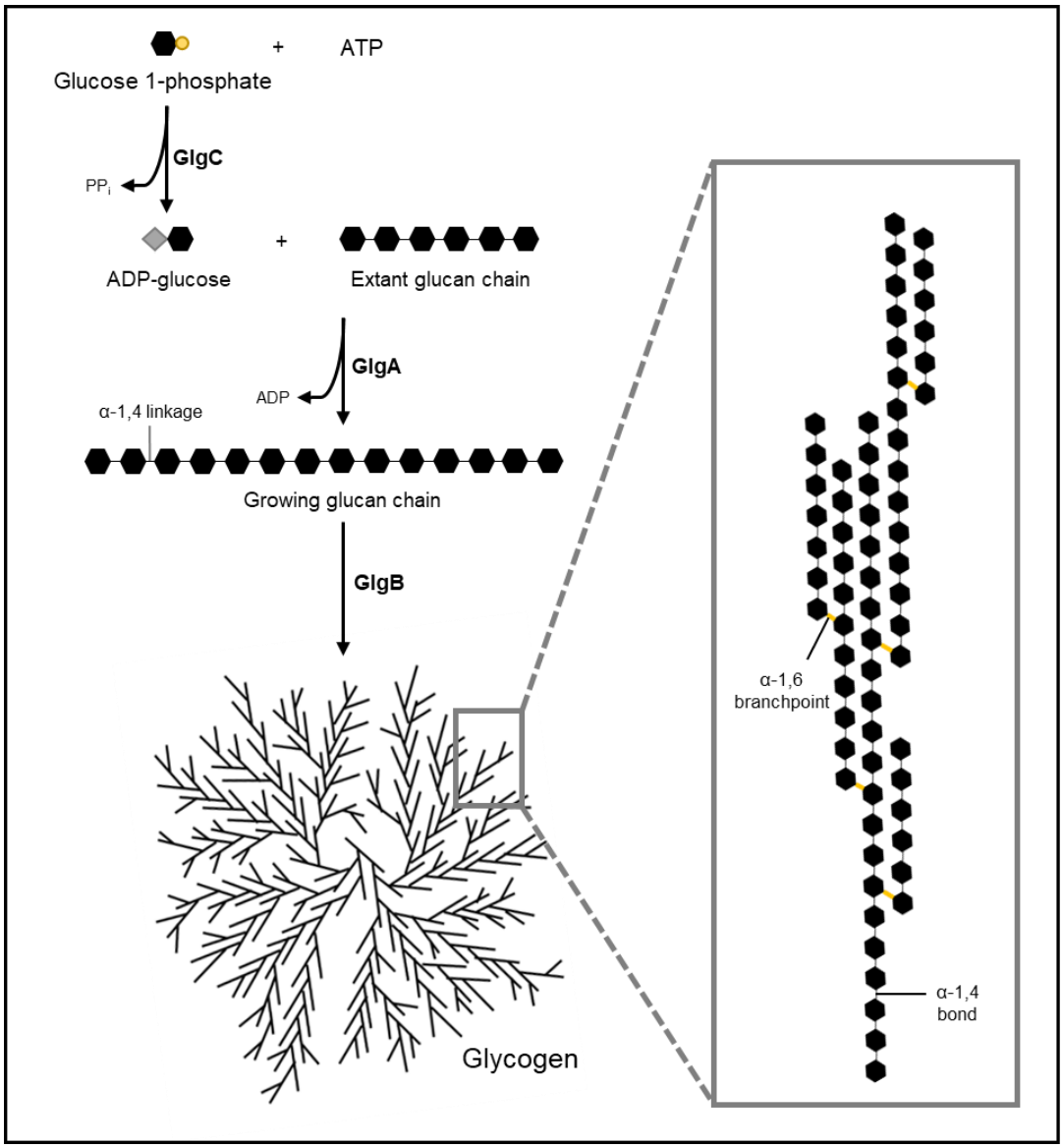

Figure 1.1. Glucose-dependent synthesis of the glycogen polymer. Glucan chains are elongated by GlgA which attaches glucose residues from ADPG via α-1,4 glycosidic linkages onto an existing glucan primer. Once these chains are of a specific length they may serve as substrate for GlgB, which cleaves and reattaches these stubs via α -1,6 branchpoints elsewhere in the growing glycogen molecule. Controlling the rates of chain propagation (by GlgA) and stoppage (by GlgB) largely determines the structure of this biopolymer.

Polymer elongation is accomplished by glycogen synthase[26] (GlgA; EC 2.4.1.21), which catalyses the transfer of a glucosyl unit from ADPG onto an extant glucan primer. An endogenous glucan chain attached to GlgA is polymerized through the addition of glucose moieties from ADPG onto the non-reducing ends of these bound linear dextrin acceptors via α-1,4-glucosidic bonds[27,28]. Glycogen branching enzyme[29] (GlgB; EC 2.4.1.18) introduces branch points by preferentially transferring short oligosaccharide chains of 5 to 11 glucose residues[30] from the non-reducing end of an oligosaccharide chain and reattaching these via α-1,6-linkages at another glucose unit elsewhere in the growing polymer[31,32] (Figure 1.1). Though this pathway represents the main route of glycogen synthesis in *E. coli*, it is not the only one utilized for *de novo* glycogen formation[28,33] (See section 3.1 below for details).

2.2. Regulation of glycogen synthesis

2.2.1. Transcriptional regulation

Glycogen biosynthesis is tightly coupled to the physiological status of the cell and many factors regulate its metabolism[2]. The main signal prompting its accumulation appears to be the depletion of some extracellular nutrient that limits growth, which may be nitrogen, sulphur or phosphorus[34–36], whilst extracellular carbon is plentiful. This prompts elicitation of the stringent response[37] which leads to extensive reprogramming of transcription, allowing the cell to prepare itself for long-term survival in stationary phase[38].

This adaptive response is controlled by the accumulation of the alarmones, guanosine tetraphosphate and pentaphosphate, collectively called ppGpp[39–41], formed by RelA[40] (GTP pyrophosphokinase; EC 2.7.6.5) from ATP and GTP in response to amino acid starvation[40] or by SpoT[40] (a bifunctional ppGpp synthase/hydrolase; EC 2.7.6.5) when carbon[42], iron[43] or fatty acid[44] limitation occurs. This hyperphosphorylated nucleotide can bind directly to the active site of RNAP which affects RNAP's efficiency and reduces transcription at stringent promoters. Auxiliary factors like DksA[45] (RNA polymerase-binding transcription factor) can also help promote binding to RNAP. Stringent growth arrest is hallmarked by ppGpp downregulating transcription of stable RNA genes, like those encoding ribosomal RNA (rRNA) and transfer RNA (tRNA). Since these RNA species form an integral part of the translation machinery, ppGpp indirectly reduces transcription rates by regulating gene expression levels[46–48].

The liberating effect ppGpp has on RNAP bound at certain promoters during the stringent response also increases the pool of free RNAP, which may now be redirected to bind at specific promoters and express genes whose protein products will help the cell prepare itself against the impending cataclysm of long-term famine. It has been proposed that this effect is responsible for the well-documented enhancement of *glg* gene expression at the onset of stationary phase[14,38,49]. It has also been suggested that energy-dependent glycogen synthesis is further enhanced by elevated ATP pools that result from ppGpp-dependent inhibition of protein, nucleic acid and lipid

biosyntheses[50,51]. Conflicting data exists regarding the regulation of *glgCAP* expression by the cAMP-CRP complex.

In vitro data showed that both RelA (by producing ppGpp) and the cAMP/CRP system stimulate transcription of the genes encoding GlgC and GlgA[36,52]. In *E. coli*, CyaA (adenylate cyclase; EC 4.6.1.1) is responsible for the synthesis of cAMP from ATP and forms this cyclic nucleotide in response to a drop in extracellular glucose levels. When bound to the transcriptional regulator CRP (cAMP receptor protein), the cAMP/CRP complex regulates genes at diverse promoters and plays an indispensable role in catabolite de-repression, stimulating the expression of an array of genes that allow cells to transport and use less favourable carbon sources when glycolytic ones have been depleted from the environment. Mutants with a lesion either in *cyaA* or *crp* have been shown to display marked glycogen-deficient phenotypes[51,53].

Recent transcriptomic approaches have failed to identify any *glg* genes belonging to the CRP regulon[54,55] and other studies have shown that mutant bacteria lacking either CRP or CyaA activity accumulate wild type levels of glycogen[56,57]. Expression of the *glgCAP* operon appears to be unaffected by low cAMP levels in a *cyaA* mutant[51] and earlier observations of glycogen deficiency in *cyaA* or *crp* mutants may be ascribed to the importance of cAMP/CRP in efficient activation of PTS-related genes. Altogether, these findings point to an indirect positive effect of cAMP/CRP on *glg* gene transcription.

The expression of *glgC* appears to be coupled to extracellular Mg^{2+}, through the PhoPQ two-component system[20,51]. This regulatory system involves PhoQ sensing extra-cellular levels of Mg^{2+} and influencing the PhoP regulatory protein leading to alterations in transcription of various magnesium-response genes[58–60]. This system allows the cell to tune the expression of genes in response to exogenous Mg^{2+} levels. Under conditions of limited Mg^{2+}, mutants lacking either PhoP or PhoQ activity show reduced glycogen amounts and GlgC protein levels and these reductions are restored when the growth medium is supplemented with high levels of Mg^{2+}.

These results imply that expression of *glgCAP* is subject to regulation by PhoPQ in response to low environmental Mg^{2+} levels, which allows further integration of glycogen synthesis with the energetic and nutritional status of the cell[51]. Absence of a PhoP binding site upstream of the *glgBXCAP* operon suggests this control is likely indirect[2,59,60] . Expression of all five *glg* genes is downregulated in a *phoP* mutant background when exogenous Mg^{2+} is low[20] which indicates that expression of the entire *glgBXCAP* operon is under positive directive by the PhoPQ regulon.

2.2.2. Allosteric regulation and quorum sensing dictate ADPG pools

The activity of GlgC, which synthesizes ADPG, is allosterically activated by fructose-1,6-bisphosphate (glycolytic intermediate, which implies high carbon and energy levels in the cell) and inhibited by AMP (which signifies a low energy status in the cell). Glycogen formation is thus finely tuned to the nutrient and energy status of the cell through intracellular ppGpp and AMP levels. The

enzyme AspP[61,62] (adenosine diphosphate sugar pyrophosphatase; EC 3.6.1.21) can catalyze the breakdown of ADPG into G1P and AMP, diverting carbon flux away from glycogen biosynthesis and into other biosynthetic pathways in response to diverse signals[61–63], including intercellular communication.

Activation of cytosolic AspP enhances the hydrolysis of ADPG keeping the levels of this nucleotide sugar low. However, as the population density of the culture increases and nutritional conditions deteriorate, AspP becomes membrane bound and this sequestration keeps cytosolic levels of AspP low, allowing the cell to form ADPG, synthesize glycogen and prepare for inevitable starvation[63].

2.2.3. Post-transcriptional regulation

Manipulations of carbon fluxes through central carbon metabolism (CCM) are regulated at several levels and the main posttranscriptional regulator of CCM appears to be the carbon storage regulator (Csr) system[64–67]. This system influences several aspects of CCM[66] and is involved in various survival and adaptive strategies including the stringent response[64], glycogen production[65,68], cellular fitness by facilitating metabolic adaptation[19] and even aging[7]. The main effector of this system is CsrA, which binds to specific mRNAs facilitating either targeted transcript stabilization or degradation. CsrA negatively regulates glycogen biosynthesis mainly by preventing translation of *glgC*[65,68,69], and disruptions to the *csrA* gene lead to significant over-accumulation of glycogen in mutant cells[7,19,65].

2.3. Glycogen degradation

Catabolism of the glycogen polymer is initiated by glycogen phosphorylase[11] (GlgP; EC 2.4.1.1), which sequentially cleaves glucose residues from the non-reducing ends of glycogen outer chains via phosphorolysis (Figure 1.2). This continues until stubs of at least 4 residues remain[4], allowing the debranching enzyme[30] (GlgX; EC 3.2.1.33) to remove GlgP-limit dextrins via direct debranching at α-1,6 linkages[70]. It has been proposed that GlgX could shorten glycogen chains during biosynthesis, ensuring balance between that process and degradation[30]. GlgX favors the release of maltotetraosyl units from GlgP-limit glycogen, which may then be elongated or processed by enzymes related to maltose/maltodextrin metabolism[4,71] (See section 3.3 below for details).

2.3.1. HPr influences glycogen phosphorylase activity

If stationary phase cells are introduced into fresh medium containing an abundance of glucose, the phosphorylation state of the PTS partners is reduced. Glycogen degradation serves as the primary source of glucose during this adaptive phase[19,72,73], allowing rapid metabolic adaptation when cells are exposed to a new environment. One of the members of the PTS system, HPr, stimulates GlgP activity when it is not phosphorylated. This enhances breakdown of glycogen reserves accumulated in the previous growth phase[73], providing the cell with immediate G1P that may fuel a variety of processes, including sugar transport. As exogenous glucose becomes depleted

and the rate of sugar import dwindles, the phosphorylated form of HPr accumulates. This results in reduced GlgP activity, allowing glycogen accumulation. This strategy provides a direct link between two important processes involved in carbohydrate metabolism, glycogen turnover and sugar transport, that work to promote rapid metabolic adaptation to new conditions[72].

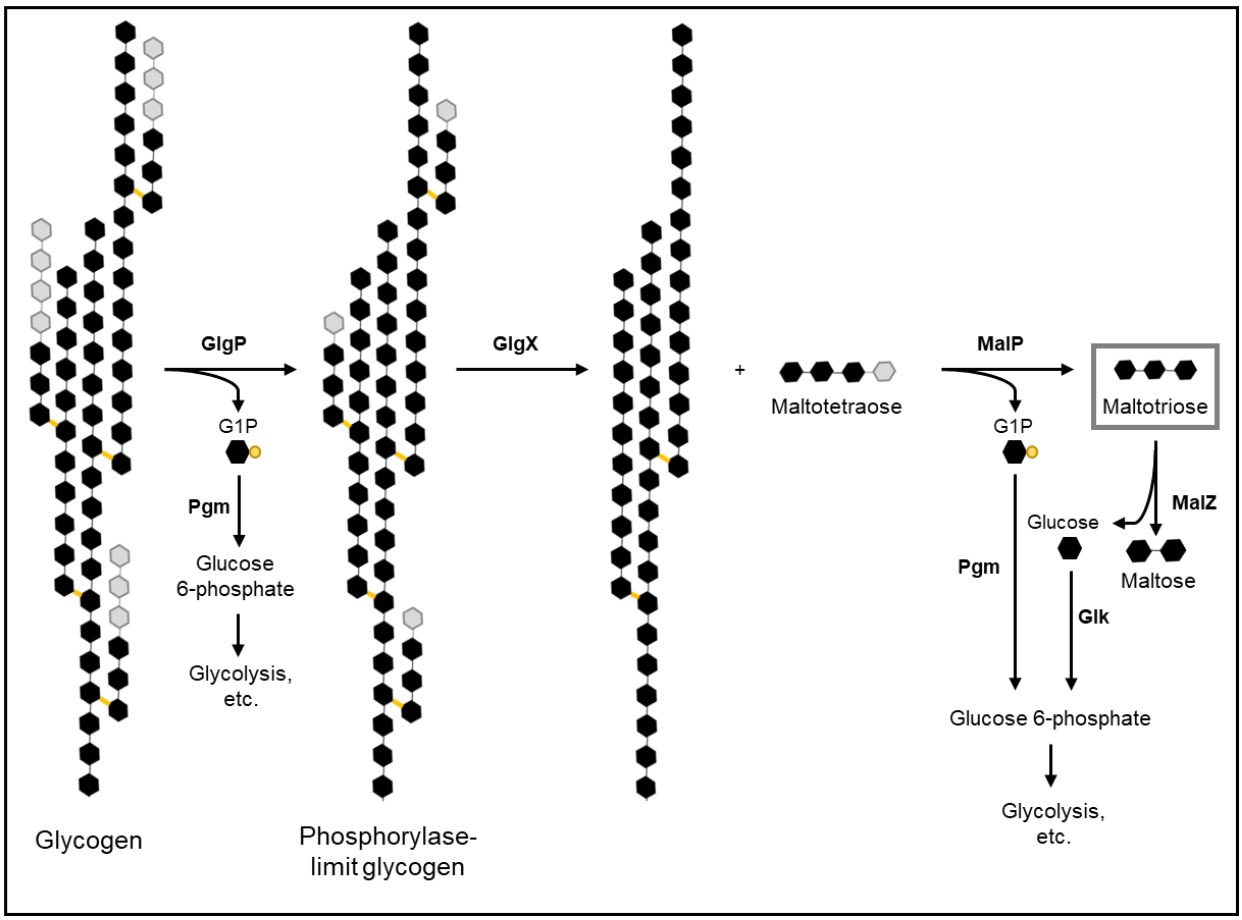

Figure 1.2. Glycogen degradation is linked to maltose/maltodextrin metabolism. Glycogen outer chains are recessed by GlgP until it reaches the end of its phosphorolytic cleavage activity, leaving behind short maltotetraosyl stubs that are debranched by GlgX. The maltotetraose liberated in this way is further processed by enzymes of maltose/maltodextrin metabolism and this degradation liberates substantial amounts of G6P that may be channelled into glycolysis and anabolic processes (adapted from Boos & Shuman, 1998)[71]. Pgm, phosphoglucomutase; Glk, glucokinase.

3. Maltose/maltodextrin metabolism influences glycogen synthesis

Branched glycogen can store substantial amounts of glucose and while it has generally been accepted that its degradation provides the cell with carbon to sustain viability only for a short duration[15], glycogen with shorter external chains may retard degradation rates, allowing this biopolymer to support long-term survival as a durable energy reserve[74]. Other sugars, like maltose or linear maltodextrin, may be scavenged from the environment and used for gluconeogenesis or for the formation of longer dextrins in the cell[75]. These linear polyglucans, like glycogen, may be degraded to fuel cellular processes that require energy/carbon, though their turnover would unlikely sustain survival for long bouts of famine due to several structural nuances between maltodextrins and glycogen. These two types of glucose polymers are, however, similar in their fundamental

composition (linear α-1,4-linked glucose residues) so it is unsurprising that the metabolism of both are interlinked.

3.1. *De novo* glycogen synthesis through maltose/maltodextrin turnover

Two enzymes that are essential for maltose/maltodextrin utilization are amylomaltase (MalQ) and maltodextrin phosphorylase (MalP)[75,76]. The genes encoding these proteins are arranged within a single operon, *malPQ*, with transcription driven from a main promoter located upstream of *malP*, that is positively regulated by the regulator MalT, whilst an internal promoter drives expression of *malQ*. It has been shown that MalQ may form the primer required for initiation of glycogen granule formation (independent of GlgA action) through its disproportionating activity[28].

MalQ preferentially binds to maltose and short maltodextrins, liberating glucose from the reducing ends of its substrate and transferring the remaining protein-bound glucan to the non-reducing end of an existing oligosaccharide (Figure 1.3). In this way MalQ elongates dextrins within the cytosol. These serve as substrate for MalP, which acts on maltotetraose and longer dextrins[77,78], releasing G1P from the non-reducing ends of linear glucans via phosphorolysis. MalP will not utilize maltotriose and, together with MalQ, ensures endogenous dextrins are the optimal length for incorporation by GlgB into the expanding glycogen molecule[28] (Figure 1.3).

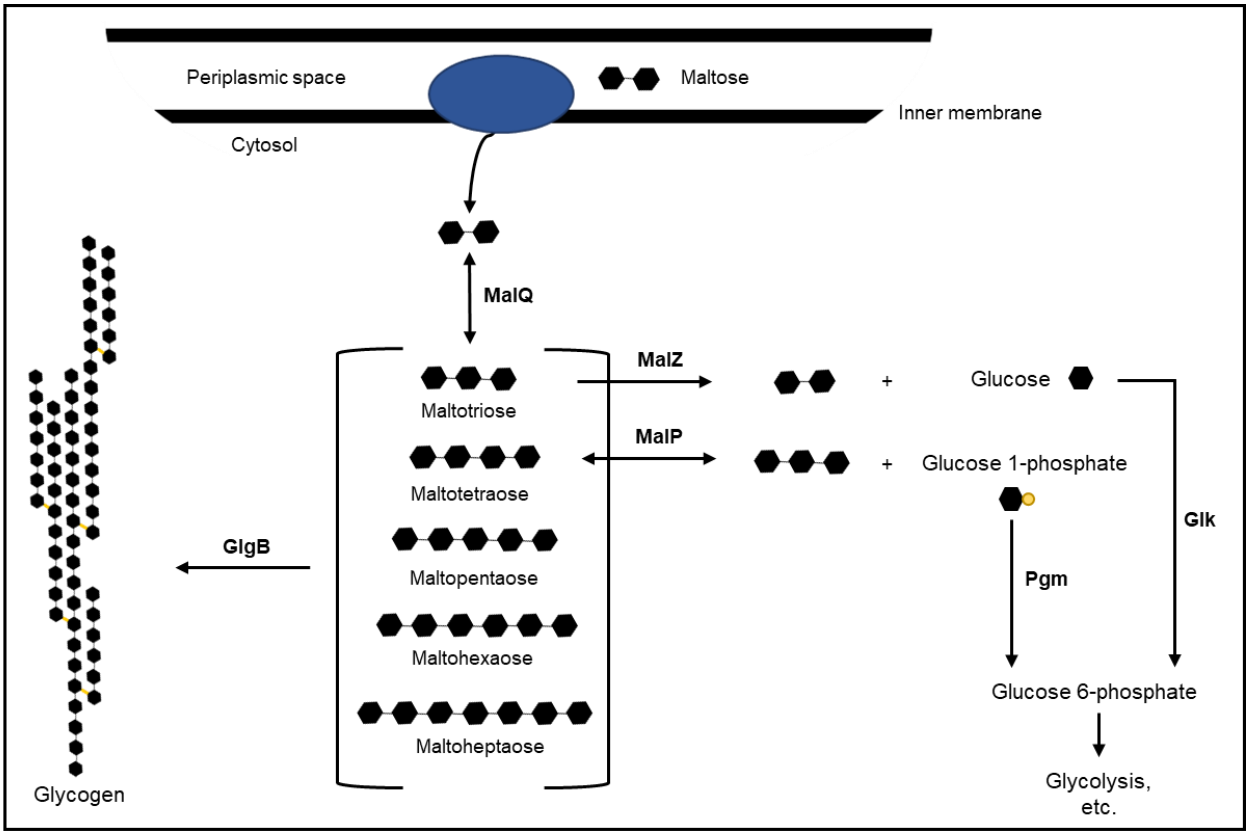

Figure 1.3. Maltose/maltodextrin metabolism is linked to glycogen biosynthesis. Once maltose has entered the cytosol it may serve as substrate for elongation by MalQ. Maltodextrin chain lengths are manipulated by MalP and MalZ. Once glucan chains have reached a certain length, they may be acted upon by GlgB which introduces these cleaved dextrinyl stubs into the growing glycogen polymer facilitating GlgA-independent glycogen synthesis (adapted from Boos & Shuman, 1998; Park et al. 2011). Pgm, phosphoglucomutase; Glk, glucokinase.

Though not essential, another degradative enzyme, amyloglucosidase (MalZ), can manipulate the length of linear dextrins produced by MalQ by removing glucose from the reducing ends of maltodextrins with maltotriose being its smallest substrate[77,79]. These enzymes (Figure 1.3) may thus facilitate *de novo* glycogen formation from maltose and short maltodextrins[28] independent of the GlgA-dependent pathway.

3.2. Regulation of maltodextrin phosphorylase expression

The activity of MalP is primarily controlled at the level of gene expression. Despite the occurrence of a cAMP-CAP binding site upstream of MalP's promoter region, this complex does not appear to directly affect expression of the *malPQ* operon[80]. Instead, it likely affects MalP expression indirectly via MalT, which is subject to catabolite repression and thus requires the presence of the cAMP/CAP complex for induction[81]. MalT activity is stimulated when it is bound to maltotriose and MalP can form maltotriose from glycogen-derived breakdown products when cells are cultured on glucose.

As outlined above, other proteins of the *mal* regulon act upon maltotriose and may control the degree of induction of this system (Figures 1.2 & 1.3). Regulation of MalP by HPr in *E. coli* appears to be absent[72]; however, in *C. glutamicum*, a functional PEP: carbohydrate PTS is essential for transcription of MalP as elimination of HPr or EI activity impairs *malP* transcription[82]. Sugar transport in *C. glutamicum* differs markedly from that of *E. coli*, as the former organism co-transports both glycolytic PTS substrates, like glucose, along with non-PTS substrates, like maltose[82].

Transcriptomic approaches examining mutants lacking either the transcription factor FNR or combinations of the two histone-like DNA-binding proteins HUα and/or HUβ, revealed that the *malPQ* operon may additionally be regulated by both FNR[83] and HU[84]. These two systems drive diverse processes, but appear to influence several complementary pathways that promote survival, with HU functioning under aerobic conditions and FNR fulfilling this role under anoxic conditions[84]. An FNR binding site has been mapped upstream of the *malPQ* operon[83], and transcription initiation from the *malP* promoter is stimulated by both FNR and maltotriose-bound MalT interacting with RNAP. FNR is known to reprogram the cell, allowing a switch from aerobiosis to anaerobiosis[83]. HU fulfils various roles in the cell[84–86], and it controls the expression of genes whose products aid the cell with stress survival, DNA repair and osmoregulation. The mechanism(s)/reason(s) underlying activation of *malP* transcription by HU and FNR remain open for investigation.

3.3. Links between glycogen and maltodextrin metabolism

Despite MalP and GlgP catalyzing similar reactions, they differ in their substrate specificities, with MalP showing a clear preference for short chain maltodextrins, though it can act on glycogen[87]. GlgP's affinity for glycogen is higher than that of MalP and it may also act on maltodextrins consisting of at least 5 glucosyl residues[71]. Though GlgP cannot substitute MalP's role in maltose/maltodextrin

metabolism[71], it is reasonable to assume that either MalP or GlgP may act on maltodextrins liberated by the debranching activity of GlgX during glycogen degradation.

Under specific conditions (low extracellular glucose, high endogenous cAMP alongside the presence of maltose or longer dextrins[22,28]) the cAMP/CRP system enhances expression of the transcriptional activator, MalT[75,88]. Transcription of this gene is subject to additional regulatory control and the protein directly recognizes and responds to endogenous maltotriose, which acts as inducer of the *mal* system. Enzymes involved in maltodextrin metabolism can influence maltotriose amounts and, therefore, affect intracellular levels of the inducer of MalT activation[71]. Glycogen-derived maltotetraose can be acted upon by MalP, to form maltotriose providing a link between glycogen and maltodextrin metabolism (Figure 1.2).

4. Glycogen, maltodextrins and endogenous carbon metabolism

It had been postulated that glycogen serves an integral role in bacterial metabolism, being degraded when nutrients are limiting, thereby sparing other macromolecules from turnover[89,90]. Given the centrality of this biopolymer to endogenous metabolism it is unsurprising that its turnover is linked to diverse cellular processes[2,17,57].

Both glycogen degradation and maltose/maltodextrin metabolism supply the cell with substantial amounts of G1P (Figures 1.2 and 1.3) which may be used by GalU[91,92] (UTP:glucose 1-phosphate uridylyltransferase; EC 2.7.7.9) to form UDP-glucose (UDPG) or for G6P generation via Pgm (Figure 1.4). UDPG fulfils various roles in the cell, which include acting as a link between nutrient availability and cell division[93] and serving as substrate for the synthesis of parts of the outer membrane[94]. G6P, on the other hand, may be used to generate PEP and facilitate sugar transport or be channelled into glycolysis and anabolic pathways[72].

A role for glycogen turnover in cell cycle progression has been noted in yeast[95] and in *E. coli* grown in continuous culture[96]. In both cases evidence indicates that glycogen is stored when less-favorable nutritional conditions arise. Its rapid mobilization during growth resumption in fresh media suggests that its degradation for ATP synthesis is preferred over energy expenditure on PTS-dependent glucose transport and subsequent assimilation. A role for glycogen as the preferred glucose source during the lag phase (or the growth phase succeeding the one it was amassed in) has been corroborated in *E. coli* by more recent studies[19,72,73]. We are only beginning to appreciate glycogen's function within the context of endogenous carbon and energy metabolism and assessing the influences its turnover has on central metabolism and essential processes, like division and DNA replication, remain tantalizing avenues to explore.

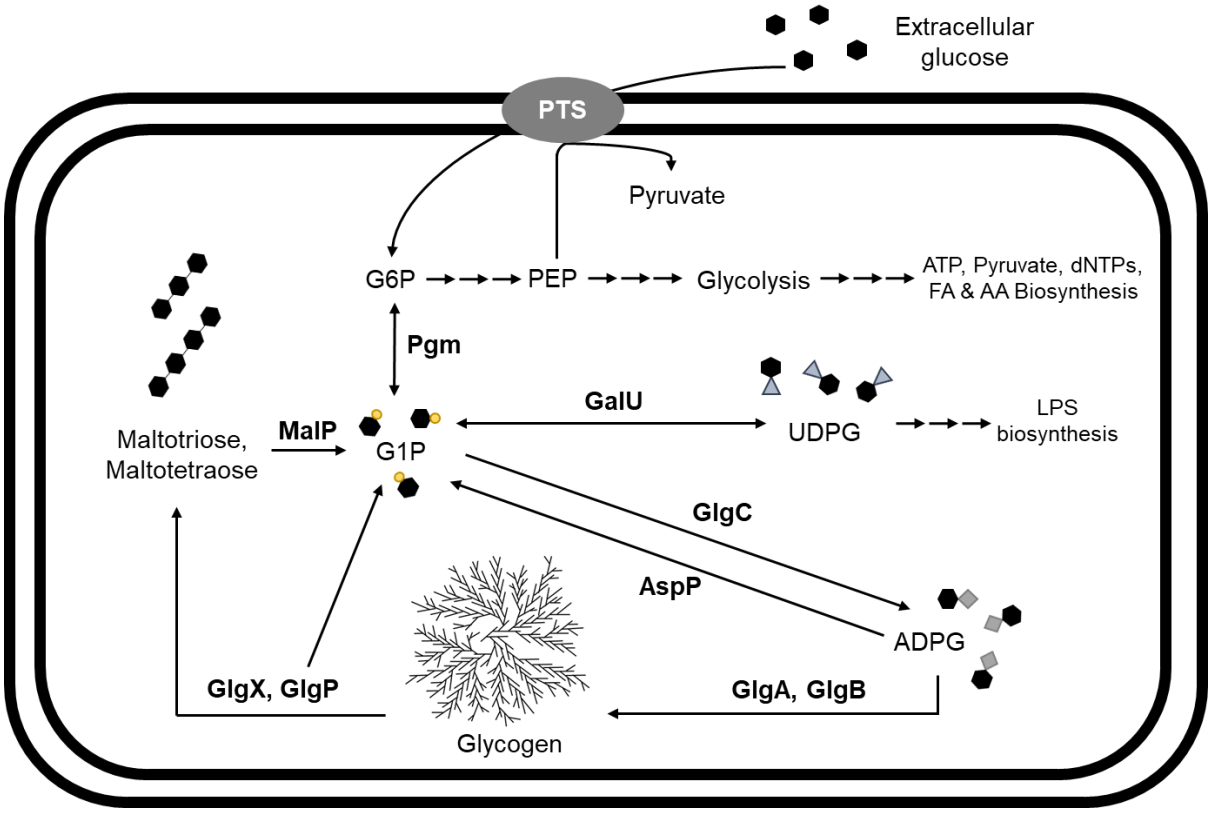

Figure 1.4. Glycogen metabolism within the context of central metabolism. The concerted actions of GlgP, GlgX and MalP yield G1P from stored glycogen. This may be used for UDPG biogenesis by GalU or be channelled into other processes, like glycolysis, after interconversion to G6P by Pgm. Extracellular glucose, upon being transported into the cell via the glucose PTS, may enter various pathways as G6P. Should nutritional conditions permit, glycogen will be formed from extracellular glucose, through the activities of GlgC, GlgA and GlgB.

5. Sensing cell size and maintaining size homeostasis in *E. coli*

Bacteria are the smallest living organisms capable of independent growth and reproduction and the impact of environmental changes and genetics on cell size and reproduction has been the subject of elaborate investigations over the past few decades. Whereas environmental cues like pH[97] and osmolarity[98] have been shown to affect cell size by modulating progression of the cell through the cell cycle, several pioneering works have led to models of bacterial size control in response to nutrient availability[93,99–107]. For single-celled *E. coli*, size certainly matters as changes in cell volume or surface area will inevitably affect the cell's metabolic flux and capacity for biosynthesis and nutrient exchange[108].

5.1. The nutrient growth law

More than 60 years ago the first experimental work was undertaken examining control of bacterial cell size. *Salmonella enterica* serovar Typhimurium was cultured under various nutritional regimes at different temperatures[99]. Richer media not only supported the growth of larger bacteria, but also cell populations that grew faster and contained proportionally more DNA and RNA than small, slow-growing cells cultured under nutrient-poor conditions. It was proposed that a balance between macromolecular biosynthetic rates and cell size ensures that DNA/RNA concentrations remain constant across varying growth conditions[99]. Manipulating growth rate by varying culturing

temperature had no effect on cell size or composition, suggesting that these parameters were specifically influenced by nutrient-dependent metabolic changes and gave birth to what has colloquially been referred to as Schaechter's nutrient growth law[99]. This states that average cell size scales linearly with the nutrient-imposed growth rate and has been demonstrated to apply to other bacteria, including *E. coli*[109] and *B. subtilis*[110].

5.2. The bacterial cell cycle

Seminal work by Cooper and Helmstetter[111] solved a long-standing mystery as to how fast-growing bacteria (doubling times <60 mins) remain viable when they divide more quickly than it takes them to replicate and segregate their chromosomes (60 – 90 mins). A model for multifork replication was proposed based on past experimental evaluations of the DNA synthesis rates in *E. coli* undergoing different nutrient-dependent growth rates[100]. This phenomenon requires that new rounds of DNA replication are initiated before the current one is complete, allowing maternal cells to give rise to daughters whose nucleoids may actively be firing from multiple origins. A single initiation event will always precede a single division event so that two identical daughter cells arise, each containing at least one fully replicated chromosome.

The cell cycle of a slow-growing bacterium may be seen in terms of three phases (Figure 1.5a). The first of these comprises the period from inception to initiation of DNA replication (B period), followed by the time it takes to replicate the genome (C period) and finally the time from terminating DNA replication to division (D period). The distinct gap period (B phase) preceding replication initiation is notably absent in fast-growing cells, where the C and D periods overlap as multiple rounds of replication are initiated to keep up with the fast pace of growth and division[100] (Figure 1.5b). This also provides an explanation as to why large, fast-growing cells in nutrient-rich media contain more DNA than their slow-growing nutrient-deprived counterparts[99]. By initiating and extending new forks or elongating partially completed DNA chains, replication rates keep up with rapid division rates when nutrients are abundant. Coupling between replication initiation and cell division was further implied by the observation that the timing of initiation could accurately be predicted by assuming that a constant time elapses between triggering a round of replication and completing cell division[111].

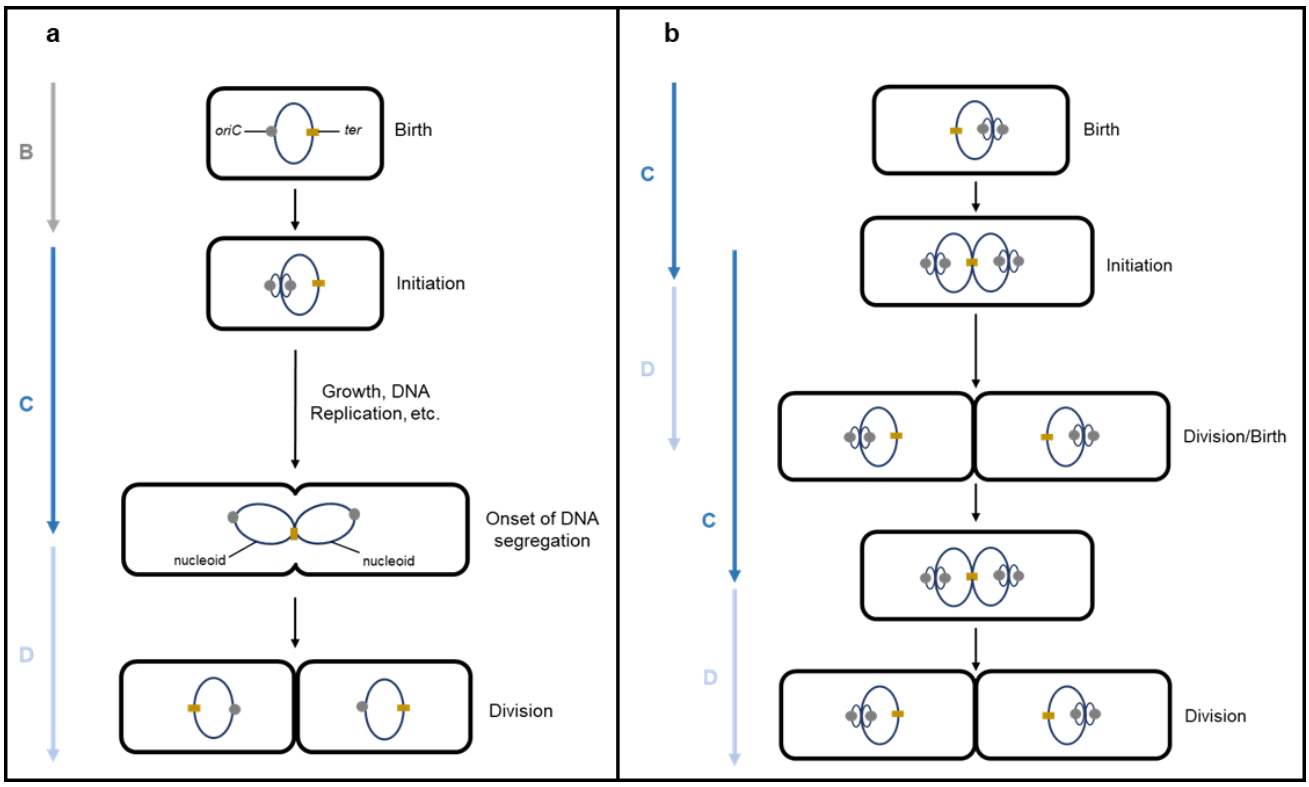

Figure 1.5. The bacterial cell cycle according to Cooper and Helmstetter. Under conditions of slow growth (**a**) the cell cycle consists of three distinct periods and bacteria have enough time to initiate and replicate their genomes only once per division cycle. When nutrient abundance supports fast growth (**b**) cells are born with active replication fork. A new initiation event may be triggered before the cell has completely replicated its genome and divided, but septation occurs only once per round of replication to ensure a one-to-one ratio between initiation and division events (adapted from Levin & Taheri-Araghi, 2019).

5.3. Discovering a link between cell size and replication initiation

An analysis by Donachie[101] combined the proposed cell cycle model of *E. coli*[111] with the nutrient growth law[99] observed in *S. typhimurium* to provide evidence for a critical size model in *E. coli*. He suggested that a cell will initiate replication only upon attainment of a size that is a multiple of a critical mass (initiation mass). This initiation mass appears to be a fixed constant when doubling times are slow (>60 min) and becomes twice that value when cells divide more frequently (30 – 60 min). The initiation mass was found to coincide with an average cell volume per origin that was invariable at different growth rates, suggesting some form of size control linked to DNA replication initiation.

Furthermore, it was suggested that some factor was accumulating in a growth-dependent way and triggering initiation upon reaching a threshold level in the cell, with its accumulation being proportional to the rate of synthesis of molecules like DNA/RNA[99]. If replication and division were coupled as suggested[111], then the latter, like size, would be subject to control by replication initiation, though whether this assumption made on population-averaged data held at single-cell level was also unknown.

Subsequent work proposed this growth-dependent initiation protein to be DnaA[112,113], an ATPase which may take on either an active, ATP-bound form (ATP-DnaA), or an inactive state where it is bound to ADP (ADP-DnaA)[114]. ATP-DnaA binds to specific sequences within the origin region (*oriC*), melting the DNA double helix and allowing subsequent loading of the proteins needed for DNA synthesis (replisome). Support for this proposed role comes from the observation that it accumulates in individual cells in a size-dependent manner, while its concentration remains invariable across numerous growth conditions[115].

It would follow that its elimination from the cell would delay initiation and increase average cell size while overproduction would cause the cell to over-initiate and trigger origin firing at a reduced mass. This has been observed to varying degrees[115,116], DnaA is unlikely the only factor needed to reach threshold to trigger origin firing[117]. Moreover, observations that division plates may form regardless of whether replication initiation has occurred[118], and that septation may occur through an incompletely replicated nucleoid[119] raised important concerns over the reported degree of coupling between replication initiation and cell division[100,101,120].

5.4. Sizers, timers and adders

Early works assumed that cell division in steady-state *E. coli* was symmetrical and would occur only once the cell had doubled in size, partitioning equal amounts of cellular constituents to daughters upon division. Until recently, cell size homeostasis was believed to involve division being triggered by the cell actively sensing either time or space. Whether division was dictated by a timer (occurring once the cell has reached a certain age after a constant time has elapsed) or a sizer (occurring once the cell has grown by enough to reach a constant size at division) remained unclear[121,122].

The advent of robust single-cell analysis techniques, such as the ‘mother machine’[123] has provided unprecedented insight into cell size homeostasis and the regulatory mechanisms used to maintain this. The use of microfluidic devices for single-cell examination permits observations of size and growth to be made of thousands of cells tracked over multiple generations. Pioneering work using the ‘mother machine’ revealed that cell size during exponential, steady-state growth is surprisingly variable, which would argue against a size sensor ensuring cell size homeostasis[123].

Such analysis demonstrates that daughter cells are occasionally born which are larger or smaller than their ancestors. Stochastic differences in gene expression levels between cells[120], or the fact that division is functionally asymmetrical[123] may help to describe some of the heterogeneity observed in cell size during balanced exponential growth. Subsequent analyses[102,103] revealed that in lieu of actively sensing either time or space, deviant fluctuations in size are passively corrected by cells adding a constant volume (cell unit) between division events, regardless of the size at birth (Figure 1.6).

While this adder model does not provide an immediate return of cells with stochastically different sizes to the ideal population size (i.e. convergence of cell size/ cell size homeostasis), it instead permits cells to correct these changes over multiple generations by adding a fixed size increment. This has revolutionized the way cell size homeostasis is described in *E. coli*, other bacteria and even some eukaryotes[122]. Despite solving an elusive conundrum regarding cell size homeostasis in *E. coli*, open questions remained regarding how cells sense their absolute size (size control) and implement this adder mechanism.

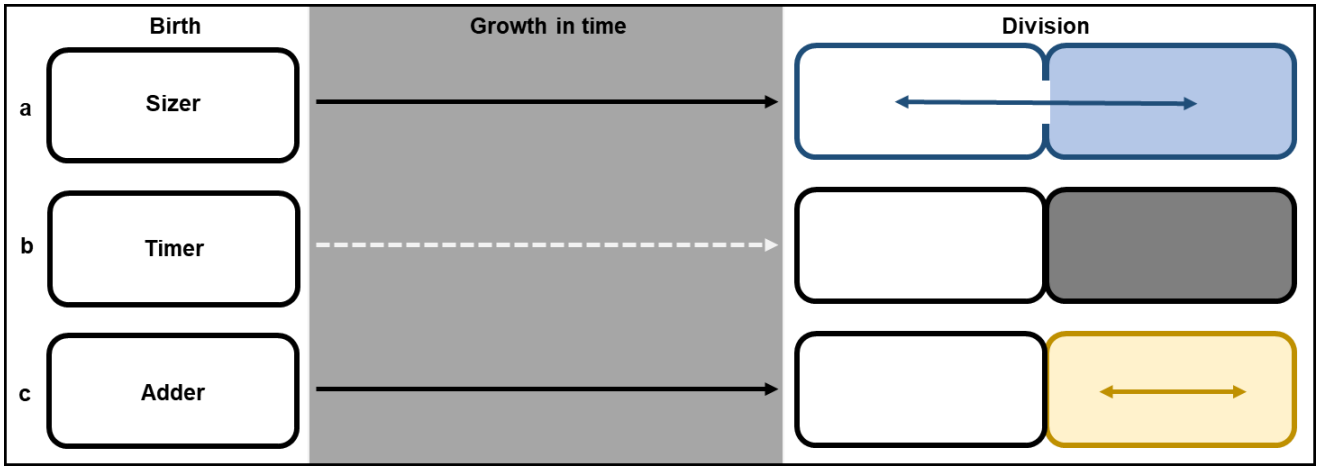

Figure 1.6. Proposed mechanisms ensuring cell size homeostasis in *E. coli*. The hypothesis that size is actively sensed and symmetric division implemented by (**a**) cells sensing the space they occupy and dividing at a constant size or (**b**) cells sensing time and triggering division at a constant age have been replaced by (**c**) the adder model where size homeostasis is passively ensured by cells dividing after a constant cell volume has been added since being born, allowing cell size to converge at an idealized 'norm' after several division events (adapted from Morcinek-Orłowska et al. 2019).

5.5. Uncovering the mechanisms behind adder and homeostatic size control

To test the adder model studies have artificially altered the volume of the cell unit added before division. This leads to cells born demonstrating deviant sizes, which return to an idealized average size after several division cycles, highlighting the robustness of adder and cell size homeostasis mechanisms to genetic and chemical intervention[104,124]. Furthermore, the point at which adder is implemented during the cell cycle had been the subject of serious debate over the past decade. Some have argued that timing of division depends on DNA replication firing at a certain size, supported by data acquired at population[104] and single-cell level[125]. This initiation size coincides with a cell volume per origin that is invariable at various growth rates[101,104,125]. Based on *in silico* modelling[102,103] and studies manipulating the allocation of resources to protein synthesis[126] , others favoured the idea that adder was controlled at the level of division. An integrated view where size control is implemented at both replication initiation and division has also been proposed[127,128].

By modulating amounts of DnaA and the essential Z-ring forming divisome protein, FtsZ, it was recently demonstrated that cells grown under steady state conditions possess two adders that ensure cell size homeostasis[105]. An initiation adder functions at the level of origin firing and depends on the cell growing to a size where it has formed, and accumulated threshold amounts of the proteins

and factors required to trigger this event. However, cells also possess a division adder, where cell division only occurs when bacteria are large enough and have accumulated those molecules needed for septation to threshold levels[105]. By varying the intracellular concentration of FtsZ it was furthermore demonstrated that division solely ensures cell size homeostasis, whilst being independent of replication initiation[105]. Although disrupting the concentration of DnaA changed cell size it did not affect the ability of the cell to return to an idealized size through homeostatic control. In this way, cells sense their size by synthesizing initiator molecules at rates proportional to size increases and accumulating these initiators to critical levels to unlock specific 'achievements' – either entry into the cell cycle by triggering replication initiation or birthing progeny by dividing (Figure 1.7).

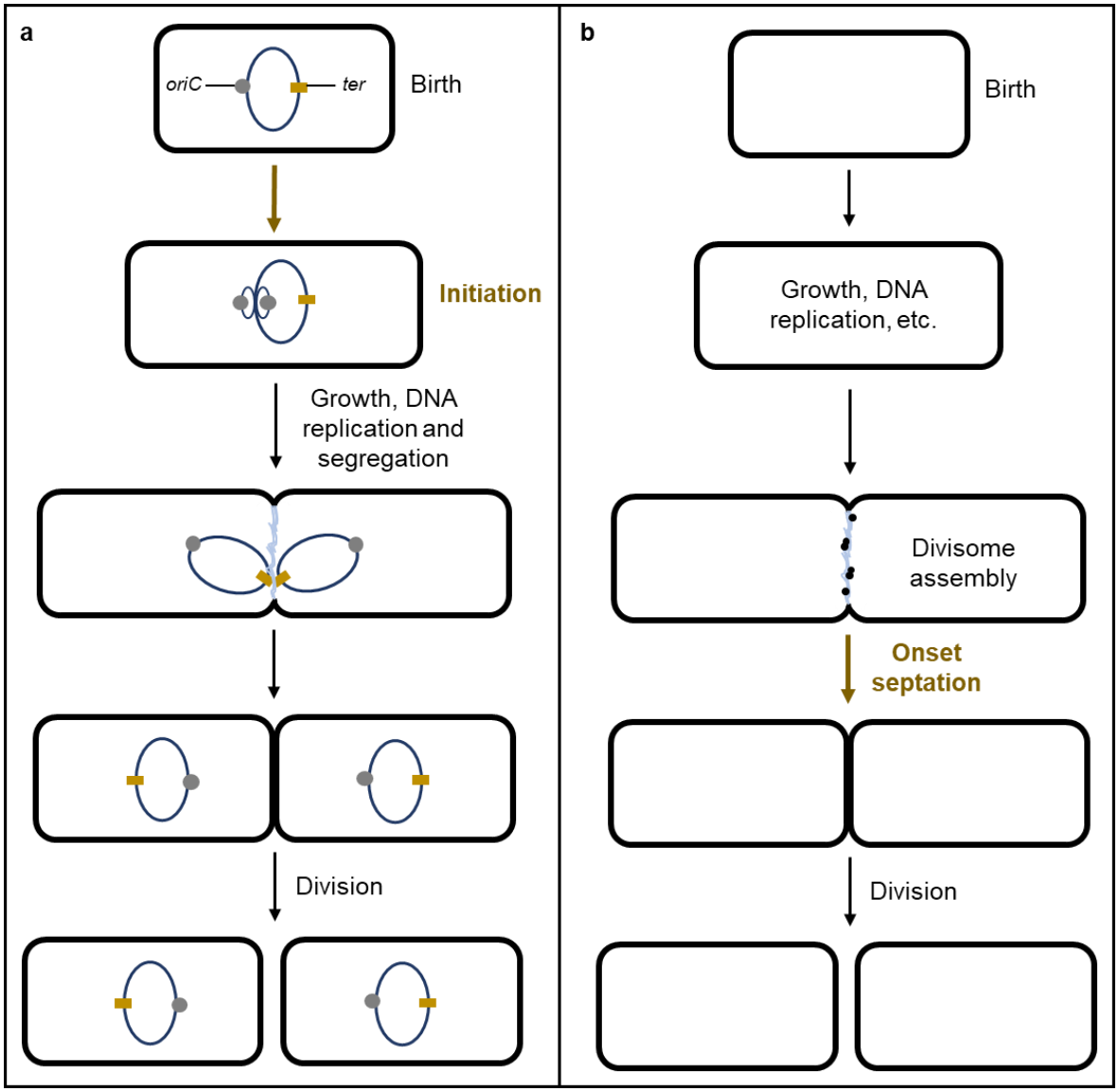

Figure 1.7. Implementation points of initiation and division adder under steady-state growth. (**a**) Cells initiate DNA replication upon adding a constant size that corresponds to the number of replication origins in the cell and the accumulation of those initiating molecules needed to trigger this event (like DnaA) to threshold. (**b**) At the same time, cells only divide after adding a constant cell volume, and this added size corresponds to accumulations of those molecules needed to trigger septation to critical levels. The division adder acting solely and independently of the initiation adder ensures size homeostasis, which is typified under a stressed regime (adapted from Morcinek-Orłowska et al. 2019).

Division must be coordinated with initiation to make sure that a cell divides only once per round of replication to ensure progeny are born viable and devoid of genetic defects[105,106,120]. For example, under conditions that provide stress[129], bacterial cells can develop into filaments[130] where the cell elongates but fails to divide (See section 6.2.1 below for details). In such filaments the volume added between division events that give birth to 'normal' daughters is independent of the number of origins of replication in the maternal cell[129]. Instead, division appears to be a highly dynamic process in such cells and cell size is sensed by employing an adder-like sensing mechanism and manipulating the position of Z-rings so they are always either one cell unit away from the cell pole, or two such units from each other[129].

6. Synchronizing DNA replication with cell division

Strict regulatory mechanisms exist that ensure replication initiation is triggered synchronously and at the correct time, whilst chromosome segregation is coordinated with cell division to prevent bisection of the genome. The strategies employed by *E. coli* to synchronize these events have been extensively studied using diverse mutant strains and culturing conditions, though certain aspects of control and regulation remain poorly understood[120].

6.1. Regulating replication initiation

Two independent cycles operate within *E. coli* that ensure synchronous origin firing and either activate or inactive the chromosomal replication initiator DnaA[131]. This involves the regulatory inactivation of DnaA (RIDA) where ATP-DnaA is hydrolyzed into inactive ADP-DnaA[132]. Rejuvenation of ATP-DnaA from ADP-DnaA is proposed to occur by nucleotide exchange (ADP for ATP) in the presence of acidic phospholipids at the inner membrane[133]. DnaA may autoregulate its own expression by binding to the *dnaA* promoter[134]. With the help of accessory factors such as DiaA[135] and HU[85] that help stabilize DnaA binding at a methylated origin, double-stranded DNA is melted and origin firing triggered. Since only one strand is methylated upon DNA unwinding and ATP-DnaA is always present in the cell, untimely origin firing must actively be prevented at the hemimethylated origin. In this regard, the *oriC* cycle involves sequestration of such sites by SeqA until they are methylated by Dam[136,137].

6.2. Cell division and the Z-ring

The GTPase, FtsZ, is an essential division protein[138,139] and polypeptide monomers bound to GTP assemble at midcell as flexible filaments, forming the Z-ring[140]. This structure is indirectly tethered to the cell membrane via ZipA and/or FtsA[141], forming a proto-ring which acts as a scaffold for at least ten other proteins that facilitate septation[142]. A role for FtsZ polymers in the generation of contractile force during division has been proposed, while peptidoglycan (PG) synthesis at the septum has been found to make a significant contribution to this force generation during septation[143,144]. FtsZ filaments appear to direct the localization of PG synthesizing enzymes through treadmilling, directing PG synthesis and reinforcing membrane invaginations mediated by FtsZ[145]. In

this sense, the energy required to drive cells apart during cytokinesis may come from both FtsZ polymers and PG, whilst synthesis of cell wall components limits this process[120,146].

6.2.1. Spatiotemporal control of division

Two primary systems that provide spatial and temporal control over Z-ring placement in *E. coli* are the Min system and nucleoid occlusion (NO)[147]. Three Min proteins, MinC, MinD and MinE play key roles in centring the Z-ring under steady state conditions, by preventing the assembly of FtsZ polymers at DNA-free cell poles[139,148]. Once MinD binds ATP (ATP-MinD) it interacts with the inner membrane and localizes to polar regions where it binds to the effector MinC, and this MinCD complex blocks septal ring formation (Figure 1.8). The hallmark of this system is its ability to oscillate from pole to pole, which occurs once MinE accumulates at a pole and binds to MinD, stimulating the dissociation of this system into the cytosol. Regenerated ATP-MinD moves to the opposite end of the cell where the concentration of MinE is low and repeated cycles of polar association and disassociation between Min partners create a negative regulatory zone at the poles for FtsZ. This system thus provides spatial control over division plate formation by limiting septation to midcell[149].

In stressed filaments, dynamic remodelling of Z-rings helps ensure daughter cells are born the right size, even when faced with adverse conditions[129]. In such a regime, absolute size of a filament is sensed by employing adder-like mechanisms while Min protein oscillations re-organize and place Z-rings at specific subcellular locations. It is likely that other growth-dependent regulatory systems act in synchrony with the Min system to ensure cell size homeostasis in stressed, filamentous *E. coli*, but these remain to be elucidated[129].

A link between the replication genome and cell division had long been proposed based on observations made examining temperature sensitive mutants of *E. coli* that are unable to replicate or segregate their nucleoids[150]. Division plates do not form over the nucleoids of these mutants and it was initially believed that as chromosomes are active sites of transcription and translation, these processes produce a short-range but potent inhibitory effect on division.

Subsequent work in *B. subtilis* and *E. coli* identified the nucleoid occlusion factors Noc[151] and SlmA[152] in the respective organisms. The binding of SlmA proteins to specific SlmA binding sites (SBSs) that are abundant in the origin region, but less so at the terminus, allows this protein to destabilize FtsZ filaments that may accumulate over an unsegregated nucleoid (Figure 1.8)[153]. This ensures temporal control over constriction and ensures it does not occur before replication is completed and sister chromosomes have been driven apart.

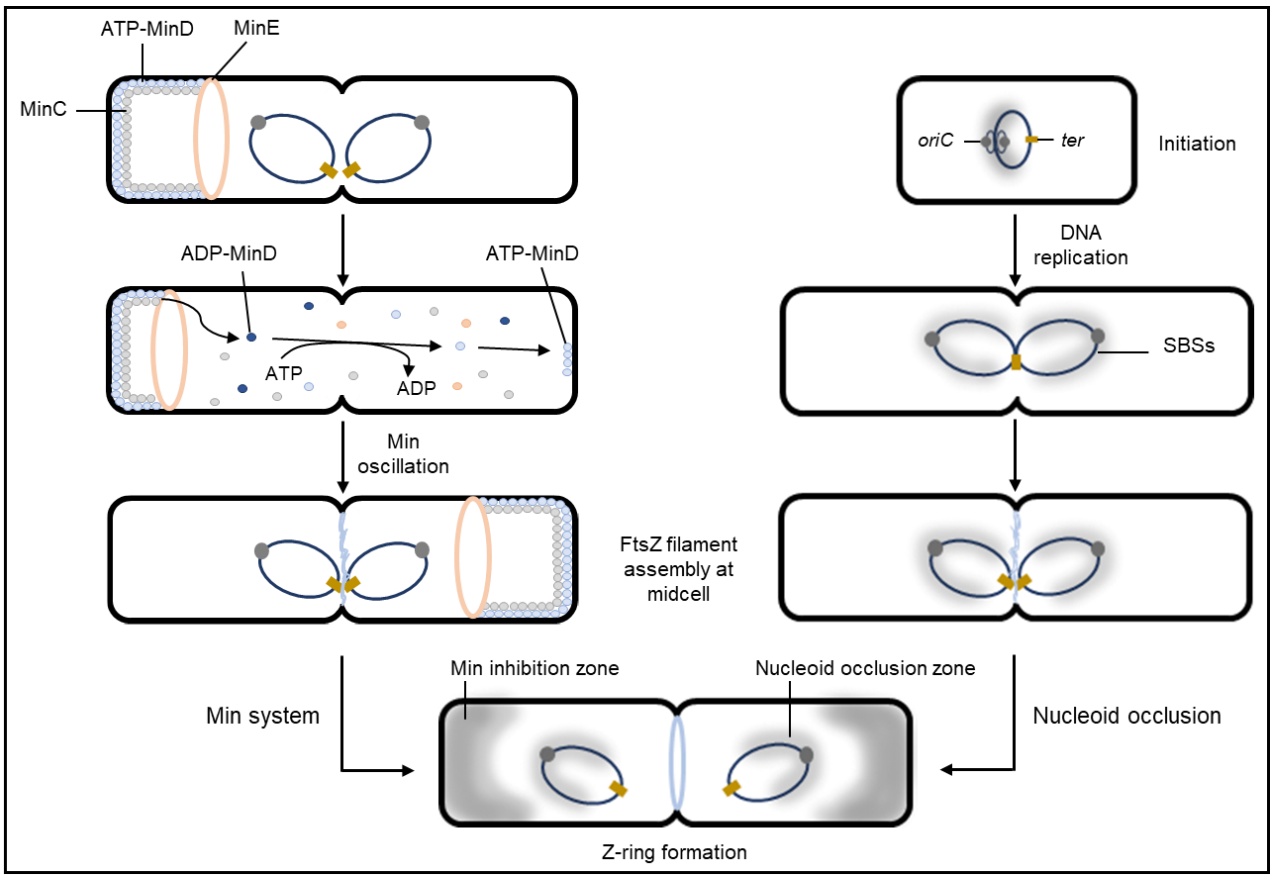

Figure 1.8. Spatiotemporal control of the Z-ring. Polar oscillations by the Min proteins (left) prevent Z-rings from forming at the cell poles. Concurrent prevention of FtsZ polymerization over the replication nucleoid (right) by SlmA binding at specific chromosomal binding sites prevalent at the proximal origin region (SBSs) ensures division plates are positioned at midcell and do not bisect an unsegregated chromosome (adapted from Pinho et al. 2013).

6.3. The SOS response – an inducible DNA damage checkpoint

When a cell is faced with severe stresses like carbon[154,155] or amino acid[156] starvation, being blocked in cell wall synthesis by antibiotic treatment[157], or some form of DNA damage[155,157,158,159,160] it may grow into filaments as a protective strategy[161,162] by eliciting the SOS response. The purpose of this emergency division block is to halt cell division and provide time to repair damaged DNA and restart stalled replication machinery. If such a division block is maintained, normal-sized rods elongate into multinucleate filaments[130] that form septa between separated nucleoids and divide in an ordered manner to give birth to normal-sized progeny[129].

Induction of this response is well characterized[163] and involves recruitment of the recombination protein, RecA, to the site of single-strand DNA breakage, typically found at stalled replication forks[155]. The activation of RecA upon ATP binding allows it to function as a coprotease, facilitating degradation of the transcriptional repressor and negative regulator of the SOS response, LexA. This activates transcription of a suite of unlinked genes[155] - most notably *sulA* which encodes a strong, global inhibitor of Z-ring assembly, that is rapidly degraded once damaged DNA has been repaired and arrested forks restarted[161].

At least one other inhibitory mechanism exists in *E. coli* that connects DNA replication to the division machinery, as an unsegregated nucleoid at midcell will prevent Z-ring formation in the absence of SulA, SlmA and MinC[164]. The division inhibitor, OpgH (See section 7.2 below for details), could, in theory[93], account for such a septation block at midcell, though its activity is primarily stimulated in response to nutrient availability while its role in delaying division is less clear in response to stresses (like osmotic shock[98]) that may affect DNA replication rates and/or nucleoid segregation.

7. Carbon metabolism and cell size

Given the importance of cell cycle progression both in size control and homeostasis, it is unsurprising that direct strategies have evolved in bacteria that allow direct coupling between cell cycle events and nutrient status[120]. This allows cells to grow large when nutrients are abundant and give birth to larger daughter cells. Nutrient-dependent increases in size are believed to help the cell interior accommodate extra DNA produced by multifork replication, preventing Z-ring formation over unsegregated chromosomes[93,165]. By coupling nutrient availability to size, parental cells can also store nutrients and give birth to larger progeny, potentially enhancing the vigour of future generations[166].

7.1. Lipid availability dictates cell size

Bacteria appear to follow an outside-in model of cell expansion, where external nutrient availability sets the capacity of the cell membrane, which in turn dictates the rate of anabolism in the cytosol[106]. Manipulating fatty acid synthesis by antibiotic treatment or genetic disruption changes both cell length and width in a manner which mimics nutrient availability. This finding answered a long-standing question as to whether some anabolic processes were more important than others in determining cell size. The alarmone ppGpp serves a central role in coupling cell envelope expansion to the rate of anabolic cytosolic processes. Its build-up during times of nutrient deficiency, when resources limit lipid synthesis, prevents cytosolic anabolic metabolism from outpacing cell envelope biogenesis.

These methods of size control prevent cells from funnelling nutrients into fatty acid synthesis, growing exceptionally long and eventually lysing; conversely, they also prevent cellular contents from exceeding the volumetric capacity of the cell, preventing rupturing from the build-up of internal pressure[106]. Due to their impact on biosynthetic capacity, nutrients clearly affect growth rate and cell size by affecting lipid biosynthesis and progression of the cell through the cell cycle[106].

7.2. Nutrient-dependent regulation of cell division

Recent advances have identified the metabolic sensors UgtP in *B. subtilis*[165] and OpgH in *E. coli*[93] that delay cytokinesis in response to high intracellular UDP-glucose (UDPG) levels that typically reflect a high carbon and energy status[167]. The discovery of the moonlighting role of OpgH[93], alongside its ability to produce osmoregulated periplasmic glucans (OPGs) that aid in osmotic

stress[168], provided concrete evidence for a regulatory mechanism that responds to extracellular carbon availability and manipulates cell division accordingly. The proposed mode of action of this glucosyltransferase involves its ability to bind both FtsZ and the metabolite UDP-glucose (Figure 1.9).

Under conditions of carbon abundance, more intracellular G1P would be available for the synthesis of ADPG (permitting glycogen biosynthesis) and UDPG[167]. Binding of UDPG to OpgH, results in a conformational change that allows this protein to directly interact with FtsZ monomers, delaying assembly of the Z-ring. By sequestering FtsZ monomers, OpgH delays septation by raising the threshold for FtsZ to trigger division, so cells grow larger when nutrients are readily available[122]. Disrupting OpgH activity causes division to occur more frequently. Cell size is reduced when OpgH, or proteins involved in UDPG biosynthesis[93] are mutated.

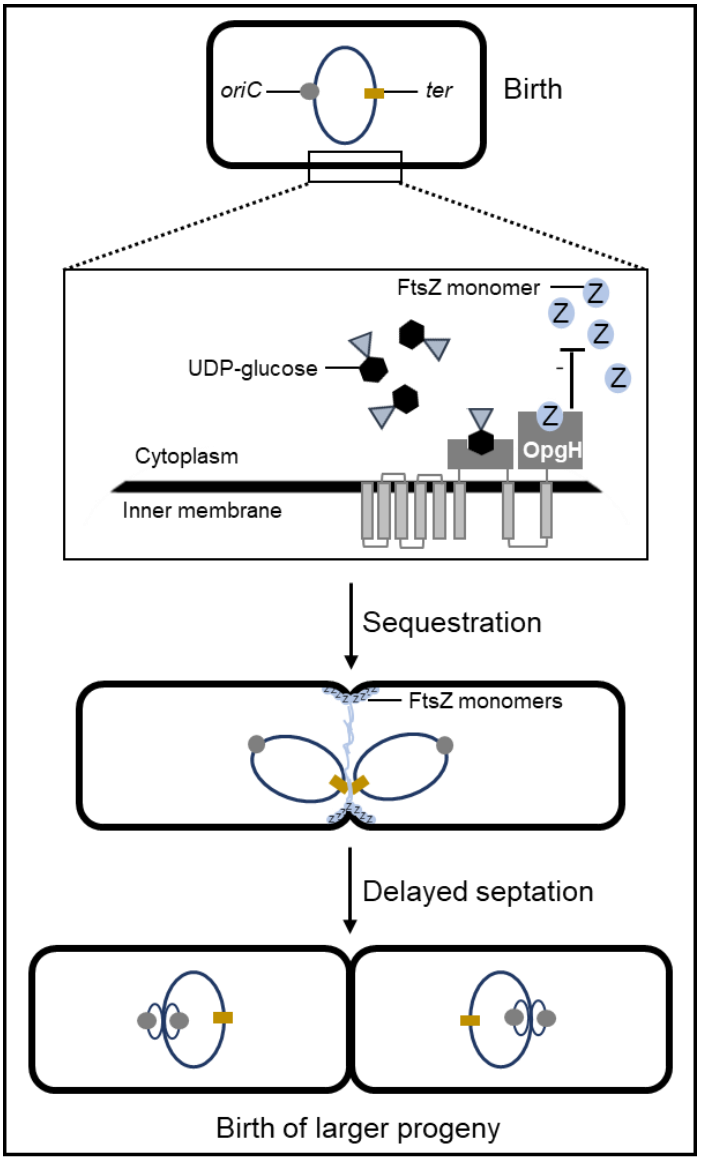

Figure 1.9. Carbon-dependent control of cell division via UDPG metabolism. Under conditions of carbon excess, high intracellular UDPG levels stimulate the activity of membrane bound OpgH which sequesters FtsZ monomers to delay the onset of division. Consequently, larger daughter cells containing multiple replication cycles are born when conditions are favorable (adapted from Hill et al. 2013).

A role for glycolysis in *B. subtilis* cell division has been suggested for the metabolite pyruvate[169]. Pyruvate kinase (Pyk) is a glycolytic enzyme that catalyzes the conversion of phosphoenolpyruvate (PEP) to pyruvate. Pyruvate has several important fates in the cell, including generation of ATP and reducing power. Through its conversion to acetyl-coenzyme A (acetyl-CoA) by the multienzyme pyruvate dehydrogenase complex (PDH^c) it provides an important link between glycolysis, the tricarboxylic acid (TCA) cycle, amino acid turnover and fatty acid metabolism[107]. Given the importance of pyruvate at crucial nodes in central metabolism linking carbon flux through anabolism, catabolism and energy production[170,171], it is unsurprising that this molecule fulfils additional regulatory roles within the cell. This link in *B. subtilis* between glycolysis and cell division is proposed to involve the E1α subunit of the PDH^c which responds to pyruvate levels in a nutrient-dependent manner and associates strongly with the nucleoid at midcell when nutrients are abundant, whereas this association is less obvious when nutrient conditions are poor[169] (Figure 1.10).

Since the Min system oscillates between poles and nucleoid occlusion factor binding sites are sparse or absent at the terminus region which is found at the cell center during the early stage of DNA segregation, it is proposed that the presence of E1α at midcell somehow positively regulates division. Whilst the exact mechanism of this interaction remains obscure, positive regulation is corroborated by the observation that disruption of Pyk activity in *B. subtilis*, which impairs the cell's ability to synthesize this metabolite, causes E1α to localize at the cell poles, which could explain polar divisions occurring in a *pyk* mutant[169].

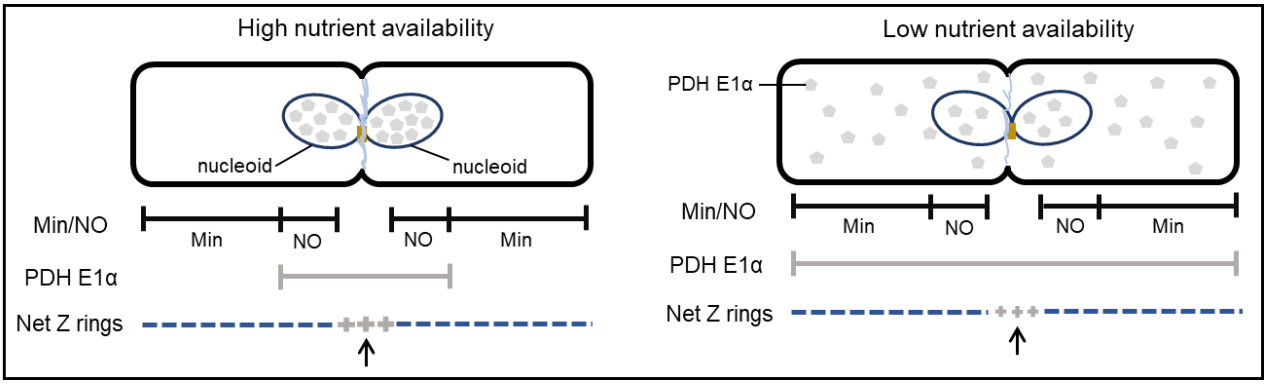

Figure 1.10. Linking glycolysis to cell division in *B. subtilis*. Under nutrient-rich conditions (left) the E1α subunit of PDH^c associates strongly over the nucleoids, presumably exerting some sort of positive effect over Z-ring formation at midcell. When nutrient access is restricted (right), the activity of the PDH^c is reduced and its E1α subunit is found diffused throughout the cell (adapted from Monahan et al. 2014).

7.3. Linking carbon metabolism to DNA replication

Several studies have linked enzymes of central carbon metabolism (CCM) with amelioration of phenotypes observed in temperature sensitive mutants affecting proteins involved in initiation, elongation and fidelity of DNA replication[172–176]. For example, disruption of genes needed for DNA replication are known to cause changes in cell size in *E. coli*[116,174,177]. Disrupting specific CCM enzymes can rescue or partially reduce the filamentation seen in such mutants, though it remains to be shown how this is accomplished[174,176].

It is likely that certain enzymes of CCM fulfil unappreciated roles in the cell that either directly or indirectly couple cell growth with DNA replication[172–176] and cell size by interacting with other proteins or influencing metabolite levels that are expected to impact signal transduction pathways that co-ordinate cell cycle progression and cell morphology[107]. While significant progress has been made linking some aspects of CCM to cell size, for example cAMP levels to cell width and acetyl-CoA levels to cell size and division through fatty acid metabolism[106,107], the extent of CCM influence on cell size remains poorly understood. It is unlikely that UDPG-dependent increases in cell size alone link nutrient availability to size through the cell cycle[93,107,165,167]. A complex relationship exists between nitrogen and carbon metabolism and coordination between these processes and cell size has been linked to AspC, an enzyme involved in amino acid metabolism[178]. While the exact mechanism of its action remains obscure, it is proposed that AspC alters carbon flux and manipulates UDPG levels to regulate division, while it also appears to somehow control replication initiation through DnaA[178].

When the rate of glycolysis exceeds the rate at which carbon is channelled into the TCA cycle[179], for example during exponential growth on glucose, bacteria may excrete acetate into the medium as a waste product of metabolic overflow[19]. When glucose is depleted from the environment, this acetate (and/or amassed glycogen) may be consumed to fuel those processes that sustain growth (i.e. for maintenance energy)[19]. Acetate is formed in a two-step process by Pta and AckA that generate acetyl-phosphate (acetyl-P) and acetate from acetyl-CoA, respectively. Disrupting the activity of either Pta or AckA delays growth and diminishes cell size, highlighting the importance of the overflow pathway in maximizing glycolytic flux[107,171].

When either *pta* or *ackA* is disrupted in a temperature sensitive *dnaA* mutant[171,172], they fully suppress the inability of this mutant to grow at the non-permissive temperature. It has recently been proposed that fluctuations in the activity of the PDH^c in response to pyruvate levels in *E. coli* is responsible for this observation, providing a potential link between nutrient availability and initiation of DNA replication[171]. Though *pta* and *ackA* mutants overaccumulate pyruvate (presumably as glycolytic flux to pyruvate is greater than the capacity of the PDH^c to form acetyl-CoA), this does not appear to be the primary effect leading to suppression of the phenotype observed in *dnaA* mutants.

Instead, changes to PDH^c activity likely account for this suppression, which was corroborated by disruptions to partners of the multienzyme complex similarly rescuing mutants producing defective DnaA protein. Further investigation is required to fully characterize the nature of this relationship between glycolysis and DNA replication in *E. coli*[171]. In *B. subtilis* the membrane-bound E2 subunit of the PDH^c was found to interact with DNA primase using a yeast two-hybrid system to detect protein-protein interactions[180], whilst another putative role in DNA replication for this protein partner of the PDH^c has been suggested to occur by it binding to AT-rich regions within the replication origin and delaying initiation in a nutrient-dependent manner[181,182].

7.4. Cell size and stringent response

Upon nutrient (carbon) deprivation and entry into stationary phase, *E. coli* cells undergo dramatic reductions in size and growth rate by eliciting the stringent response[37] which allows the cell to prepare itself for long-term survival in stationary phase[38]. Stringent growth arrest is accompanied by the build-up of ppGpp[39]. Cell size is diminished indirectly by ppGpp restricting fatty acid synthesis whilst reductions in growth rate likely result from it leading to downregulation of various growth-related biosynthetic processes[106].

7.5. Cell size within the context of endogenous metabolism

A wealth of research has been presented providing significant insight into how *E. coli* sense and respond to nutritional conditions. This involves sensing extracellular nutrients, synthesizing lipids, DNA, RNA and protein and triggering specific cell cycle events when their triggering molecules have accumulated to critical levels in the cell. Cell size is clearly a complex trait that involves coordinating cellular expansion, growth and cell cycle progression with nutrient status. Given the importance of glycogen within the context of endogenous carbon energy metabolism it is surprising that little work exists in *E. coli* assessing the affect its metabolism has on cell size[65] and cell cycle progression[96].

8. Aim and objectives

8.1. Aim

The aim of this study is to elucidate the link between glycogen turnover and cell size in *E. coli*.

8.2. Objectives

1. Measure cell size of strains affected in glycogen degradation when cultured in defined media at different stages of growth.
2. Assess mass doubling, viability, culturability and glycogen amounts in the different strains over time.
3. Examine FtsZ and DnaA protein levels through immunoblotting.
4. Analyze DNA amounts and replication patterns via flow cytometry.
5. Determine the subcellular localization of Z-rings and glycogen aggregates in the strains using confocal fluorescence microscopy.
6. Examine the effect of other genes on cell size.

2. Chapter 2 – Disruption of glycogen metabolism alters cell size in *Escherichia coli*

This chapter will be submitted to *Scientific Reports* and has been written in compliance with its submission guidelines. Complementary data may be found under Addendum A. Author contributions are acknowledged below:

Felix van der Walt

Performed experiments, participated in manuscript writing and conceptualized parts of the project

Léo Bürgy

Performed cell sizing analysis, created coliseg and edited the manuscript

Lindi Strydom

Generated the triple mutant and edited the manuscript

Jessica de Stadler

Manually analysed micrographs

Lize Engelbrecht

Assisted with confocal microscopy experiments and edited the manuscript

Rozanne CM Adams

Assisted with flow cytometry experiments

Gavin M George

Edited the manuscript

Samuel Zeeman

Edited the manuscript

Jens Kossmann

Edited the manuscript, funding

James R Lloyd

Conceptualized parts of the project, participated in manuscript writing, funding

Disruption of glycogen metabolism alters cell size in *Escherichia coli*

Felix van der Walt[1], Léo Bürgy[2], Lindi Strydom[1], Jessica de Stadler[1], Lize Engelbrecht[3], Rozanne CM Adams[3], Gavin M George[2], Samuel Zeeman[2], Jens Kossmann[1], James R Lloyd[1*]

[1]Institute for Plant Biotechnology, Department of Genetics, University of Stellenbosch, Private Bag X1, 7602 Matieland, Stellenbosch, South Africa

[2]Institute for Agricultural Sciences, ETH Zurich, 8092 Zurich, Switzerland

[3]Central Analytical Facility, University of Stellenbosch, Private Bag X1, 7602 Matieland, Stellenbosch, South Africa

[*]**Corresponding author:** Institute for Plant Biotechnology, Department of Genetics, Stellenbosch University, Private Bag X1, Matieland 7602, Stellenbosch, South Africa. Tel: +27218083837; Fax: +27218083835; Email: Lloyd@sun.ac.za

Nutrients impact cell size and growth rate in a variety of organisms. Research in *E. coli* has traditionally focused on the influence of exogenous nutrient sources on cell size through their effect on growth and cell cycle progression. Using a set of mutants progressively impaired in their ability to degrade the carbon store glycogen, we tried to establish whether impairment of polyglucan degradation affects cell size. Morphological changes to mutants include increased lengths and substantial heterogeneity associated specifically with a lesion in *malP*, encoding maltodextrin phosphorylase. This was more apparent during exponential growth than in stationary phase and occurred without detectably changing the portion of cells with Z-rings, cellular FtsZ levels or generation times. Run-out experiments demonstrated that DNA replication was affected in a variety of ways in mutants of glycogen catabolism, whilst Δ*malP* mutant cells contained increased DnaA amounts at late growth stages. Mutant bacteria with a disruption to *glgX*, encoding glycogen debranching enzyme, accumulated coinciding glycogen and protein inclusion bodies that were especially obvious during early exponential growth.

INTRODUCTION

Robust adaptive and survival strategies are employed by bacteria to promote fitness. Most notably, when nutrients are abundant, bacterial cells show dramatic increases in size and growth rate[99] which permits parental cells to promote the vigour of future generations by storing nutrients and giving birth to larger progeny[166]. Enhanced rates of macromolecular biosynthesis accompany nutrient-dependent size and growth increases to ensure that larger cells are also born with more DNA, RNA and protein[100,101,109,110].

The positive scaling relationship between size and nutrient-imposed growth rate has historically been termed Schaechter's nutrient growth law[99]. Several well-known exceptions to this rule exist, including mutants impaired in fatty acid[183] or carbon metabolism[93,107], and in genes of unknown function[124]. A more inclusive growth law in *Escherichia coli* suggests that individual cell size and average growth rate are mainly dictated by the initiation mass of the cell and the time it takes to execute the cell cycle[104]. Regulatory mechanisms ensure that progeny persist at an appropriate size for the ambient condition and *E. coli* is known to passively correct deviant changes to cell size by adding a constant volume of cellular material (cell unit) between division events, regardless of size at birth[102,103]. In contrast to earlier active models proposed for size homeostasis[101], this adder model ensures that cells born either too short or too long return to a population average size after multiple division cycles. Several studies have reported that the volume of this cell unit is proportional to the number of origins of replication in the cell[101,184], suggesting that cell size is controlled at the level of replication initiation.

Under steady-state conditions, this cell unit is dictated by an initiation adder[105], which ensures that origin firing is triggered only when the cell has grown and amassed factors, such as DnaA, to a threshold required to initiate this event. Initiation mass coincides with a cell volume per origin that is invariable at different growth rates[101,104,125]. Strict regulatory mechanisms ensure timely triggering of replication initiation and co-ordinated progression of elongation and chromosome segregation before cytokinesis occurs[131,185]. Size control in *E. coli*, however, is also subject to a division adder[105]. This means that cells only commit to division upon reaching a critical size, accumulating factors like the divisome protein FtsZ to a threshold concentration that allows formation of the Z ring, recruitment of other essential divisome proteins and eventual triggering of septation[120]. By varying the levels of FtsZ, it was demonstrated that division, independent of replication initiation, solely ensures cell size homeostasis[105].

Apart from the extensive direct control mechanisms that synchronize cell cycle events[120], progression may be indirectly influenced by environmental cues, like nutritional availability[93,171,178]. This affords the cell a way of integrating external signals with proliferation by manipulating the duration of the cell cycle. Central carbon metabolism (CCM) refers to a complex network of pathways involved in the transport and utilization of carbon for growth and may impact cell size and morphology in diverse ways[93,106,107,169,171]. The absence of certain CCM enzymes suppresses deleterious

phenotypes observed in mutants carrying temperature sensitive disruptions to genes encoding members of the replisome and DnaA[171–173]. This indicates that some CCM enzymes may link nutrient abundance to initiation, elongation and fidelity of DNA replication either directly through their activity[171] or by unknown mechanisms[172,173].

Glycogen is the main carbon store in *E. coli* and its turnover is linked to many CCM pathways, such as glycolysis. The first step in glycogen biosynthesis, catalysed by ADP-glucose pyrophosphorylase (GlgC)[3], utilizes the same substrate (G1P) that is used to synthesize UDPG[2]. On the other hand, G1P is formed when endogenous glycogen is catabolized through the combined actions of the glycogen and maltodextrin phosphorylases (GlgP[11] and MalP[76]). One other enzyme, glycogen debranching enzyme (GlgX)[30] is also involved in this process, producing linear glucan chains used as substrate by MalP[4,186].

Cell size, growth and cell cycle progression are known to be influenced by extracellular nutrient abundance. However, the role of intracellular nutrients in this process is less clear. Recent work within our research group generated an *E. coli* Δ*malP*/Δ*glgP*/Δ*glgX* triple mutant strain capable of glycogen synthesis, but severely impaired in its ability to degrade this polymer[186]. In this study we employed a defined, nutrient-rich medium and assessed the effect of glycogen breakdown impairment on *E. coli* cell size. We demonstrate that a lesion in *malP* leads to substantial heterogeneity in length. Our results also point to a link between glycogen turnover and DNA replication.

RESULTS

Mutants strains lacking glycogen catabolic enzymes grow at the same rate, are equally viable, but show reduced culturability. In this study we used a synthetic, rich medium and examined if growth was affected in isogenic mutant strains lacking *malP*, *glgP* and/or *glgX*[186] (Table 2.1). No significant differences in growth or doubling time were observed between the strains (Fig. 2.1a). We decided to examine the colony forming capacity of the strains at three different time points (Fig. 2.1a) that coincide with early exponential (OD_{450} of ~ 0.15), onset of stationary (OD_{450} ~ 4.0) and late stationary phase (OD_{450} ~ 7.0). During exponential growth, all MalP-deficient strains showed significant reductions in bacterial titre compared to strains with a wild type (WT) *malP* allele (Fig. 2.1b). During stationary growth, however, none of the mutants differed from the parental strain, though some differences were detected between the mutants.

Cell viability was assessed (Fig. 2.1c; Supplementary Figs. 1-6) and no differences were observed between any of the strains during exponential growth or at the onset of stationary phase, though during late stationary phase mutants with a disrupted *malP* allele produced significantly fewer dead cells than both the parental strain and Δ*glgP*/Δ*glgX*. Furthermore, both Δ*malP* and Δ*malP*/Δ*glgP* formed more viable cells at this stage than either Δ*glgP* or Δ*glgX*, though these single mutants did not differ from either Δ*malP*/Δ*glgX* or the triple mutant.

Table 2.1. Genotypes of bacterial strains used in the study. Strains were either acquired from the *E. coli* Genetic Stock Center or manufactured in our laboratory.

Strain	Description	Reference
Wild type (BW25113)	*Δ(araD-araB)567 ΔlacZ4787(::rrnB-3) λ- rph-1 Δ(rhaD-rhaB)568 hsdR514*	187
ΔmalP(kan)	BW25113*ΔmalP::kan*	188
ΔglgP(kan)	BW25113*ΔglgP::kan*	188
ΔglgX(kan)	BW25113*ΔglgX::kan*	188
ΔmalPΔglgP(kan)	BW25113*ΔmalP::ΔglgP::kan*	186
ΔmalPΔglgX(kan)	BW25113*ΔmalP::ΔglgX::kan*	186
ΔglgPΔglgX(kan)	BW25113*ΔglgP::ΔglgX::kan*	186
ΔmalPΔglgPΔglgX(kan)	BW25113*ΔmalP::ΔglgP::ΔglgX::kan*	186
ΔglgA(kan)	BW25113*ΔglgA::kan*	188
CM742	F-, *ara-19*, *fhuA1*, *lacY1 or lacZ4*, *tsx-33*, *glnX44*(AS), *galK2*(Oc), *λ*$^{-}$, *Rac-0*, *hisG4*(Oc), *rfbC1*, *rpsL8*, *mtl-1*, *dnaA46*(ts), *metE46*, *thiE1*	189

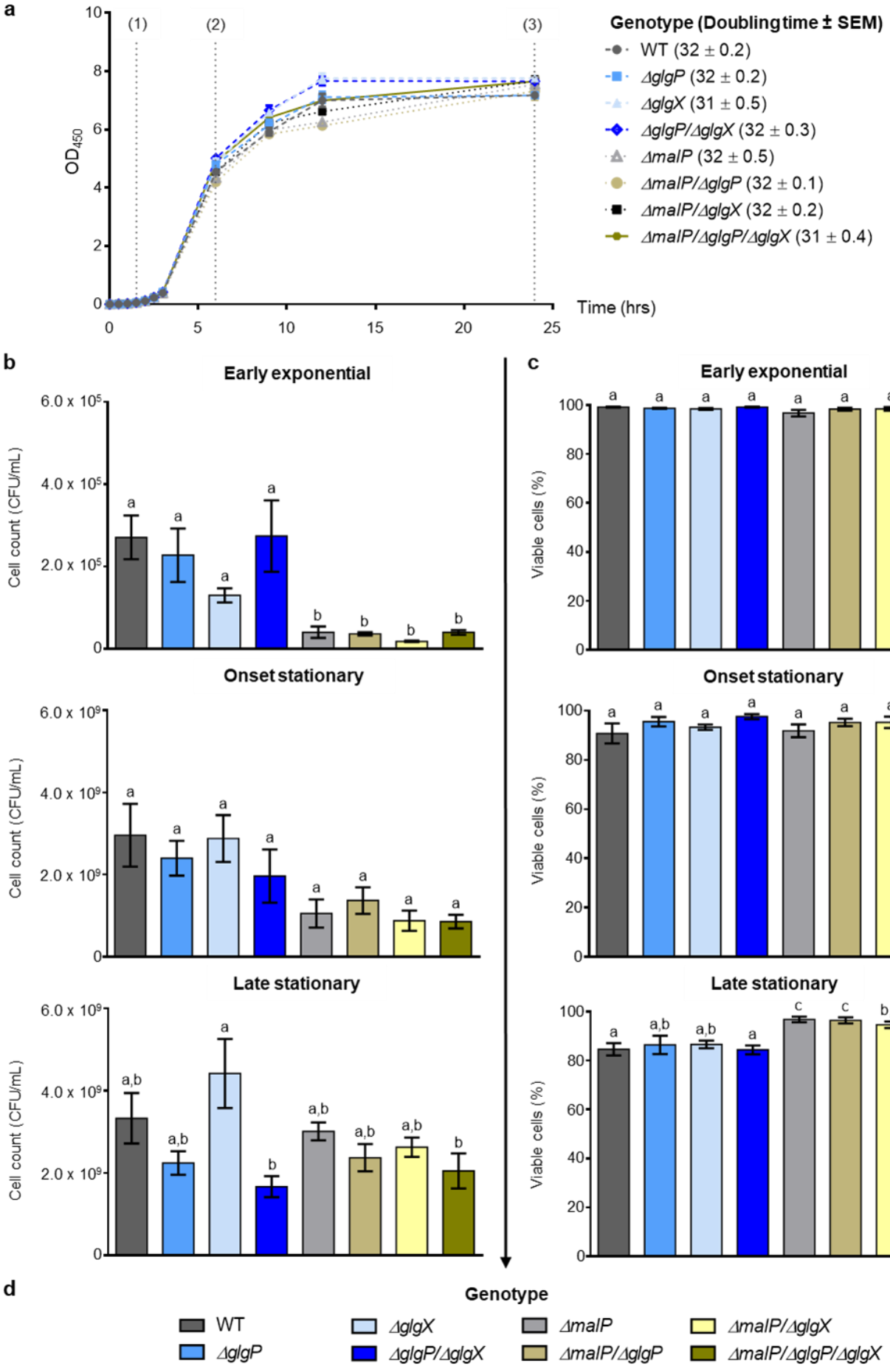

Figure 2.1. Growth, bacterial culturability and viability assessed over time. (**a**) Growth curves were generated by determining OD_{450} over a 24-hour period. The mean values from three independent replicates are plotted ± SEM and values within the linear portion of growth were used to calculate doubling times, shown after each strain name in parentheses in minutes ± SEM. The three time points investigated in this study are indicated by vertical dotted lines. (**b**) Cell counts were ascertained by diluting cells harvested at the indicated times and plating suspensions on LB plates, which were incubated overnight. Colonies were manually scored, and plotted values are the means from three independent replicates ± SEM. (**c**) The percentage of viable cells were determined over time from confocal images, with plotted values being the mean counts from three separate experiments assessing, in total, ≥ 5 000 cells ± SEM. (**d**) Different genotypes depicted in (**b**) and (**c**) are represented by the colours shown here. Different letters in (**b**) and (**c**) denote significant differences ($p \leq 0.05$) between group means as determined by a one-way ANOVA with Tukey's correction.

Mutants inhibiting glycogen breakdown produce longer cells than the parent strain. Cell length was examined at the same three growth stages. Cells longer than 2 µm were considered elongated and heat maps were created to summarize the mean differences in proportion of elongated cells between genotypes (Figs. 2.2a-c), whilst single data points for line charts were obtained by grouping cell lengths of each strain into four bins, according to specified cut-off points (Figs. 2.2d-f). Data were also used to generate weighted histograms by sorting cell lengths into defined bins and creating difference plots by using bin counts to compare the relative frequency of cell lengths in each genotype/condition (Supplementary Figure 7). Width was found to be essentially identical between strains (Supplementary Table 1).

Compared to the WT, substantial proportions of elongated cells were formed by the Δ*glgX*, Δ*glgP*/Δ*glgX* and Δ*malP*/Δ*glgX* mutant strains during early logarithmic growth (Fig. 2.2a) and by the Δ*malP*/Δ*glgX* strain when compared to the Δ*glgP* strain. Length distribution profiles of the Δ*glgP* single mutant were essentially identical to the WT at all three time points (Figs. 2.2a-c, Supplementary Figs. 7a-c). During early exponential growth, most cells from all strains ranged between 2 to 4 µm (Fig. 2.2d) and the range of cell lengths was also broader here than during stationary phase (Supplementary Figs. 7a-c), as all strains contained a small proportion of bacteria greater than 4 µm (Fig. 2.2d) while cells of these lengths were rarely found at the later two sampling points (Figs. 2.2e, f). Strains with a mutated *malP* allele demonstrated greater heterogeneity in length during early logarithmic growth with histograms (Supplementary Fig. 7a) revealing a marked shift in the prevalence of longer cells, whilst mean lengths increased from between 2.60-2.82 µm in strains with a WT *malP* allele to between 3.25-3.65 µm in Δ*malP* mutants (Supplementary Fig. 7a).

Variability in cell lengths were higher in Δ*malP* mutant strains, with the standard deviation being over 70% of the mean compared to less than 40% for the other strains during early exponential growth (Supplementary Fig. 7a). MalP-deficient mutants produced substantial proportions of abnormally long cells (Fig. 2.2d) with some bacteria growing into filaments longer than 40 µm. By stationary phase, the marked proportion of filamentous cells seen in the Δ*malP* mutants was almost eliminated (Figs. 2.2e, f) and the proportion of cells between 2 and 4 µm was enhanced in all the strains with a disrupted *glgX* or *malP* allele (Figs. 2.2e, f). Compared to the WT and Δ*glgP* mutant, all other mutant strains formed greater proportions of elongated cells during stationary phase (Figs. 2.2b, c). During the late stages of growth, the Δ*malP*/Δ*glgX* and triple mutant strains differed

markedly in their production of abnormally long cells when likened to all the other strains, though barely differed when compared to each other (Figs. 2.2b, c, e, f; Supplementary Figs. 7b, c).

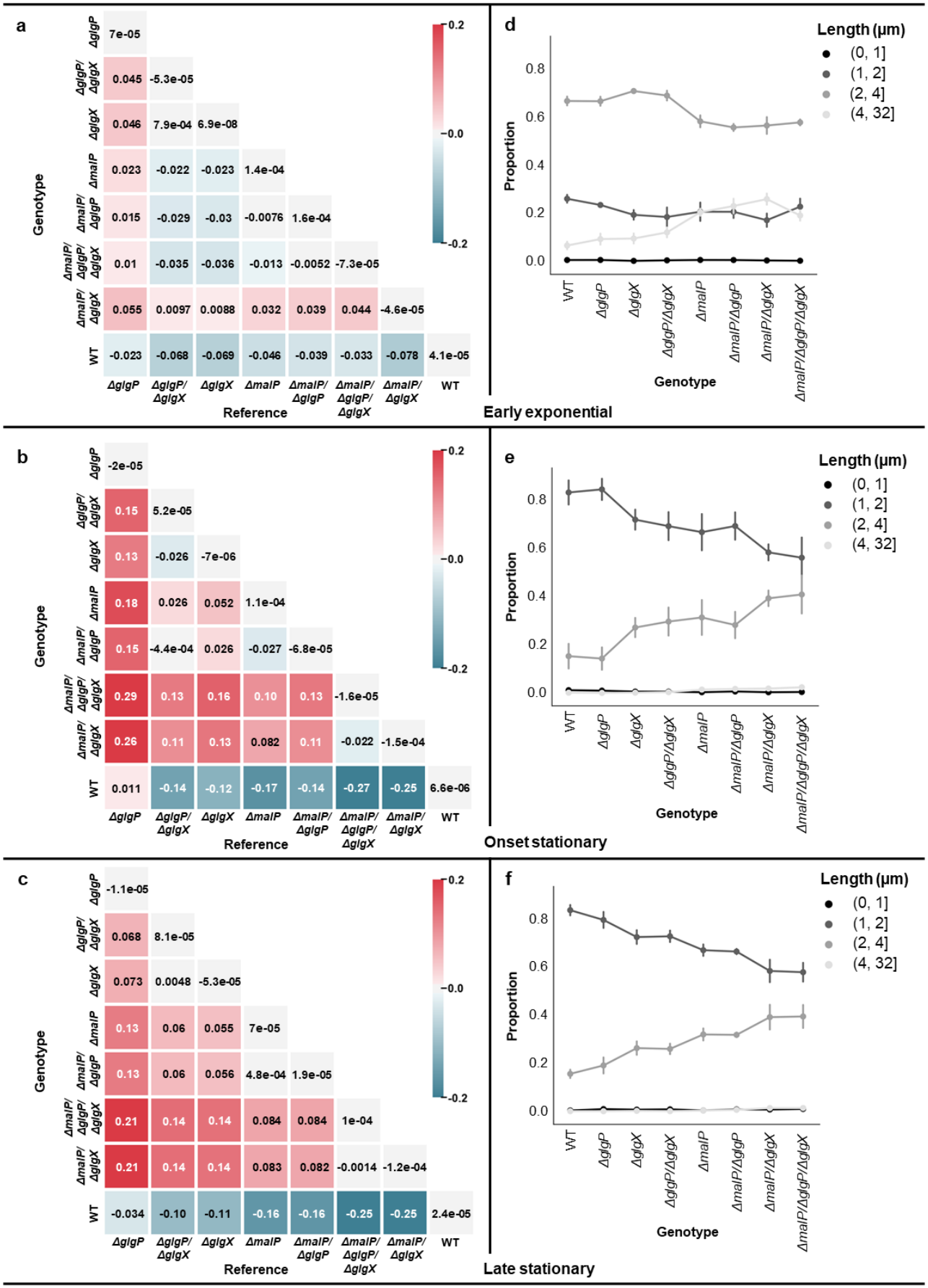

Figure 2.2. Cell length examination of the *E. coli* strains over time.(**a-c**) Heat maps plotted with the mean difference in proportion of elongated cells between strains. Red indicates a substantial difference in the proportion of elongated cells (>2 µm) between the genotype of interest (row) – the reference (column), whilst blue signifies the converse. (**d-f**) Line charts were created by grouping lengths into four bins according to cut-off points that are displayed at the upper right corner of each plot. Single data points represent mean ± standard deviation. Data were obtained from ≥ 5 000 bacteria overall, measured across three independent replicates.

Division does not exclusively occur at midcell in filamentous Δ*malP* mutants. Membrane-staining revealed invaginating septa at midcell in normal and elongated Δ*malP* mutant cells, along with cell walls forming at the ¼ or ¾ cell position in abnormally long bacteria (Supplementary Fig. 2). To assess whether Z-ring assembly was perturbed in the mutant strains, the percentage of cells with division rings during early exponential growth was determined. We found that Z-ring formation was unchanged in the different strains, with ~70% of cells from all strains showing visible rings during this growth phase and rarely forming more than one division plate per bacterium (Table 2.2). Whilst rings were limited to the middle of the cell in bacteria with a WT *malP* allele (Fig. 2.3a), Δ*malP* mutants formed division rings at midcell in both normal and long cells and at the ¼ and/or ¾ cell position in abnormally long cells. Diffuse fluorescent signal was observed in areas between segregated nucleoids in elongated Δ*malP* mutants, suggesting that FtsZ accumulated at putative division sites, but that Z-ring assembly was inhibited.

Immunoblots showed that there were no differences in FtsZ levels between any of the strains at any of the time points examined (Fig. 2.3b, Supplementary Fig. 8).

Table 2.2. Analysis of Z-rings in cells. Confocal images of immunolabeled early logarithmic phase cells were inspected for the presence of Z-rings. Data represent means from two independent replicates ± standard deviation, assessing ~450 cells per repeat.

Strain	Sample size	Proportion of cells containing Z-rings (%)	Proportion of cells containing more than one Z-ring (%)
Wild type	1 470	69.25 ± 1.6	0.27 ± 0.1
ΔglgP	1 187	67.65 ± 2.8	0.76 ± 0.5
ΔglgX	1 676	66.77 ± 0.8	0.89 ± 0.5
ΔglgP/ΔglgX	981	66.06 ± 2.5	0.92 ± 0.1
ΔmalP	1 428	69.12 ± 4.0	5.32 ± 0.7
ΔmalP/ΔglgP	1 080	70.09 ± 4.1	8.43 ± 0.6
ΔmalP/ΔglgX	1 236	67.56 ± 0.2	9.14 ± 2.8
ΔmalP/ΔglgP/ΔglgX	1 105	67.60 ± 0.3	8.60 ± 4.8

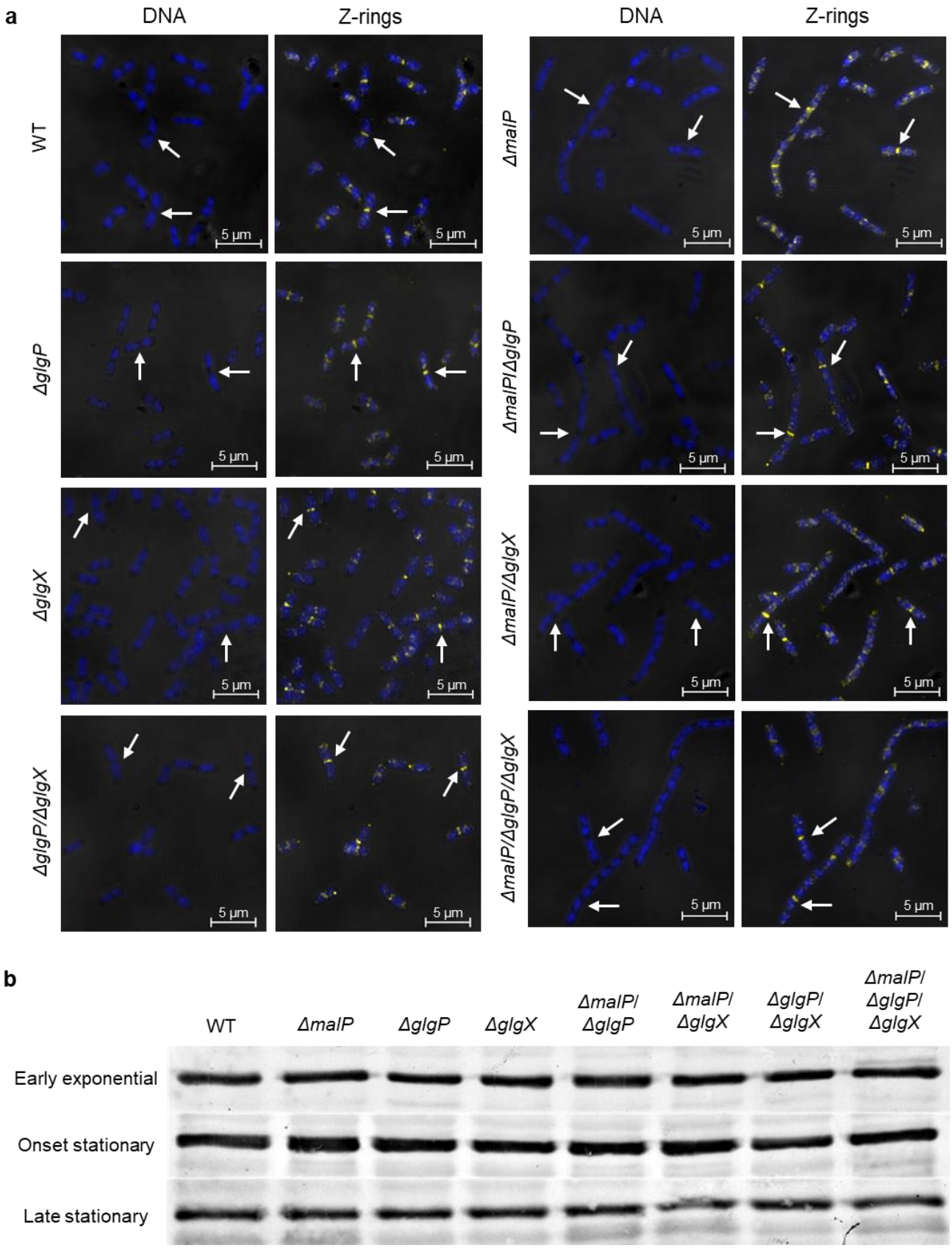

Figure 2.3. Z-ring formation and FtsZ amounts. (a) Bacteria harvested at OD_{450} of ~0.15 were fixed and immunolabelled using an α-FtsZ antibody. Phase contrast and confocal microscopy images depict the positions of Z-rings in cells during early logarithmic growth. These structures are shown in yellow, whilst DAPI-stained nucleoids are displayed in blue. White arrows demarcate FtsZ-rings. (**b**) Immunoblot analysis of relative FtsZ levels. Ten micrograms of total protein were separated by 10% (w/v) SDS-PAGE and visualized following labelling with an α-FtsZ antibody.

Glycogen aggregates are observed in Δ*glgX* mutants during exponential growth. Glycogen amounts increased in all the strains upon entry into stationary phase, with cells in late stationary phase containing the most (Fig. 2.4a). The triple mutant accumulated significantly more glycogen than the WT both at the onset ($p \leq 0.026$) and in late ($p \leq 0.038$) stationary phase, although these were the only significant differences detected within any timepoint.

We visualized glycogen aggregates in the strains as well as in a glycogen synthase (Δ*glgA*) mutant. As expected[28], no staining was observed in the Δ*glgA* strain (Fig. 2.4b; Supplementary Figs. 9-10) demonstrating the specificity of the stain. We observed substantial glycogen bodies in all strains with a defective *glgX* allele during early exponential growth (Fig. 2.4b). Whilst polar glycogen aggregates were observed in these strains, we also noted glycogen bodies in nucleoid-free regions and infrequently at midcell within elongated bacteria where both *malP* and *glgX* are mutated (Δ*malP*/Δ*glgX* and Δ*malP*/Δ*glgP*/Δ*glgX*). Polar polyglucan bodies appeared in all strains upon entry into stationary phase, with some diffuse signal detected along the cell peripheries (Supplementary Fig. 9). Glycogen bodies were particularly pronounced in strains with a defective *glgX* allele and were again detected in inter-nucleoid zones within elongated Δ*malP*/Δ*glgX* and Δ*malP*/Δ*glgP*/Δ*glgX* cells. This phenotype was less apparent in all cells cultured to late stationary phase (Supplementary Fig. 10) as staining was restricted to the cell poles and periphery.

Protein aggregates, stained by the amine-reactive viability dye, were observed only in GlgX-deficient strains during early logarithmic growth, and their spatial arrangement at midcell and polar regions coincides with that of glycogen bodies (Supplementary Figs. 1-2). At later growth stages, protein granules of various sizes are observed mainly at the poles of all strains (Supplementary Figs. 3-6).

Strains lacking MalP produce multinucleate filaments. During early exponential phase, DNA staining indicated no phenotypic differences between Δ*glgP*, Δ*glgX* and Δ*glgP*/Δ*glgX* mutants and the WT (Figs. 2.3a, 2.4b; Supplementary Fig. 1). Genetic material within elongated cells from Δ*malP* mutants appeared as unsegregated masses or as regularly spaced nucleoids along the length of the cell (Figs. 2.3a, 2.4b; Supplementary Fig. 2). During stationary growth MalP deficient mutants again demonstrated aberrant nucleoid partitioning, characterized by clumps of DAPI-stained DNA (Supplementary Figs. 4, 6, 9, 10), whilst this was not observed in the other strains (Supplementary Figs. 3, 5, 9, 10).

We determined the percentage of achromosomal cells formed by the strains over time and observed no significant differences in anucleate cell production between any of the strains during exponential growth or at the onset of stationary phase (Fig. 2.5a). In late stationary phase, the Δ*glgX* mutant produced significantly fewer anucleate cells than the WT ($p \leq 0.035$), though it did not differ markedly compared to the other strains.

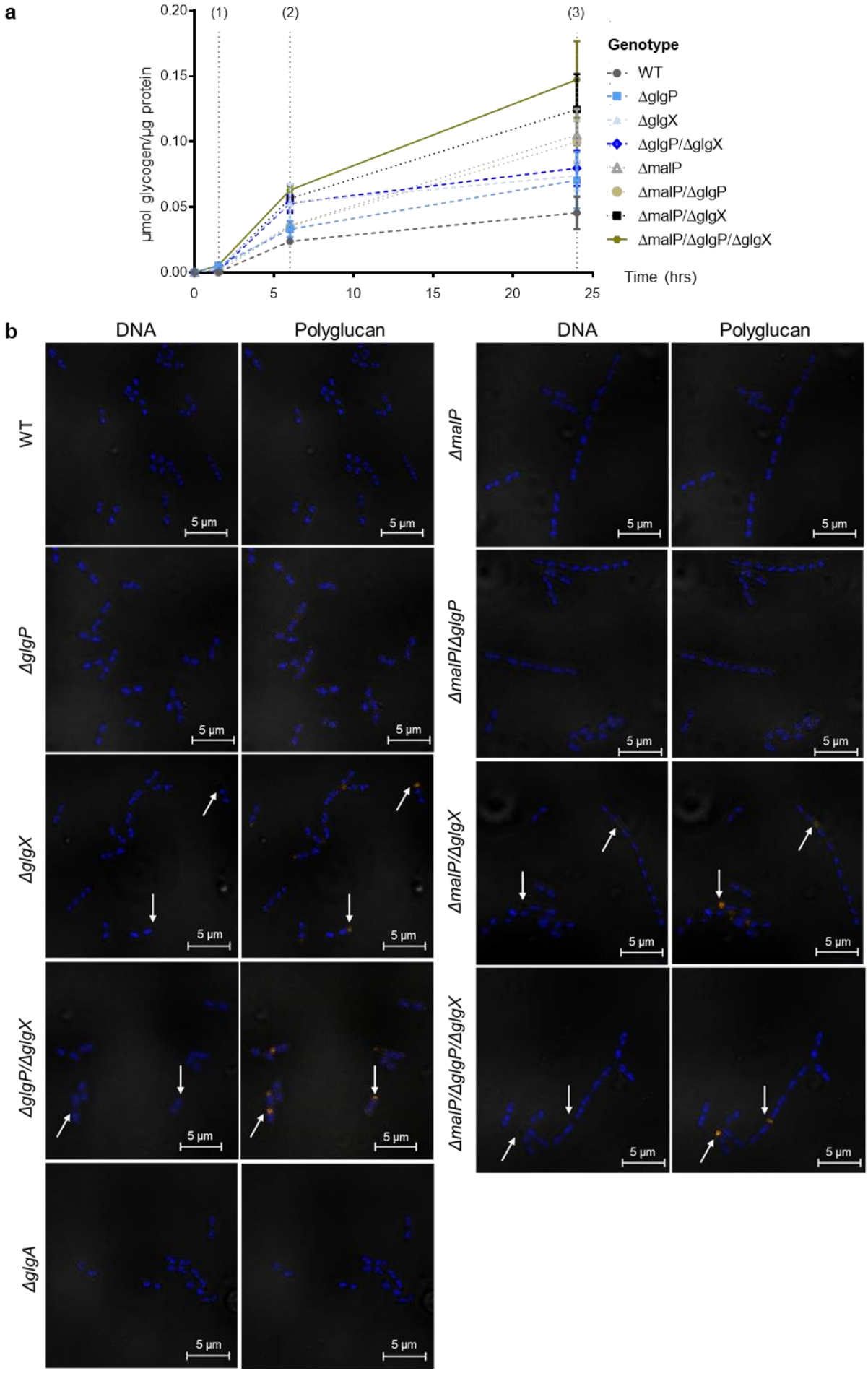

Figure 2.4. Glycogen amounts over time and PAS staining of glycogen bodies in exponentially growing bacteria. (**a**) Glycogen concentrations were determined at the three indicated time points, by harvesting cells, extracting this polymer and quantifying it via an enzyme-linked assay. Values plotted are mean values from three independent repeats ± SEM. (**b**) Cells were cultured to early logarithmic phase and then harvested, fixed and stained for polyglucan and DNA using PAS and DAPI respectively, before being imaged by confocal and phase contrast microscopy. DNA is shown in blue and glycogen in orange. White arrows point to glycogen bodies.

Mutant strains have altered DNA concentrations and diverse replication patterns. DNA concentrations, relative to the WT (Table 2.3), and replication patterns (Fig. 2.5b) were assessed during early logarithmic growth. The mean DNA content, cell mass (protein content) and DNA/mass of the Δ*glgP* and Δ*glgX* single mutants were nearly identical to the WT (Table 2.3). Cell mass was slightly elevated in the Δ*glgP*/Δ*glgX* double mutant while DNA content was essentially the same as was observed for the WT. As such its DNA concentration appeared to be lower than either of its parental single mutants and the WT strain. Mean DNA content, cell mass and DNA/mass of the Δ*malP* single mutant was somewhat higher than in the other MalP-deficient strains. DNA concentrations were furthermore marginally reduced in all strains with a disrupted *malP* and *glgX* allele (Table 2.3).

Run-out histograms revealed diverse DNA replication patterns amongst the different strains (Fig. 2.5b). In the WT strain, DNA resolved as three distinct peaks correlating to 2, 4 or 6 chromosome equivalents. The largest proportion of initiated cells contained 4 origins, indicating synchronous origin firing, though the presence of 6 origin cells suggests a degree of replication asynchrony under our experimental conditions. The peak of cells with 2 genome equivalents represents bacteria that had not initiated replication when antibiotics were added, and a delay in initiation would increase the proportion of such cells in a population[115]. Such a delay is observed in most of the mutants whilst problems with completing ongoing replication, are apparent from poorly resolved peaks[190–192].

Mutant Δ*glgP* cells showed two distinct peaks corresponding to cells with 2 or 4 chromosomes, though these did not separate completely, suggesting the existence of a subpopulation of cells containing non-integer chromosome amounts between 2 and 4 genome equivalents. There appeared to be a considerable initiation delay in this strain, indicated by the presence of a large proportion of cells with 2 origins. The presence of bacteria containing between 2 and 4 origins probably indicates that replication forks could not reach the termini, despite the length of this assay (3 hours). Initiation is also clearly delayed in the Δ*glgX* mutant, though the broadness of the peak suggests that existing replication cycles could not be completed in this strain and thus denotes cells with at least 2 and 4 origins.

The replication pattern in the Δ*glgP*/Δ*glgX* strain appears to be intermediate between the Δ*glgP* and Δ*glgX* single mutants where initiation is delayed, and elongation perturbed. Cells with at least 2 and 4 origins are present, though peaks are poorly separated and not as distinct as in the Δ*glgP* single mutant, indicating that disruption of *glgX* possibly has an additional negative effect on replication fork progression in this strain. Furthermore, the Δ*malP* single mutant showed a similar

broad and undefined peak of 2 to 4 origin cells, though cells containing up to 6 chromosomes are also present.

The severe replication problem observed in Δ*malP* single mutant cells is partially alleviated when *glgX* is also mutated. An initiation delay is still apparent from the substantial proportion of 2 chromosome cells, though the appearance of a distinct subpopulation of 4 origin cells in the Δ*malP*/Δ*glgX* strain implies that origin firing more closely resembles that of the WT than either of the single mutants (Δ*malP* or Δ*glgX*). Problems with stalled forks were less severe in this double mutant than the Δ*malP* single mutant, though cells with partially replicated chromosomes are still apparent, containing between 2 and 4 or 4 and 6 genome equivalents. Disruptions to replication fork progression seen in the Δ*malP* single mutant also appear to be ameliorated by delaying initiation upon elimination of *glgP* in either a Δ*malP* or Δ*malP*/Δ*glgX* mutant background. Both Δ*malP*/Δ*glgP* and the triple mutant produce identical replication patterns with large proportions of uninitiated, two origin cells. Bacteria with 4 origins are also present along with those where replication could not be completed, and such cells thus contain between 2 and 4 chromosomes.

Relative DnaA amounts are altered in Δ*malP* mutants during stationary growth. To ascertain whether DnaA levels were altered we performed immunoblots at all three time points. During exponential phase no marked differences were observed between any of the strains (Fig. 2.5c; Supplementary Fig. 11), however, DnaA amounts were elevated in Δ*malP* mutants upon entry into stationary phase with these differences becoming greater by late stationary phase.

Table 2.3. Mean relative cell mass, DNA content and DNA/mass ratios. Mean DNA content, cell mass and DNA/mass of untreated mutant *E. coli* strains, relative to the wild type. Data represent means ± standard deviation calculated from four independent samples surveying ~ 20 000 cells per run.

Strain	Relative DNA content	Relative mass	DNA/mass
Wild type	1.0 ± 0.0	1.0 ± 0.0	1.0 ± 0.0
ΔglgP	1.06 ± 0.1	1.02 ± 0.1	1.04 ± 0.1
ΔglgX	1.06 ± 0.2	1.09 ± 0.1	0.98 ± 0.1
ΔglgP/ΔglgX	1.02 ± 0.3	1.20 ± 0.2	0.85 ± 0.1
ΔmalP	1.77 ± 0.6	1.59 ± 0.3	1.10 ± 0.2
ΔmalP/ΔglgP	1.18 ± 0.1	1.18 ± 0.1	1.00 ± 0.0
ΔmalP/ΔglgX	1.19 ± 0.3	1.29 ± 0.3	0.91 ± 0.1
ΔmalP/ΔglgP/ΔglgX	1.18 ± 0.4	1.34 ± 0.3	0.87 ± 0.1

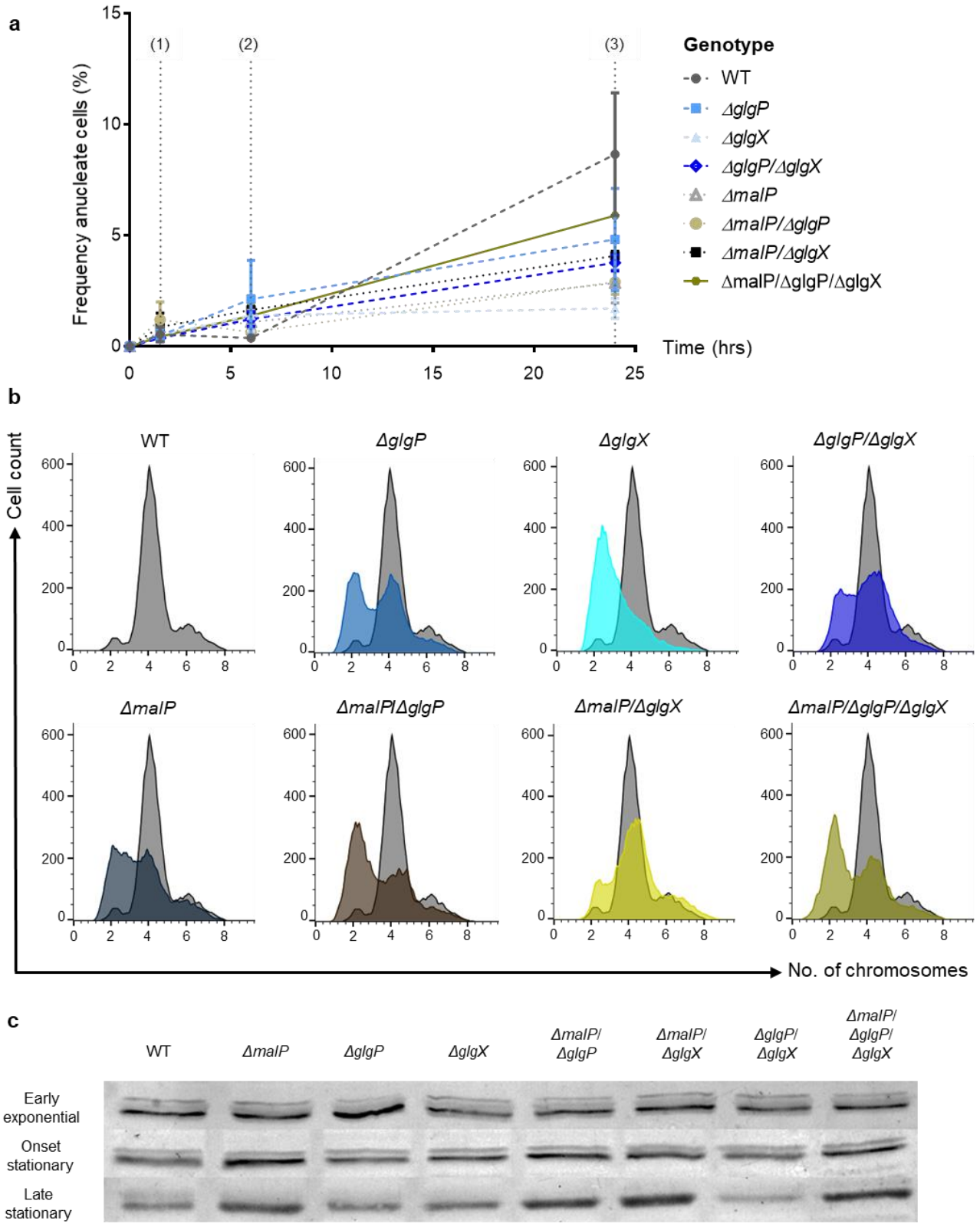

Figure 2.5. Achromosomal cell production, replication patterns and DnaA levels in the strains. (**a**) Confocal pictures of DAPI-stained bacteria were assessed at the three indicated time points to determine the percentage of achromosomal cells. Single data values represent the mean counts from three independent experiments evaluating, in total, ≥ 5 000 cells ± SEM. (**b**) Drug-treated, early logarithmic phase (OD_{450} ~ 0.15) bacteria were stained with Hoechst and analyzed by flow cytometry. Histograms depict the DNA content of such cells and mutant plots are shown superimposed over that of the wild type. The ordinate represents cell count per channel and the abscissa DNA content per cell. Diagrams depict the outcome of a single experiment where ~ 20 000 events were captured. (**c**) Immunoblot examination of relative DnaA levels. Each lane was loaded with 10 µg total protein and separated by 10% (w/v) SDS-PAGE, before being blotted onto nitrocellulose membranes and visualized following probing with an α-DnaA antibody.

DISCUSSION

One of the major carbon stores in bacteria is glycogen and its breakdown is linked to CCM. We decided to examine if glycogen degradation influences bacterial cell size using a set of mutants (Table 2.1) impaired in their ability to degrade this polyglucan. This was due to the observation that, although the cells from all strains grew at the same rate (Fig. 2.1a), the number of culturable cells in strains containing a mutant *malP* allele were reduced during exponential phase (Fig. 2.1b). As fewer culturable cells were present at the same optical density, it is plausible that bacteria were forming non-viable or anucleate cells, or were growing larger without dividing.

All eight strains were grown until late stationary phase, harvested at three time points and cell dimensions and other features were determined from confocal micrographs. During early exponential growth all strains accumulated cells which were longer than those found during stationary phase (Fig. 2.2), and strains with a mutant *malP* allele were noticeably enriched (Fig. 2.2a) in elongated cells (>2 µm) that included a small proportion of filaments longer than 4 µm (Fig. 2.2d). We observed cell walls forming at midcell or one cellular unit away from a cell pole in elongated, early logarithmic MalP-deficient bacteria (Supplementary Fig. 2). No detectable differences in viability (Fig. 2.1c) or anucleate cell formation (Fig. 2.5a) were found between strains at this growth phase, which indicates that the reason Δ*malP* mutants show reduced culturability during early log growth (Fig. 2.1b) is caused by the formation of elongated and filamentous cells.

It is well-known that delaying cell cycle progression alters cell length. For example, arresting initiation of DNA replication[105,177] or delaying the onset of septation[184] have been shown to result in significant increases in cell length whilst width is either unchanged or reduced[107]. On the other hand, disruptions to fatty acid metabolism alter cell size, but changes in length are accompanied by concurrent changes in cell width[106,183]. In our experiments cell width remained largely invariable (Supplementary Table 1) indicating that the observed alteration in cell length is most likely the result of some downstream effect on the cell cycle, rather than fatty acid metabolism.

Mutant Δ*malP* bacteria showed significant heterogeneity and enhanced lengths during early log growth (Figs. 2.2a, d; Supplementary Figs. 2, 7a) without forming fewer Z-rings (Table 2.2), producing less FtsZ (Fig. 2.3b) or dividing less frequently (Fig. 2.1a), suggesting that maternal cells have difficulty integrating signals originating from CCM with cell size and growth rate. Stochastic variability in length likely results from bacteria that are unable to control synchronous progression of cell cycle events[106,107,129] – a situation which has been reported in other CCM mutants[107]. Furthermore, MalP-deficient cells clearly showed nucleoid partitioning defects during logarithmic growth (Figs. 2.3a, 2.4b; Supplementary Fig. 2), which is expected to affect cell division dynamics. Altogether, these observations prompted us to investigate components of the cell cycle.

In filamentous cells, size homeostasis is ensured by employing adder-like mechanisms and the Min system to sense absolute size and direct division rings to form one cell unit away from the

pole, and two from another ring[129]. This allows progeny of even the longest cells to converge at a population average after multiple generations, as was observed in the MalP deficient strains by late stationary phase (Supplementary Fig. 7). The proportion of cells with division plates was determined from micrographs to assess division potential[193] and this appeared essentially identical between strains (Table 2.2).

While several non-dividing rings may be present in a filament (Fig. 2.3a; Table 2.2), only a single instance of division occurs at any given timepoint[129] (Supplementary Fig. 2). Given the lack of alteration in division plate numbers (Table 2.2), it is unsurprising that FtsZ amounts were similar in all strains at all growth stages (Fig. 2.3b). Taken together this demonstrates that the impairment of division is not caused by decreased capacity to form division rings but instead is the result of some mechanism(s) delaying septation.

We observed that elongated early logarithmic MalP-deficient cells contain multiple nucleoids which included masses of genetic material that were poorly separated (Figs. 2.3a, 2.4b; Supplementary Fig. 2). Unsegregated clumps of DNA are also evident in these strains during stationary phase (Supplementary Figs. 4, 6, 9, 10). Increasing DnaA concentrations in *E. coli* has been shown to cause over-initiation and filamentation with replication fork stalling observed under run-out conditions and flow cytometry examination[194], however, we observed no differences in DnaA amounts between strains during early exponential growth when replication patterns and DNA amounts were assessed (Fig. 2.5c). This indicates that alterations in logarithmic phase DnaA amounts do not provide an explanation for the observed fork stalling in our experiments.

We assessed DNA concentrations (DNA/mass) during early logarithmic growth and observed a marginal increase in this value in the Δ*malP* single mutant (Table 2.3), whilst this was somewhat reduced in the Δ*glgP*/Δ*glgX*, Δ*malP*/Δ*glgX* and Δ*malP*/Δ*glgP*/Δ*glgX* strains compared to the other strains. Cell mass values were slightly elevated in Δ*glgP*/Δ*glgX* and all MalP-deficient strains, consistent with the idea that larger cells are produced more often by these strains at this sampling point (Fig. 2.2d; Supplementary Fig. 7a). Fairly elevated DNA amounts were observed in strains with a mutant *malP* allele, though deleting either *glgP* and/or *glgX* alongside *malP* seems to lower both DNA and protein content (Table 2.3).

A possible explanation for this may be found from replication run-out histograms as mutations affecting *glgP* seem to stall replication initiation irrespective of genotype (Fig. 2.5b). Cells from the Δ*malP* single mutant display aborted replication forks and do not resolve into distinct populations containing an integral number of chromosomes (Fig. 2.5b). Double and triple mutants with lesions in *glgP* and *malP* produce similar run-out histograms (Fig. 2.5b). This indicates that mutations in *glgP* delays replication initiation and, therefore, likely reduces replication rates in either a Δ*malP* or Δ*malP*/Δ*glgX* mutant. This helps explain their reduced DNA amounts and DNA/mass ratios, compared to the Δ*malP* single mutant (Table 2.3).

Deleting *glgX* alone delayed replication initiation in the single mutant, while this effect appears masked when it is mutated alongside *glgP* (i.e. Δ*glgP*/Δ*glgX* and Δ*malP*/Δ*glgP*/Δ*glgX* strains). The replication patterns of a double Δ*malP*/Δ*glgX* mutant closely resembles that of the WT. It is possible that disrupting *glgX* in the Δ*malP* single mutant delays replication and affords the cell more time to overcome difficulties with stalled forks replication (Fig. 2.5b) or nucleoid segregation (Figs. 2.3a, 2.4b; Supplementary Fig. 2) and could help explain why DNA amounts are lower in this double mutant than the Δ*malP* single mutant (Table 2.3).

Length increases were not exclusive to cells from strains with a mutated *malP* allele as Δ*glgX* and Δ*glgP*/Δ*glgX* mutants formed greater proportions of longer cells more frequently than the WT at all growth stages (Figs. 2.2a-c). This was particularly evident during stationary phase (Figs. 2.2b, c), and deleting *glgX* also appears to enhance the formation of longer cells by Δ*malP*/Δ*glgX* and the triple mutant compared to the parental Δ*malP* and Δ*malP*/Δ*glgP* strains (Figs. 2.2b, c; Supplementary Figs. 7b, c). While disruptions to DNA replication (Fig. 2.5b) may certainly explain increases in cell length during early exponential growth in the Δ*glgX*, Δ*glgP*/Δ*glgX* and Δ*malP*/Δ*glgX* mutant strains (Fig. 2.2a), it is unclear whether this is the entire picture.

As culturing persists, discrepancies in the proportion of elongated cells produced by mutant strains with a lesion in *glgX* (especially in combination with a mutant *malP* allele) become more pronounced (Figs. 2.2b, c), compared to both the WT and Δ*glgP* single mutant. Since glycogen overaccumulation has been associated with cell size dysregulation upon entry into stationary growth when the pleiotropic *csrA* gene is mutated in *E. coli*[65], we investigated whether our mutant strains were collecting excessive amounts of this biopolymer.

Disruptions to *glgP* and *glgX* are known to cause overaccumulation of glycogen in mutant cells as turnover rates of this polymer are diminished[11,30,74,186]. We could not, however, detect significant differences in glycogen concentration between strains, except between the WT and triple mutant during stationary growth (Fig. 2.4a). This is most likely caused by differences in media composition in our experiment compared with previous ones[186]. Despite the low amounts of glycogen detected during exponential growth (Fig. 2.4a) we were able to visualize glycogen bodies in all strains containing a lesion in *glgX* (Fig. 2.4b). This indicates that small amounts of glycogen remain within these cells upon exiting lag growth[19,73], possibly due to structural changes that are known to increase short chains within this polymer[30,74,186] and which would be expected to delay turnover[74].

It was recently shown that cell-pole granules, termed regrowth-delay bodies, sequester various essential proteins, including FtsZ, and form under standard laboratory conditions in stationary phase cells which are dissolved upon resumption of growth by bacteria during adaptive growth in fresh medium[195]. Such protein deposits aid in growth restart, and if their dissolution is impaired, cells may take on a non-growing persister state. During lag phase, glycogen stores are preferentially degraded for glucose, allowing rapid metabolic adaptation to extracellular carbon

becoming available[19,73]. Both glycogen bodies (Fig. 2.4b) and protein aggregates (Supplementary Fig. 2) coincided spatially with FtsZ in elongated Δ*malP* mutant cells (Fig. 2.3a) during early logarithmic growth.

We show here for the first time that glycogen may collect at inter-nucleoid zones (Fig. 2.4b; Supplementary Fig. 9) and not only at the cell periphery as previously reported[2,6,7]. Glycogen deposits were, furthermore, primarily observed at polar sites in all strains at the onset of stationary phase, whilst most cells harvested during late stationary growth demonstrated a combination of polar and peripheral PAS staining (Supplementary Figs. 9, 10). We noticed protein inclusion bodies from viability micrographs only in strains lacking *glgX* during early logarithmic growth (Supplementary Figs. 1, 2), and their appearance at polar or inter-nucleoid sites seem to mimic the spatial distribution of glycogen bodies (Fig. 2.4b). In *E. coli*, sites of protein aggregation are spatially dictated by nucleoid occlusion[196], where the bacterial nucleoid sets a zone of high macromolecular crowding around itself. Damaged proteins are passively sequestered to these sites[196], effectively restricting protein inclusion bodies to DNA-free regions within the cytosol. These have been extensively tracked using single-cell analysis techniques and may appear under non-stressed conditions at cell poles or midcell or, under stressed conditions, at inter-nucleoid regions of filaments[196,197].

Excess glycogen, like polypeptides, may be passively targeted to sites of low macromolecular crowding, determined by nucleoid occlusion[196], following synthesis at the cell periphery. It appears, therefore, that glycogen is segregated alongside protein inclusion bodies in Δ*glgX* mutants. Based on the observation of similar spatial distribution of protein aggregates, glycogen bodies and FtsZ, it is possible that glycogen degradation may fuel various processes during lag growth[198] such as cell division[96], cell wall remodelling and ATP-dependent protein disaggregation and proteolysis. G1P liberated from glycogen catabolism may also be channelled into UDPG biosynthesis, which is essential for maintaining normal outer membrane morphology[91,92,94] and influences the cell division inhibitory protein, OpgH[93].

Our results provide an insight into how cell lengths are altered in mutants affecting glycogen degradation. DNA replication is clearly affected in the mutant strains. Whether this results from disturbing carbon flux and altering energy levels or the levels of specific metabolites that synchronize cell cycle events is unclear. Disruptions to DNA replication may be the result of currently unidentified protein-protein interactions between enzymes involved in glycogen catabolism or CCM and those involved in controlling certain aspects of the cell cycle. A high-throughput study of protein-protein interactions[199] in *E. coli* revealed that MalP interacts with diverse proteins known to regulate the SOS response[155], DNA damage repair and metabolism. Links between CCM and DNA replication have been shown[171–173] though how MalP helps regulate this fundamental process remains unclear. Phosphorylases produce substantial amounts of G1P during glycogen degradation, which may be fed into CCM after being converted to G6P. Disruptions to CCM and UDPG levels are known to

affect cell size[93,107], so it is tempting to speculate that these may be affected pleiotropically in the mutants in this study and our future work will examine these hypotheses.

MATERIALS AND METHODS

Strains affected in glycogen degradation and growth analysis. All strains (Table 2.1) affected in glycogen metabolism are derivatives of the BW25113[187] and form part of the isogenic Keio collection[188]. They were obtained either from the *E. coli* Genetic Stock Centre (CGSC, Yale University) or were manufactured as described previously[186].

Cells were cultured at 37°C in AB medium[200] supplemented with 10 µg/mL thiamine, 25 µg/mL uridine[201], 0.4% (w/v) glucose and 0.5% (w/v) casamino acids (ABTGCU medium). The slowly growing BW25113 cells, used as a standard for flow cytometry, were cultured in the same minimal medium, except that uridine and casamino acids were omitted (ABTG medium). To achieve balanced growth, cells were grown overnight from a single colony and then diluted 1:1000 into fresh medium. Bacteria were cultured until an OD_{450} ~ 0.2 - 0.4 was reached, at which point cells were back-diluted to an OD_{450} ~ 0.005 into fresh medium. Growth was followed spectrophotometrically at 450 nm at 30-minute intervals for the first three hours of growth and doubling times calculated from OD values using an online tool (http://www.doubling-time.com/compute_more.php). Colony forming units were assessed by serially diluting an aliquot of cells in GTE (50 mM Glucose, 25 mM Tris-HCl (pH 8.0), 10 mM EDTA) and plating 10 µL on LB agar plates. Plates were incubated for 12 hours at 37°C, at which point colonies were counted manually.

Glycogen and protein quantification. Duplicate samples of either 45 mL (logarithmic phase cells) or 2 mL (stationary phase cells) were harvested by centrifugation (20 000 x g, 10 minutes, 4°C) and cell pellets frozen at -80°C until glycogen levels were determined using a previously published method[186].

For determination of total protein, cell pellets were re-suspended in an equal volume of protein extraction buffer (PEB, 17 mM Tris-HCl pH 8.5, 5 mM EDTA, 1 mM phenylmethylsulfonyl fluoride (PMSF) and 2 mM β-mercaptoethanol) and lysed through sonication (10 bursts lasting 15 seconds each, with 1-minute cooling between bursts) at 5 W output). Cell suspensions were clarified by centrifugation (20 000 x g, 10 minutes, 4°C) and total soluble protein quantified[202] using a kit (Bio-Rad Protein Assay Kit) and BSA as a standard.

Immunoblotting. Cells were harvested, washed once in TE buffer (20 mM Tris-HCl pH 7.5, 1 mM EDTA) and re-suspended in PEB, before being lysed by sonication and using soluble protein concentrations determined as described above. Samples containing 10 µg total protein were separated by 10% (w/v) SDS-PAGE and transferred onto a PVDF membrane by semi-dry blotting using standard procedure[203]. Membranes were probed either with α-FtsZ (1:2000 dilution) serum (Agrisera) or α-DnaA (1:1500 dilution) serum followed by goat anti-rabbit secondary antibody,

conjugated to alkaline phosphatase. Immunoblots were developed by incubating in BCIP/NBT solution (Sigma) for 10 minutes before imaging.

A mutant *dnaA46* strain (CM742[189]; Table 2.1), was used as a negative control in the blots assessing DnaA protein amounts. This strain was cultured at 30°C in LB broth until early exponential phase (OD_{600} ~ 0.1 – 0.2) and then shifted to 42°C (non-permissive temperature). Growth continued for 1.5 hours at which point cells were harvested and soluble proteins extracted and quantified as described above.

Flow cytometry. Cells in early exponential phase (OD_{450} ~ 0.1 – 0.2) were either harvested by centrifugation (3 300 x g, 5 minutes, 4°C) or treated with 150 µg/mL of rifampicin (USBiological) and 45 µg/mL of cephalexin (Sigma) for at least 3 hours for replication run-out experiments[204]. Drug-treated cells were collected by centrifugation and both treated and untreated cells re-suspended in ice-cold TE buffer before being fixed by diluting tenfold in 77% (v/v) ice-cold ethanol[205].

Samples were kept at 4°C for at least 12 hours before being pelleted by centrifugation and air dried to remove any residual ethanol[206]. Untreated samples used for ratiometric analyses were washed once in 0.1 M phosphate buffer (pH 9.0) and re-suspended in the same buffer containing fluorescein isothiocyanate (FITC) at a final concentration of 5 µg/mL to stain total cellular protein. After overnight staining[207] at 4°C, cells were washed twice in TBS (20 mM Tris-HCl pH 7.5, 130 mM NaCl) and genetic content stained with 1.5 µg/mL of Hoechst 33258 (Sigma) in the same buffer[208]. Run-out samples were similarly washed in TBS and DNA stained with Hoechst in the same buffer. Hoechst staining proceeded for at least 30 minutes on ice, prior to flow analysis.

Flow cytometry was performed using a BD FACS Aria™ IIu, equipped with a violet (407 nm) and blue (488 nm) laser, and data recorded using BD FACSDIVA™ 8.0.1 software. Hoechst 33258 fluorescence was captured using a 450/40 bandpass filter, whilst FITC fluorescence was collected through a 530/30 bandpass filter. Total protein of an *E. coli* cell may be used as a measure of its mass[209] so average cell mass was taken as median FITC fluorescence, whilst average DNA content per cell was determined as median Hoechst fluorescence. The relative DNA per mass ratio (DNA concentration) was calculated by dividing average DNA content by average cell mass[210]. Data obtained from flow experiments were processed by FlowJo v10.6.1 (©Tree Star, Inc) software.

Membrane and vital staining techniques. An aliquot of cells corresponding to ~ 10^5 CFU/mL were collected at the indicated growth stages by centrifugation (3 300 x g, 5 min, 22°C) and re-suspended in 1 mL 1X PBS (137 mM NaCl, 2.68 mM KCl, 10.1 mM Na_2HPO_4, 1.76 mM KH_2PO_4). Cell envelopes were stained by adding 5 µL of 1 mg/mL FM™ 4-64FX (Thermo Fisher Scientific) and non-viable cells stained with 1 µL of the LIVE/DEAD™ cell dye (Thermo Fisher Scientific). Samples were incubated at room temperature for 5 minutes and then fixed using an established method with slight modifications[211], through the addition of 200 µL ice-cold fixative (16% (v/v) formaldehyde, 0.06% (v/v) glutaraldehyde in 1X PBS). Following incubation at room temperature for 15 minutes with slight

agitation (100 RPM), cells were kept on ice for another 30 minutes before being collected by centrifugation (20 000 x g, 1 minute, 4°C) and washed three times with 1X PBS containing 1 mM EDTA (PBS-E). Bacteria were re-suspended in GTE and stored at 4°C. Mounting and imaging occurred within 48 hours of sample preparation.

Periodic acid-Schiff (PAS) staining. An aliquot of cells corresponding to ~ 10^5 CFU/mL were collected by centrifugation (3 300 x g, 5 min, 22°C) and re-suspended in 1 mL PBS. Cells were fixed essentially as described above, except that glutaraldehyde was omitted from the fixative[212]. Following the third wash step with PBS-E, cells were instead collected and resuspended in 100 µL ice-cold TE buffer and membranes permeabilized by mixing cells with 1 mL ice-cold 77% (v/v) ethanol. Suspensions were kept on ice and periodic acid (Riedel-de Haën) in ddH_2O was added to the samples to a final concentration of 10 mg/mL.

Cells were kept on ice for at least 30 minutes, then harvested by centrifugation and re-suspended in 1 mL PBS-E following two wash steps with the same buffer. Suspensions were kept on ice prior to the dropwise addition of 25 µL Schiff's reagent (Sigma) heated to 90°C. Following three inversions, samples were incubated at room temperature with slight agitation (150 RPM) for 30 minutes. Excess dye was removed by washing the cells three times with PBS-E and bacterial pellets were finally re-suspended in GTE and stored at 4°C. Imaging occurred within 48 hours of staining.

Immunofluorescent labelling of FtsZ. Z-rings were labelled using an established protocol, with minor modifications[213]. Briefly, 15 mL exponentially growing cells (OD_{450} ~ 0.1 – 0.2) were fixed directly[211] by placing the cells in tubes containing 400 µL 1 M $NaPO_4$ pH 7.4, and 3 mL ice-cold fixative (16% (v/v) formaldehyde, 0.06% (v/v) glutaraldehyde in PBS). Fixation was carried out at room temperature for 15 minutes with agitation (100 RPM), after which samples were placed on ice for another 30 minutes. Fixed cells were harvested by centrifugation (4 500 x g, 5 mins, 4°C), washed three times with PBS-E and stored in the same buffer at 4°C. Immunolabelling procedures were carried out within 48 hours of fixation. All subsequent steps were performed in 150 µL volumes and centrifugation steps were at 4 500 x g for 5 mins at 4°C.

Permeabilization was achieved by re-suspending fixed cells in 150 µL PBS containing 0.1% (v/v) Triton X-100 (PBS-T). Bacterial cells were incubated at room temperature for 45 minutes, washed three times with PBS-E and re-suspended in PBS containing 100 µg/mL lysozyme and 5 mM EDTA. Samples were incubated for 45 minutes at room temperature before cells were collected and washed three times in PBS-E.

Cells were incubated in blocking buffer (2% BSA (w/v) in PBS) at 37°C for 30 minutes. They were collected by centrifugation and FtsZ was labelled using α-FtsZ serum (Agrisera) diluted in blocking buffer (1:500). Incubation in primary antibody occurred at 37°C for 1.5 hours with slight agitation (200 RPM). Cells were collected and washed three times in PBS-T, and then incubated in

goat anti-rabbit IgG conjugated to Alexafluor 488 fluorophore (Invitrogen) diluted 1:200 in blocking buffer. Samples were incubated at 37°C for 30 minutes with slight agitation (200 RPM), after which cells were washed three times in PBS-T, washed once in PBS and finally re-suspended in 100 µL GTE. Bacteria were kept at 4°C and were imaged within 24 hours of labelling FtsZ.

Determination of viable and achromosomal cells. The frequencies of viable and achromosomal cells were manually determined using multichannel confocal images which were contrast-corrected and superimposed in ZEN 2. Cells completely devoid of DAPI-associated fluorescence were scored as achromosomal and bacteria were classified as non-viable only if signal from the vital stain was detected throughout the entire cell. Cells showing only polar fluorescent foci were considered viable. The frequencies of cells with Z-rings were manually determined in ZEN 2 from multichannel images and cells were scored positive if they displayed a solid band of fluorescence across the width of the cell, two adjacent fluorescent foci, or a single fluorescent focus, signifying a constricting septum. Live and fixed WT and triple mutant cells (at least 5 000 bacteria measured over a total of three biological repeats) were measured during exponential growth to establish if fixation adversely affected length measurements.

Sample mounting. Approximately 20 µL of cells were air-dried either on agarose pads (1% (w/v) in PBS) or on slides coated with 0.1% (w/v) poly-l-lysine solution (Sigma) and bacterial nucleoids stained by topping cells with a drop of Fluoroshield™ containing 1.5 µg/mL 4',6-diamidino-2-phenylindole (DAPI, Sigma). Cover slips were placed over the samples and kept at room temperature for ~ 30 minutes before cells were imaged.

Confocal image acquisition. Cells were visualized using a Zeiss LSM780 ElyraPS1 confocal microscope equipped with a 100X alpha Plan-Apochromat (N.A. = 1.46) M27 objective (Carl Zeiss). For nucleoid, membrane and viability staining the 405 nm, 488 nm and 561 nm laser lines were used to excite DAPI, FM 4-64FX and the fixable LIVE/DEAD dye, respectively. Glycogen bodies were examined by exciting PAS-stained polysaccharides with a 488 nm laser, which was also used for the excitation of Alexa 488 fluorophores used for Z-ring visualizations.

Emission was detected with a GaAsP detector in the spectral ranges of 415 nm to 498 nm (λ_{em} = 450 nm) for DAPI, 572 nm to 733 nm (λ_{em} = 650 nm) for FM 4-64FX, 498 nm to 555 nm (λ_{em} = 530 nm) for the LIVE/DEAD dye, 570 nm to 695 nm (λ_{em} = 630 nm) for PAS-stained polyglucans and 499 nm to 570 nm (λ_{em} = 535 nm) for Alexa 488-conjugated secondary antibodies. ZEN 2 (Black edition, Zeiss) was used for image capturing, analysis and manipulation.

Image processing for cell size analysis. The individual dimensions of membrane-stained bacteria were determined from confocal pictures. We devised a custom Python script (coliseg) that integrates several open-source Python packages (OpenCV[214] bindings, NumPy[215], Pandas[216] and Matplotlib[217] with seaborn[218]) to permit excellent delineation of cell borders and determination of size, being particularly effective in the analysis of adherent and filamentous cells.

Image pre-processing. In order to convert 1144×1144×3 RGB images to binary ones containing bacterial outlines, they were first converted into 8-bit grey-scale images. Image contrasts were stretched using histogram equalisation and were then convolved with a 3×3 circular Gaussian kernel to decrease the rate of false positive contour detection. We then binarized the images with an intensity threshold T = 8; the contours were set with pixel intensity = 255, the background = 0. The images were convolved with an adaptive threshold in which the threshold value was derived from a weighted sum of the block size (block size = 15) region. Contours were subsequently dilated and then eroded to remove spurious blobs using the same kernel as for the initial Gaussian blurring. Images were then thinned such that contours are reduced to a 1-pixel wide thickness followed by a dilation. The resulting images contain the segmented bacteria.

Contour extraction. In order to extract the bacterial outline from the binary images into a table of lists representing raw contours, we used the function findContours using a two-level hierarchy retrieval mode without chain approximation. We opted for this retrieval mode as it better separated clumped/dividing bacteria; the outer contour is usually the clump itself whereas the inner contours are the actual bacteria.

Since the inner contours are extracted without distinction between agglutinated/isolated bacteria, we can reasonably assume that it does not create a bias. The potential holes were then discriminated on the base of their abnormal shape and surface area. We kept only contours with a ratio convex hull length / contour length greater than .9 and a contour area greater than 110 pixels. We finally modelled the bacteria shape by fitting the contours into rectangles. The length, the width of the fitted rectangle as well as the area of the raw contour were saved into a set of tuples (length, width, area).

Length analysis of whole populations. Since metric parameters of a cell are positively defined, we applied a $\log_{10}$-transformation to the width, length and area. To reduce the complexity, we binned the length of the bacteria with cuts at 1, 2, 4 and 32 µm. Using the counts in each bin, we compared the relative frequency of each bin. We visualised the proportion of long cell in each genotype at different time points using the binned cuts {0, 1, 2, 4, 32}. Finally, we plotted the difference of the bins for each genotype against the WT to better visualise the enrichment in each bin.

Analysis of the fraction of elongated cells. Because the number of elongated cells is small they will have little impact on the mean cell length. Therefore, we counted the number of elongated cells using a threshold length (2 µm) above which we considered a cell as being abnormally long. This threshold is conservative, as many cells are longer, but it improves the stability of the modelling procedure.

We assumed that the proportion of elongated cells in each pair timepoint–genotype is distributed according to a binomial distribution with parameter p = the proportion of elongated cells and N = sample size. We modelled the prior with a beta distribution with alpha = 5 and beta = 40.

Likelihood: $y \sim Binomial(N, p)$

Prior: $p \sim Beta(\alpha, \beta)$

$$\alpha = 5$$

$$\beta = 40$$

We used Stan[219] and its Python interface PyStan to implement the Bayesian inference. We ran 4 independent Markov chains during 4 000 iterations. We estimated the difference of proportion between each pair of genotypes within each time point by subtracting the posterior sample from each element of the pairs. Finally, we summarized the difference of the proportions with heat maps using seaborn[218]. We used the package ArviZ[220] to examine the distribution of the difference in detail.

Statistical analyses. A minimum of three independent replicates were performed for all experiments, unless stated otherwise. Statistical tests performed using both Prism 6 (GraphPad Software) and Statistica 13 (Dell Software). Normality of data was assessed by Shapiro-Wilk tests and homoscedasticity demonstrated using Brown-Forsythe variance tests. Significant differences ($\alpha = 0.05$) between group means were determined by performing a one-way ANOVA with Tukey's post hoc test. A $\log_{10}$-transformation was applied to culturability data prior to performing an analysis of variance to correct for heteroscedasticity and skewness of data.

FUNDING

This work was supported by the Swiss/South African Joint Research Program [grant number 87391] and the National Research Foundation's South African Research Chairs Initiative [Genetic tailoring of biopolymers] as well as by an Innovation Master's Scholarship [UID 114278] to FvdW from the South African National Research Foundation and Department of Science and Technology.

ACKNOWLEDGEMENTS

The authors would like to thank Professor Kirsten Skarstad from the Oslo University Hospital for the kind gift of the DnaA antibody. We would also like to express our gratitude towards Mr Michael Rosmarin for imaging some of the bacterial plates used for viable titre determinations and Mr Gert Grobler for general advice relating to data analytics.

Conflict of interest. None declared

ADDENDUM A

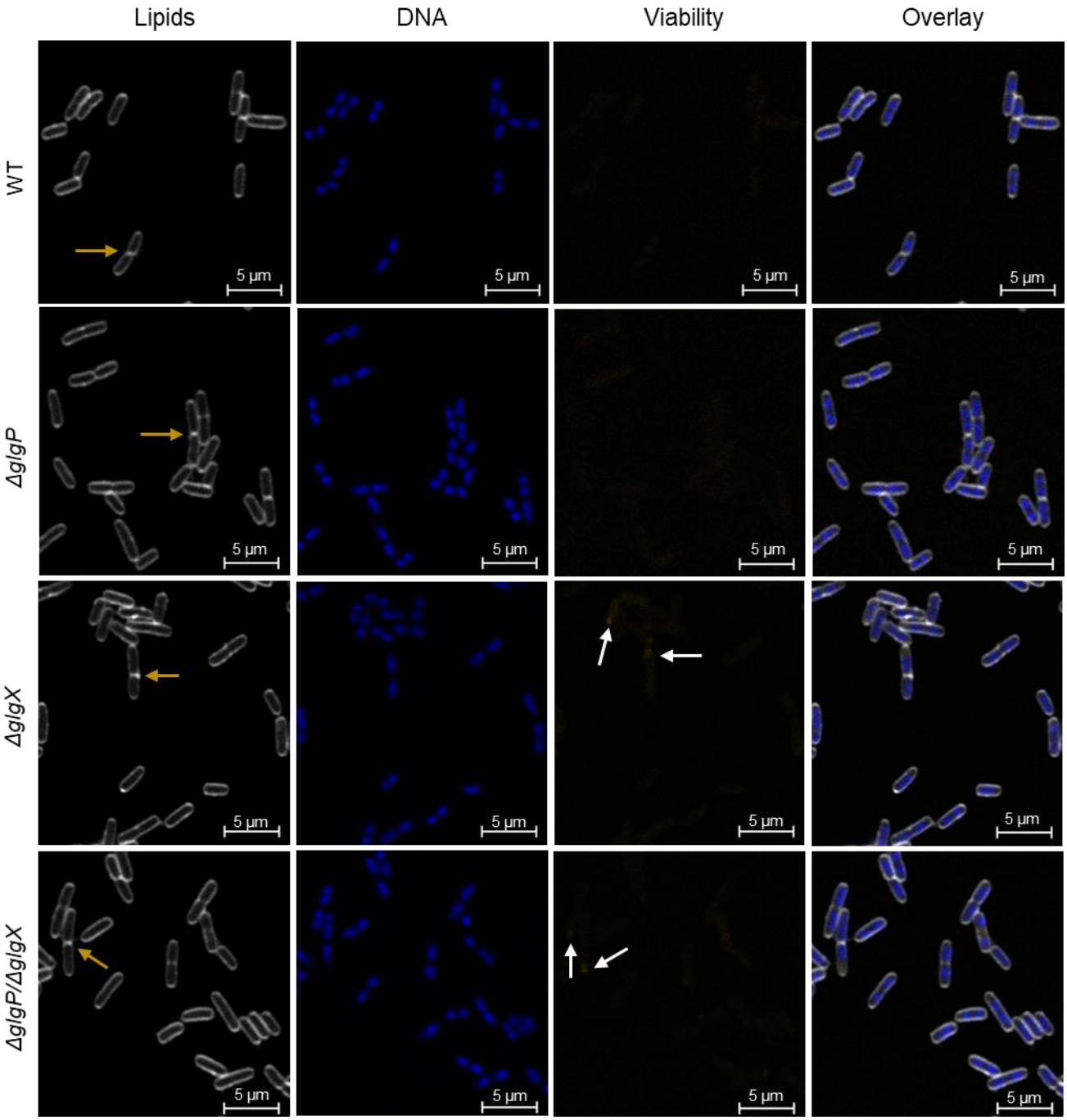

Figure S1. Representative confocal images of *E. coli* cells in early logarithmic phase. Cell membranes, DNA and viability were assessed simultaneously using multi-color fluorescent staining. The cell periphery is shown in white, DNA in blue and proteins tagged by the viability dye are shown in yellow. Golden arrows demarcate dividing cells, with lipids in the new cell wall tagged by the membrane dye. White arrows indicate putative inclusion bodies, highlighted by the amine-reactive viability stain.

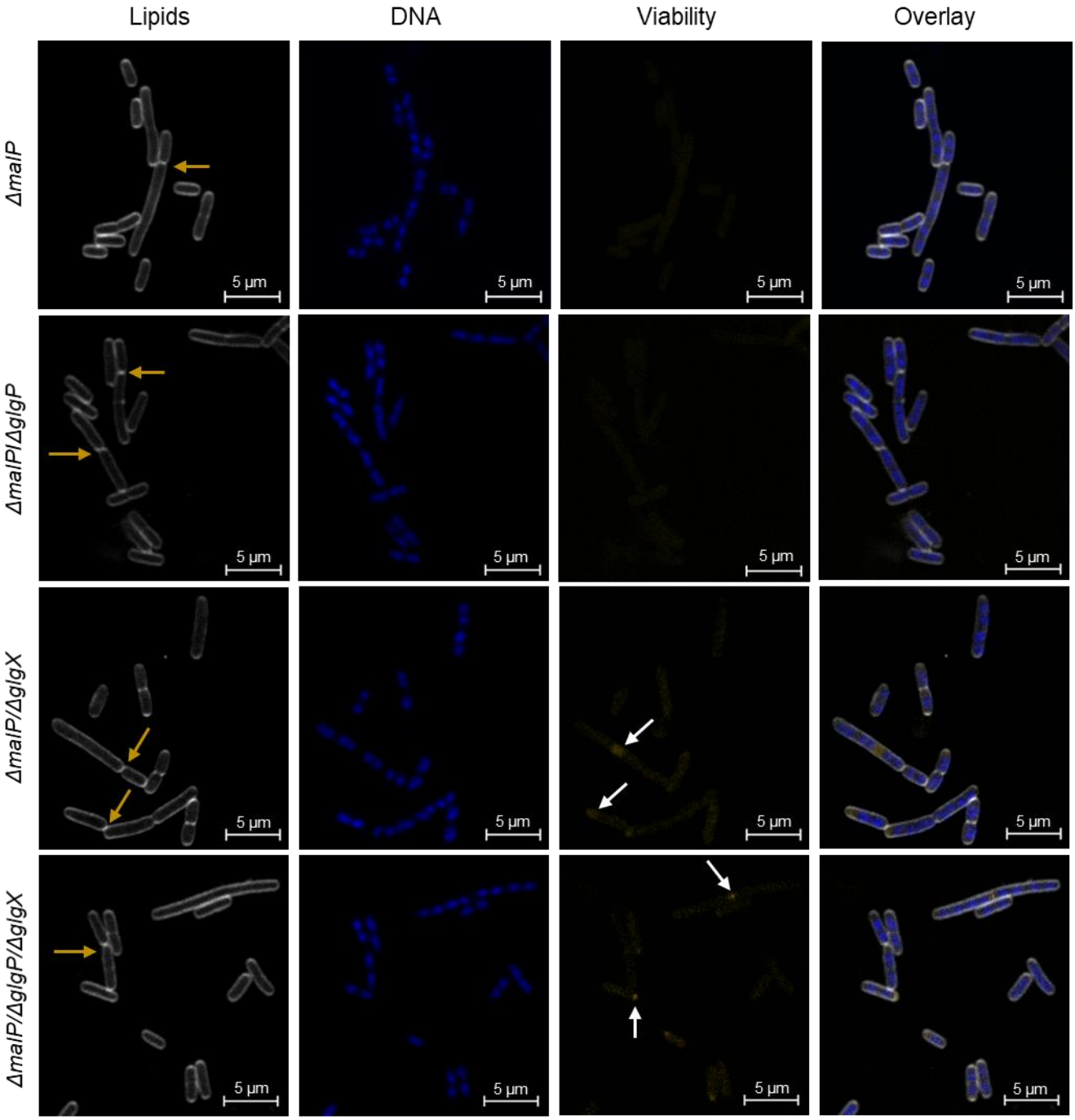

Figure S2. Confocal images of *E. coli* cells in early exponential phase. Lipids, DNA and viability were assessed simultaneously, and golden arrows point to dividing cells with lipids in invaginating septa stained by the lipophilic membrane dye. White arrows indicate protein aggregates, observed upon excitation of the amine-reactive viability stain.

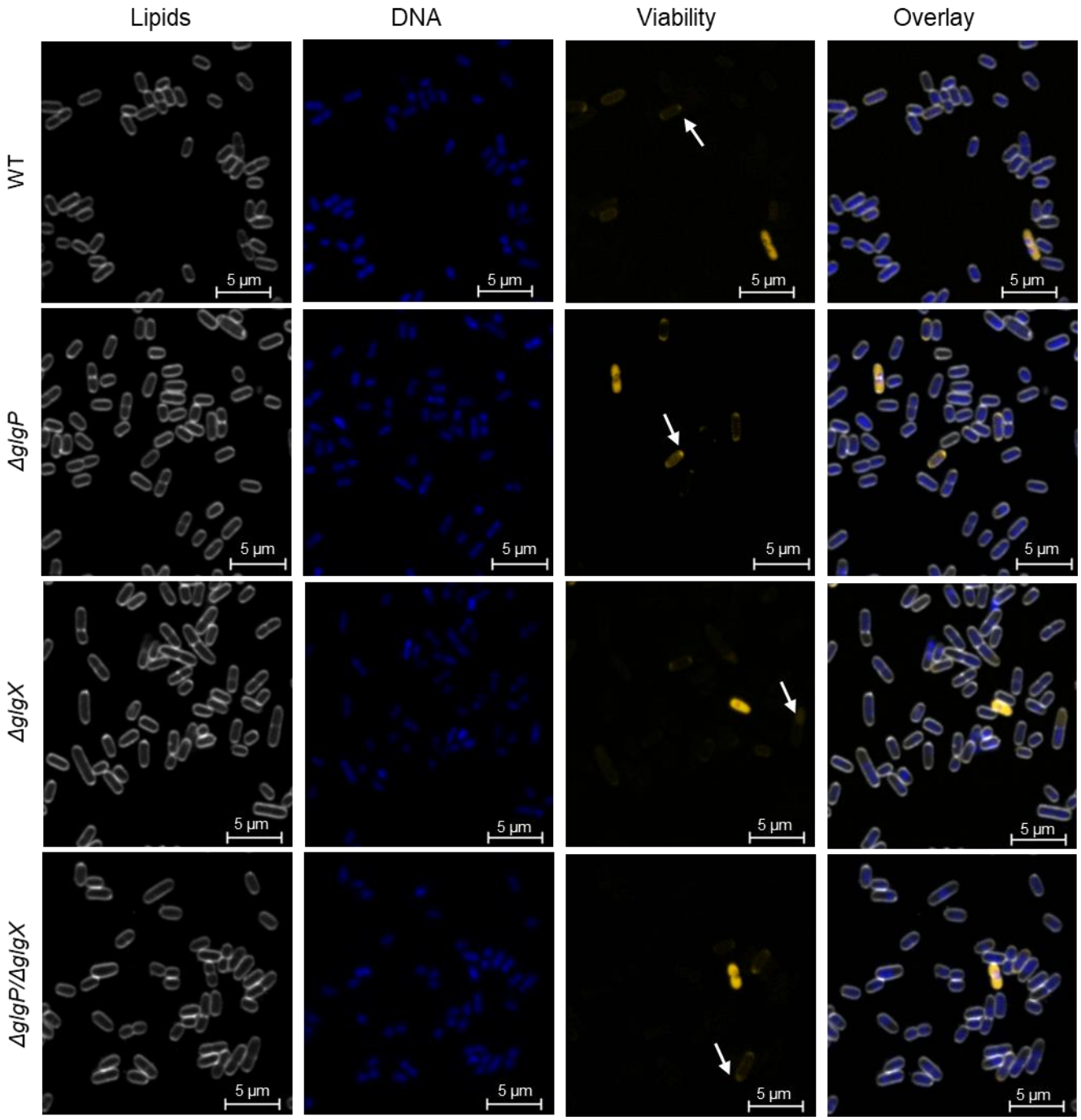

Figure S3. Representative confocal images of *E. coli* cells entering stationary phase. The cell periphery is shown in white, DNA in blue and polypeptides in yellow. Arrows indicate foci which appear to be protein masses, illuminated upon excitation of the viability stain.

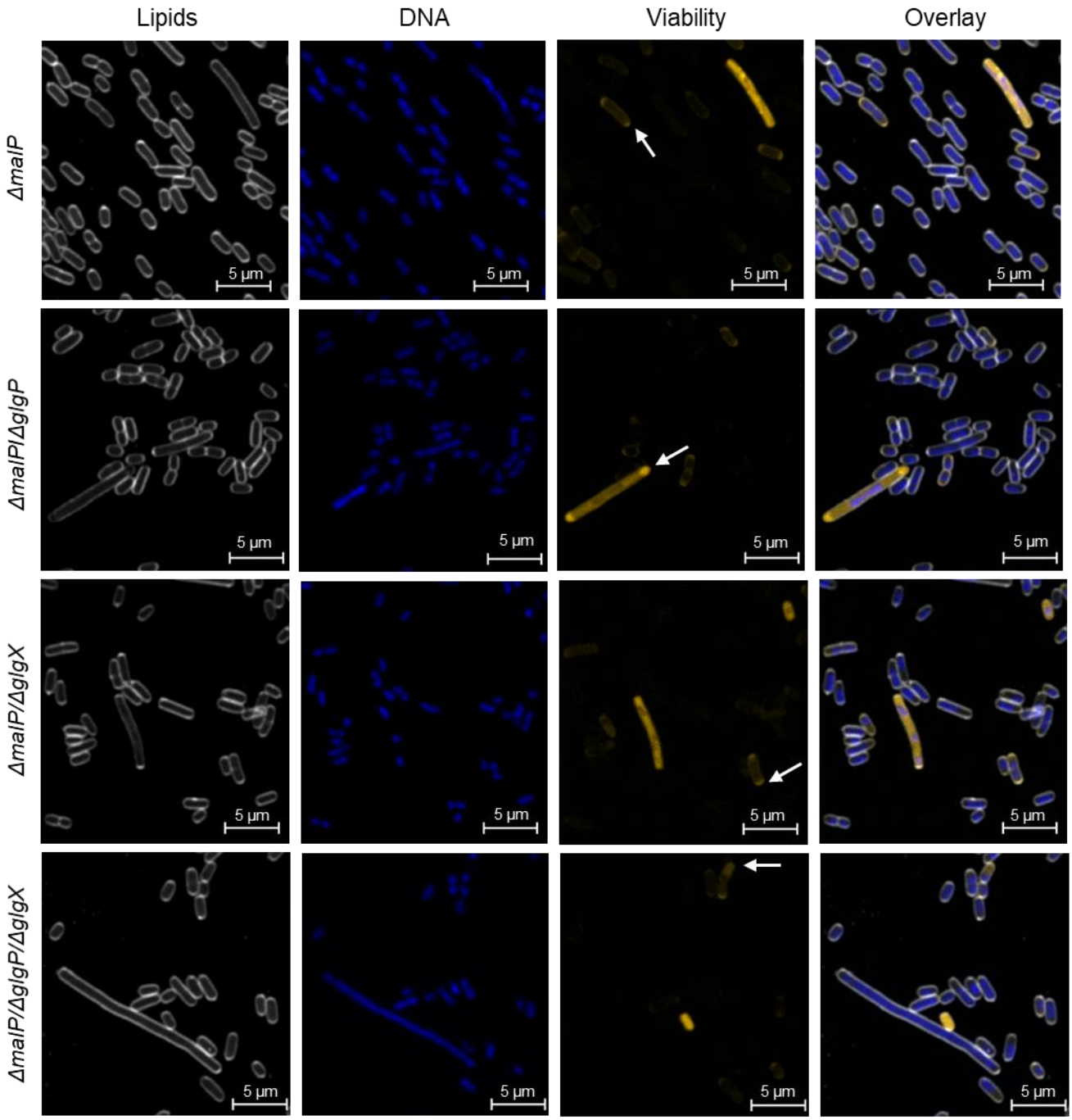

Figure S4. Confocal images of *E. coli* cells entering stationary phase. The cell envelope is shown here in white, genetic material in blue and proteins in yellow. Arrows indicate foci which appear to be protein aggregates, highlighted by the excitation of the amine-reactive viability dye.

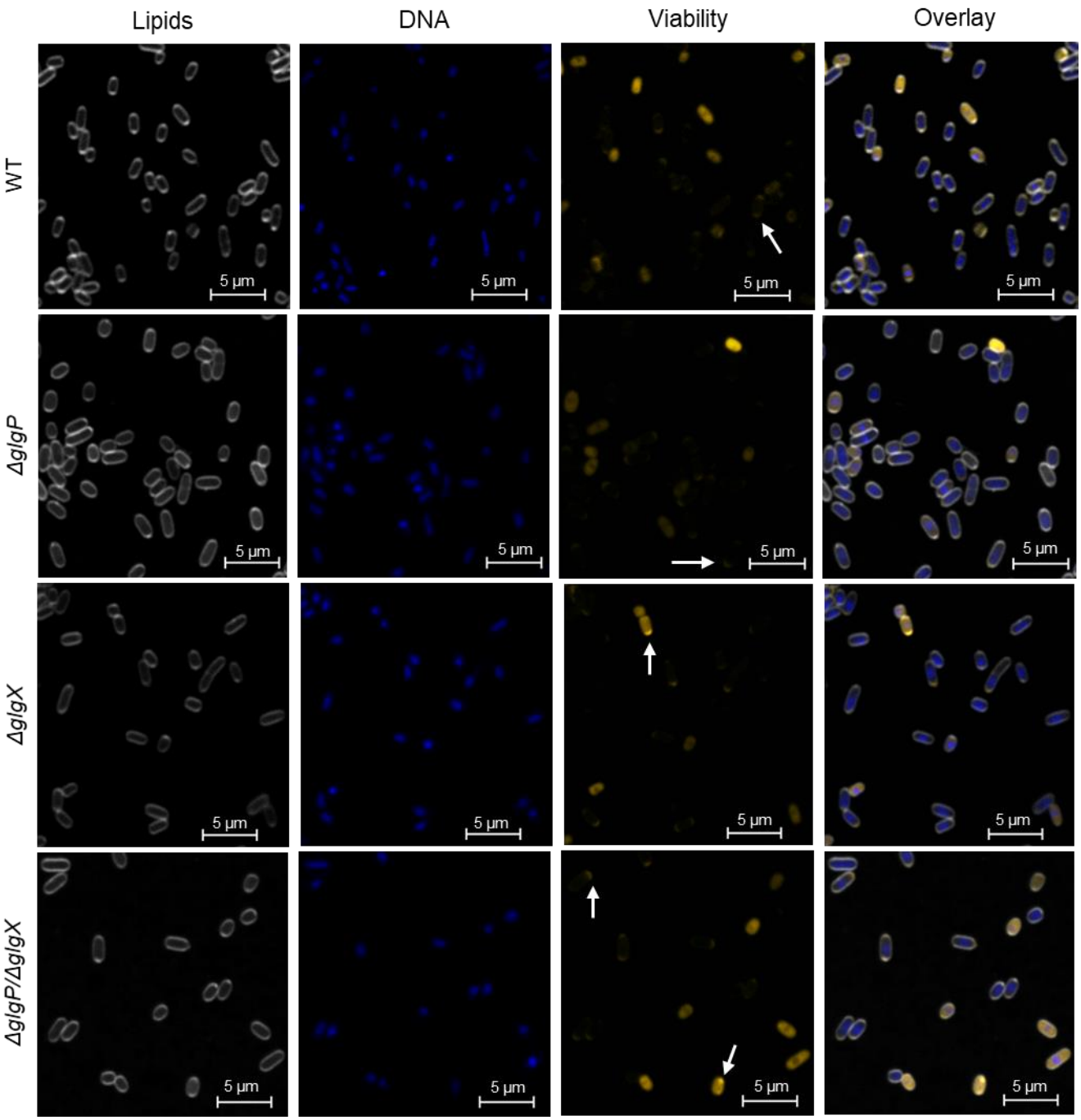

Figure S5. Confocal images of *E. coli* strain in late stationary phase. Lipids are shown in white, nucleoids in blue and polypeptides in yellow. Arrows point to what appears to be inclusion bodies, made visible with the help of the viability dye employed here.

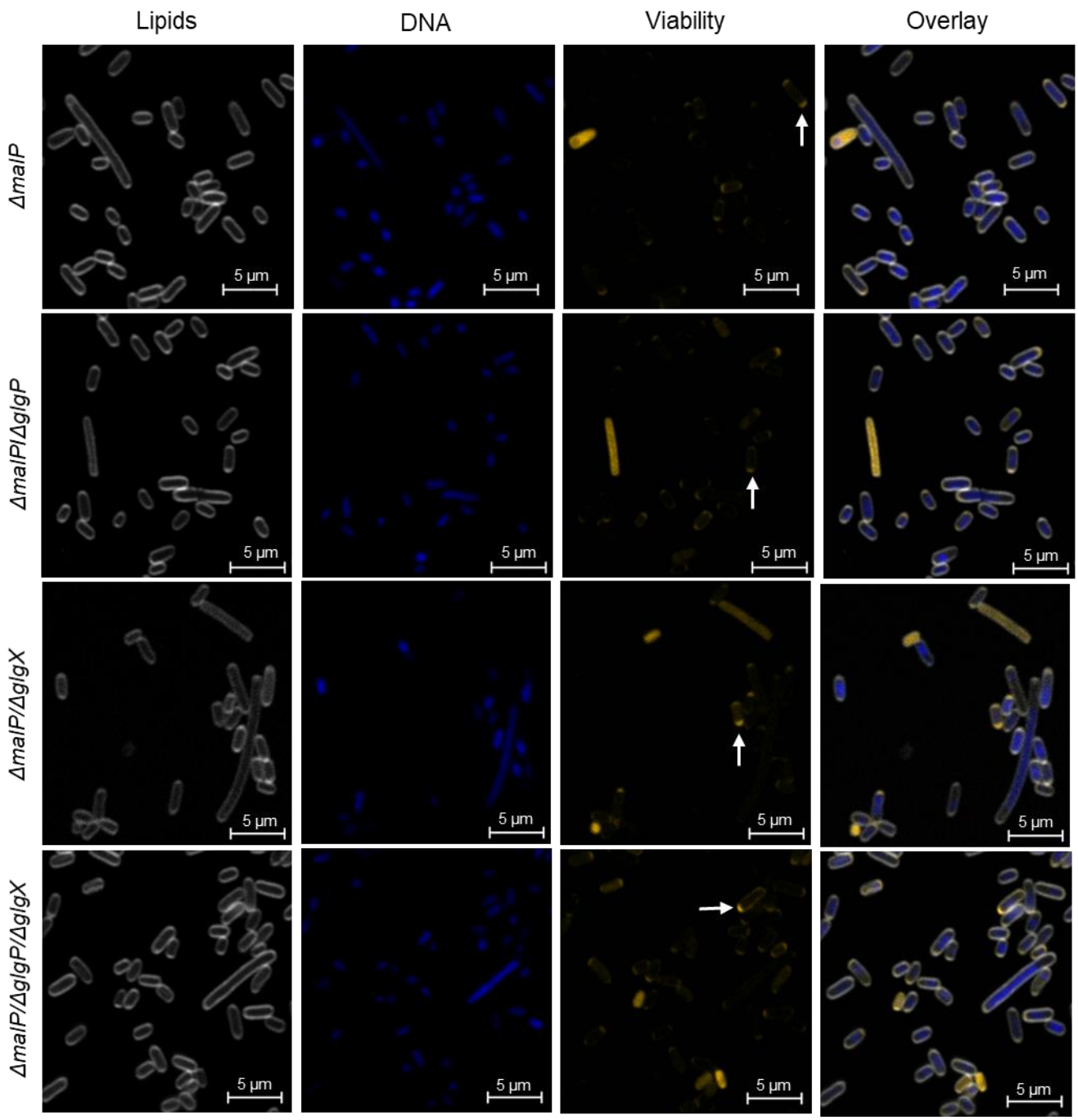

Figure S6. Representative confocal images of *E. coli* strain in late stationary phase. The cell periphery was assessed alongside DNA and proteins, shown here in white, blue and yellow respectively. Arrows point to protein aggregates, highlighted by the amine-reactive dye used to assay viability.

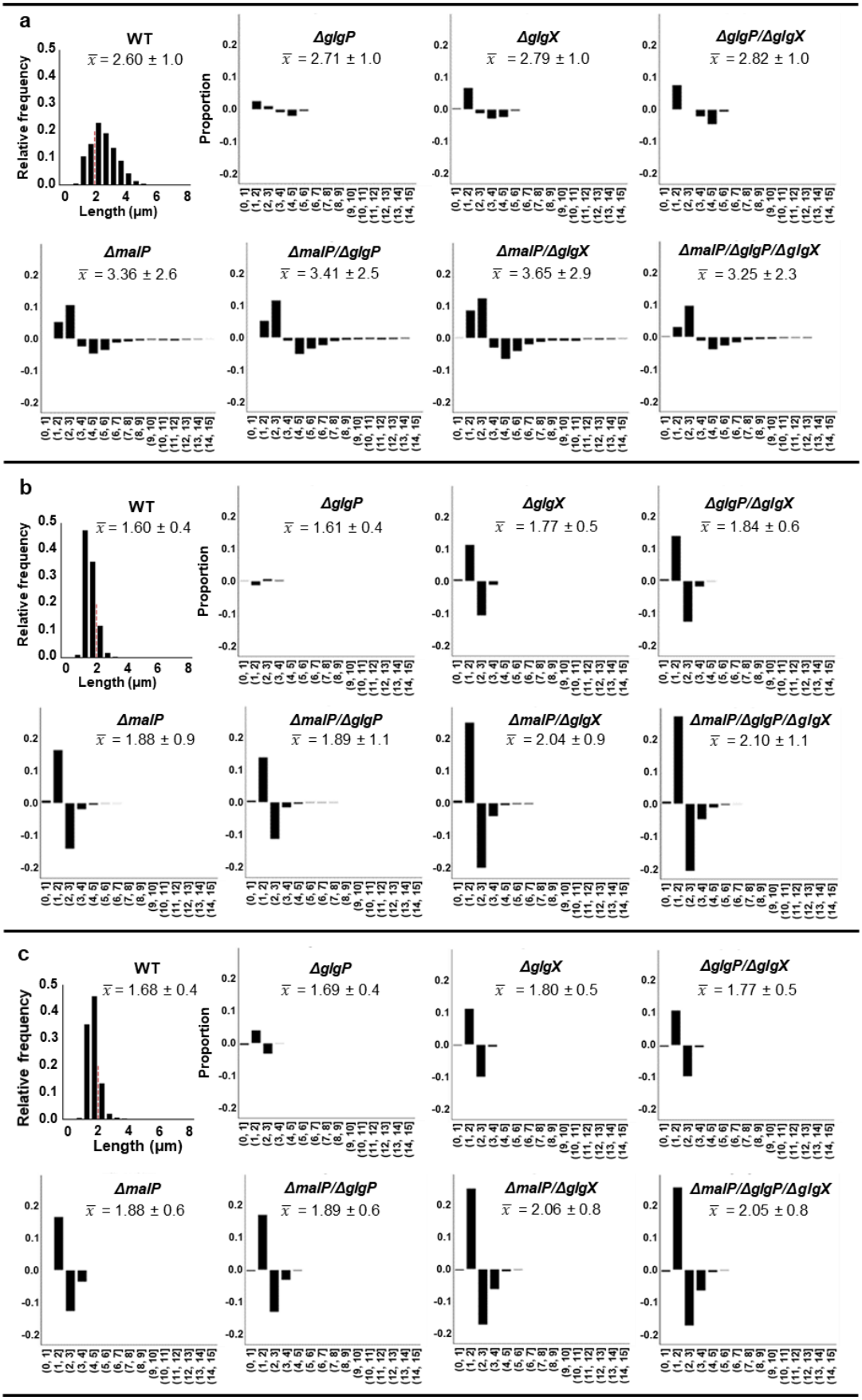

Figure S7. Length analysis of *E. coli* strains. Weighted histograms showing cell lengths during (**a**) early exponential, (**b**) onset stationary and (**c**) late stationary phase are shown for the wild type at the top left corner of each subfigure, with the 2 μm cut-off indicated by a vertical dotted line. Difference plots following these images depict discrepancies in bin counts obtained by plotting length histograms of each mutant against the wild type. Mean cell lengths in μm are displayed as insets above each plot ± standard deviation.

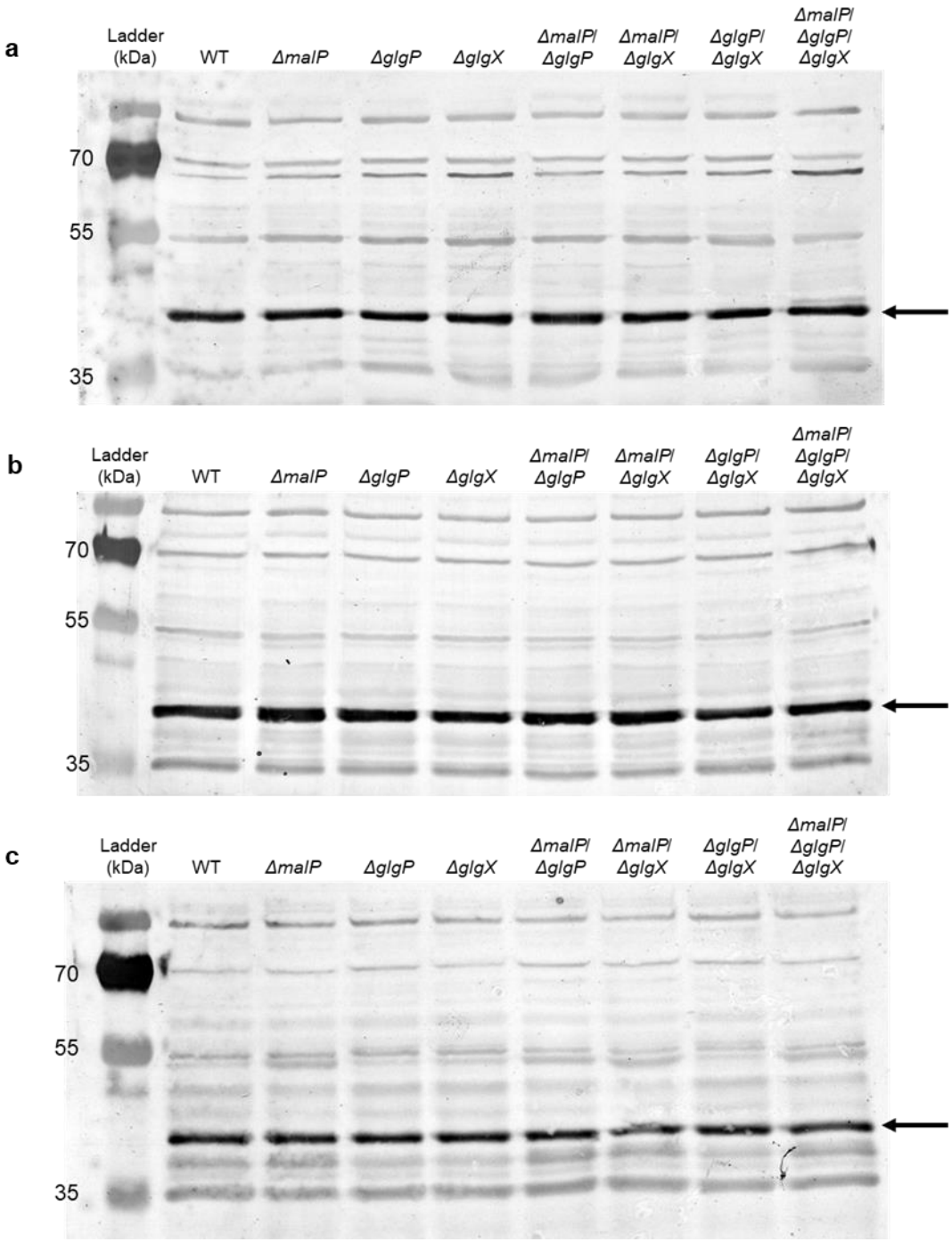

Figure S8. Immunoblot analysis of relative FtsZ levels. Protein extracts were prepared from cells (**a**) growing exponentially, (**b**) approaching stationary phase or (**c**) cultured to late stationary phase. Ten µg total protein was loaded in each lane, separated by 10% (w/v) SDS-PAGE and blotted onto nitrocellulose membranes, before being probed with an α-FtsZ antibody. The arrow indicates the position of FtsZ (~40 kDa) as estimated from the protein ladder (PageRuler Plus, Thermo Fisher Scientific).

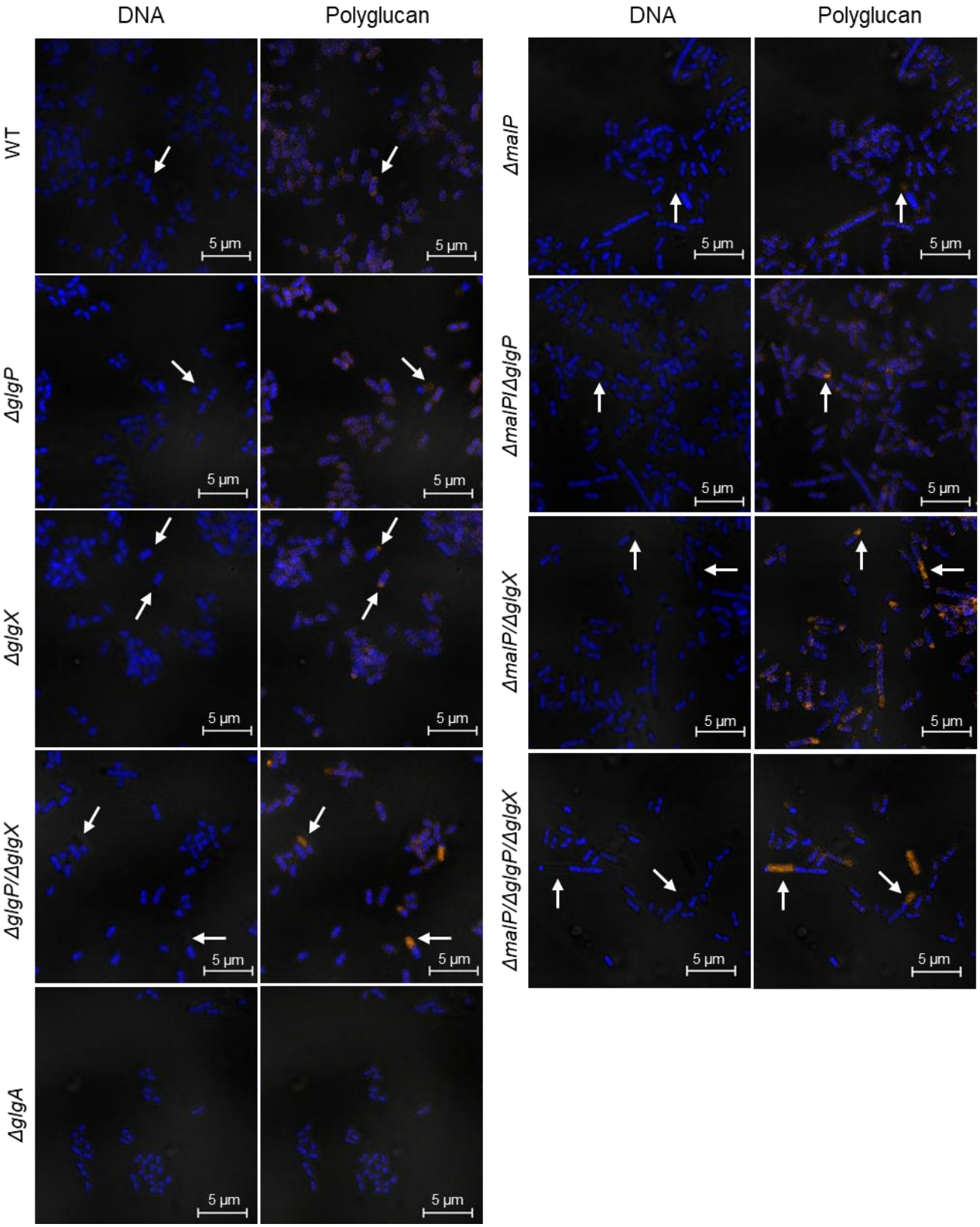

Figure S9. Confocal and phase contrast imagery of PAS-stained *E. coli* cells entering stationary phase. PAS staining procedures were performed as described and polyglucan displayed in orange, while DAPI-stained DNA is shown in blue. White arrows indicate glycogen aggregates.

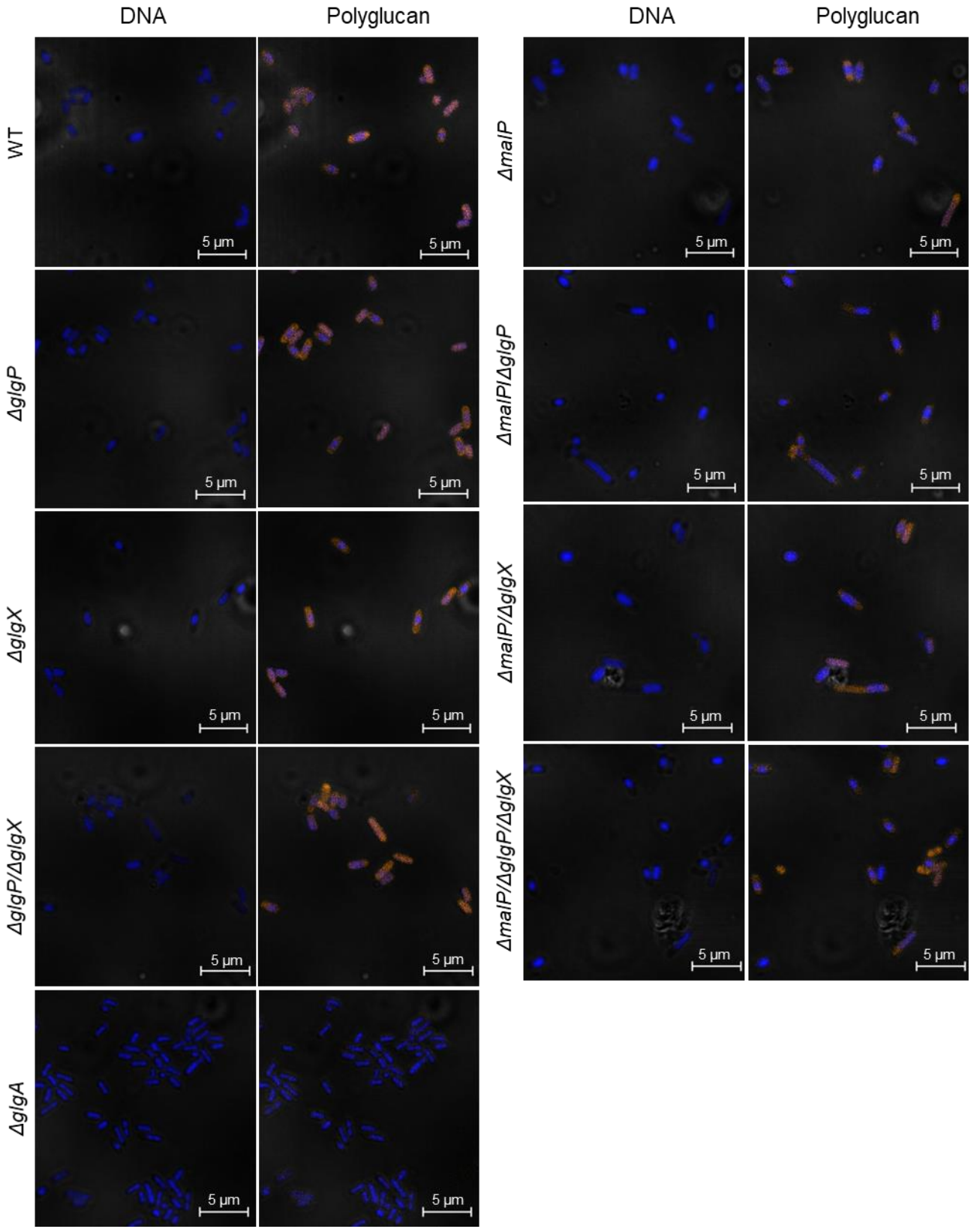

Figure S10. Phase contrast and confocal images of *E. coli* cells in late stationary phase, stained for glycogen. PAS-stained polyglucan is shown in orange and bacterial nucleoids in blue.

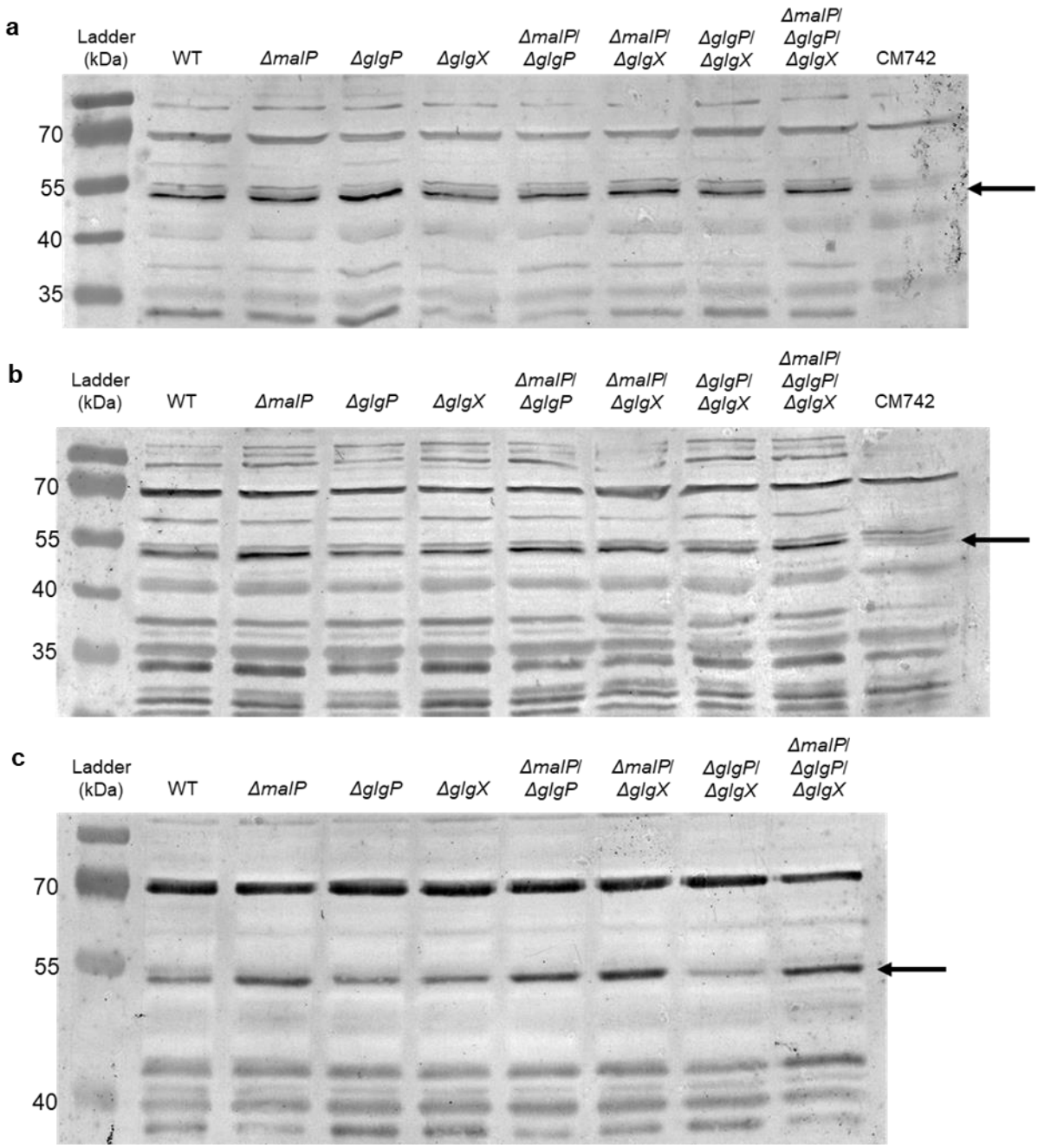

Figure S11. Immunoblot examination of relative DnaA amounts. Soluble protein was extracted from cells (**a**) growing exponentially, (**b**) entering stationary phase or (**c**) grown late into stationary phase. Ten µg total protein was separated by 10% (w/v) SDS-PAGE and blotted onto nitrocellulose membranes, before being probed with an α-DnaA antibody. The arrow points to the position of DnaA (~53 kDa) as estimated from the protein molecular size marker (PageRuler, Thermo Fisher Scientific). An extract containing ten µg of soluble protein from a mutant *dnaA46* strain (CM742), cultured exponentially under non-permissive conditions, was included as a negative control where indicated.

Table S1. Mean cellular widths of the bacterial strains over time. Cell dimensions of at least 5 000 bacteria overall were determined at the indicated growth phases from confocal micrographs across three independent replicates. Values reported are mean cell widths in µm ± standard deviation.

Strain	Early exponential	Onset stationary	Late stationary
Wild type	0.90 ± 0.14	0.78 ± 0.10	0.80 ± 0.12
ΔglgP	0.88 ± 0.15	0.78 ± 0.08	0.86 ± 0.12
ΔglgX	0.87 ± 0.15	0.77 ± 0.09	0.85 ± 0.13
ΔglgP/ΔglgX	0.89 ± 0.16	0.82 ± 0.12	0.86 ± 0.12
ΔmalP	0.88 ± 0.21	0.78 ± 0.12	0.83 ± 0.11
ΔmalP/ΔglgP	0.88 ± 0.20	0.81 ± 0.14	0.83 ± 0.11
ΔmalP/ΔglgX	0.93 ± 0.25	0.80 ± 0.12	0.94 ± 0.14
ΔmalP/ΔglgP/ΔglgX	0.90 ± 0.19	0.83 ± 0.14	0.90 ± 0.12

3. Chapter 3 – Exploration of other genes affecting *Escherichia coli* cell size

INTRODUCTION

It was shown in Chapter 2 that mutant *E. coli* cells lacking MalP activity demonstrate varying phenotypes depending on genetic background. Nucleoids appear poorly segregated in these strains, indicating that they fail to properly partition genetic material at all growth stages. Mutant cells are heterogenous in size and it is evident that they form substantial proportions of elongated and filamentous cells during exponential growth. While the Δ*malP* single mutant and the Δ*malP*/Δ*glgP*/Δ*glgX* triple mutant appear phenotypically similar they differ in two fundamental ways. The triple mutant accumulates significantly more glycogen in liquid LB than a Δ*malP* single mutant during the later stages of growth[186] and *malP* cells show more dramatic problems with DNA replication.

The phenotype observed in Chapter 2 begs the question – how do changes in glycogen metabolism alter cell size? This could be caused by glycogen and protein aggregates blocking cell division; by altered G1P pools somehow disrupting DNA replication and/or cell division (i.e. cell cycle progression) or by presently unknown/uncharacterised signal transduction pathways involving metabolite-protein, protein-protein or protein-DNA interactions.

To examine downstream processes affecting cell size in these mutants, quadruple mutants were created where genes affecting specific processes are mutated alongside *malP*, *glgP* and *glgX* to examine if this reverted the increased cell size observed in this triple mutant. The processes chosen were glycogen synthesis, UDPG generation, aspartate metabolism, nutrient perception, glycolysis, cell division and DNA replication. The reasons for choosing these are that they have been demonstrated to be involved in cell size determination[93,169,178] and/or can be linked through to glycogen metabolism[2,38,57].

ADPG (used by GlgA for glycogen synthesis) and UDPG formation in *E. coli* primarily depend on the provision of G1P (from G6P) by Pgm[57,93,221] (Fig. 3.1). The activity of Pgm is equally indispensable for funnelling glycogen derived G1P into CCM (as G6P), so this enzyme acts at a central node, regulating carbon pools for several pathways of interest[71,75]. Processes linked to the metabolism and consumption of UDPG are known to affect cell morphology and cell cycle progression[93,115]. Disruptions to the *pgm*, *galU* (See Chapter 1 Section 4) and *opgH* (See Chapter 1 Section 7.2) loci of *E. coli* significantly reduce mutant cell sizes under nutrient-rich conditions without markedly affecting growth rates[93]. Changes to size/shape in these mutants may be ascribed to the role UDPG fulfils in cell envelope composition[94] along with

changes to DNA replication (e.g. *pgm* mutant)[115] or cell division (e.g. *opgH* and *pgm* mutants)[93,115] associated with the loss of a specific enzyme's activity.

Amino acid supplies are linked to glycogen metabolism[2] and cell size, especially through the RelA-mediated synthesis of ppGpp in response to amino acids being in short supply[38]. Apart from stimulating glycogen biosynthesis (See Chapter 1 Section 2.2.1), this hyperphosphorylated nucleotide plays a central role in energy conservation during bouts of famine as its accumulation indirectly diminishes cell size[106] (by limiting fatty acid synthesis – See Chapter 1 Sections 7.1 and 7.4). Moreover, it secondarily downregulates various growth-related anabolic processes (like translation and DNA replication[192]) mainly through its inhibitory effect on transcription[38] (See Chapter 1 Section 2.2.1). Availability of the amino acid aspartate specifically impacts cell size and cell cycle progression in *E. coli* through the protein AspC[178]. This polypeptide seemingly affects both replication initiation (by indirectly affecting DnaA levels) and cell division (by somehow impacting UDPG levels and thus the activity of OpgH)[178], promoting faster replication rates and larger cell sizes when nutrients (like aspartate) are plentiful.

Disruptions to the terminal steps of glycolysis and the acetate overflow pathway, specifically where pyruvate and acetyl-CoA are generated/consumed (Fig. 3.1), differentially impact cell morphology and growth in *E. coli*[107,171,172]. Pyruvate may be generated by diverse means[222] (Fig. 3.1) and pyruvate kinase (Pyk) catalyzes the conversion of PEP (and ADP) into pyruvate (and ATP) at the final stages of glycolysis. Two isoforms of pyruvate kinase (Pyk) exist in *E. coli*, PykA and PykF, with the latter enzyme showing dominant Pyk activity when cells are cultured on glucose[223] (Fig. 3.1). Since glycogen-derived G1P is expected to be channelled into glycolysis (as G6P), the effect of knocking out *pyk* genes on cell size was investigated as this is expected to alter intracellular PEP/pyruvate ratios[179] (and indirectly impact acetyl-CoA pools - See Chapter 1 Section 7.1), the activity[169,171] of the PDH^c (and possibly DNA replication rates - See Chapter 1 Section 7.3) and sugar transport via the PTS[179,224] (See Chapter 1 Section 2.1).

To unravel the nature of the division block apparent in the triple mutant, the *minC* and *sulA* genes were eliminated in this strain as their protein products fulfil important roles either in dictating the spatial organization of Z-rings (See Chapter 1 Section 6.2.1) or coordinating DNA damage repair with division as part of the SOS response (See Chapter 1 Section 6.3), respectively. Oscillation of the Min system is energy-dependent[225], so the possibility that glycogen turnover could fuel this system was also considered.

The accessory protein, DiaA, forms a stable complex with DnaA at the replication origin and stimulates melting of *oriC* by ATP-DnaA. Though not essential, it is required for timely

triggering of replication initiation and *diaA* mutants delay origin firing and initiate replication asynchronously[135]. The bacterial nucleoid consists of genetic material associated with up to ten different nucleoid associated proteins (NAPs) and some NAPs, like the heterodimer HU that consists of HupA and HupB, not only fulfil a structural role, but also participate in processes like DNA replication, recombination and transcription[84,85,226].

HupA and HupB exist as homodimers during specific developmental stages in *E. coli* and HupA appears to play a more dominant role in replication initiation[227] than either HupB or HU. This is typified by the observation that deleting *hupB* on its own does not impact growth or DNA replication in *E. coli*, whilst mutant Δ*hupA* cells trigger origin firing asynchronously and grow slightly slower than the wild type[85]. Protein-protein interactions between MalP and both HupA and HupB have been reported; the *malPQ* operon is regulated by HU, though the reason(s) for such an interaction are currently obscure.

In this chapter, several lines of evidence are presented further corroborating the proposed link between DNA replication and glycogen turnover. Additional insight is provided into the nature of the division block underlying the filamentation and cell elongation seen in MalP-deficient strains studied in Chapter 2.

Table 3.1. Summary of genes whose involvement are investigated in the size defects of the triple mutant. Gene products are involved in processes that include glycogen biosynthesis, UDPG metabolism, cell division, glycolysis, nutrient sensing, aspartate metabolism and DNA replication.

Gene	Protein	Function(s)	Process(es)
glgA	glycogen synthase	Uses ADPG as substrate for glucose-dependent glycogen biosynthesis[26]	Glycogen biosynthesis
pgm	phosphoglucomutase	Interconverts G1P and G6P[24]. Central to glycogen (via ADPG) and UDPG biosyntheses[167]; affects cell cycle and size/shape[93,115]	Glycogen biosynthesis; UDPG synthesis
galU	UTP: glucose 1-phosphate uridylyltransferase	Forms UDPG from G1P[91,92]; affects cell cycle and size[93]	UDPG synthesis
opgH	glucans biosynthesis glucosyltransferase H	Synthesises osmoregulated periplasmic glucans (OPGs)[228]; UDPG-dependent division inhibitor[93]	Cell division
relA	GTP pyrophosphokinase	Synthesises ppGpp in response to amino acid starvation[40,161]; master regulator of glycogen biosynthesis in response to nitrogen limitation	Glycogen biosynthesis; Stringent response
aspC	aspartate aminotransferase	Interconverts aspartate and OAA[222]; aspartate-mediated regulator of cell cycle progression[178]	Aspartate metabolism; Cell cycle regulation
pykF	pyruvate kinase I	Major Pyk isoform that catalyses conversion of PEP to pyruvate in the terminal step of glycolysis[223]	Glycolysis
pykA	pyruvate kinase II	Minor Pyk isoform that catalyses conversion of PEP to pyruvate in the terminal step of glycolysis[223]	Glycolysis
minC	septum site-determining protein	Main effector of Min system that disassembles FtsZ polymers upon binding membrane-bound MinD at the cell poles[148]	Cell division
sulA	cell division inhibitor	SOS-related global division inhibitor preventing FtsZ polymerization in response to stress (usually DNA damage)[155]	Cell division
diaA	DnaA initiator-associating protein	Binds DnaA ensuring timely initiation of DNA replication[135]	DNA replication
hupA	histone-like DNA binding protein HUα	Nucleoid-associated architectural protein[229]; HU stimulates DnaA-mediated unwinding of *oriC*[230]	DNA replication
hupB	histone-like DNA binding protein HUβ	Nucleoid-associated architectural protein[229]; HU stimulates DnaA-mediated unwinding of *oriC*[230]	DNA replication

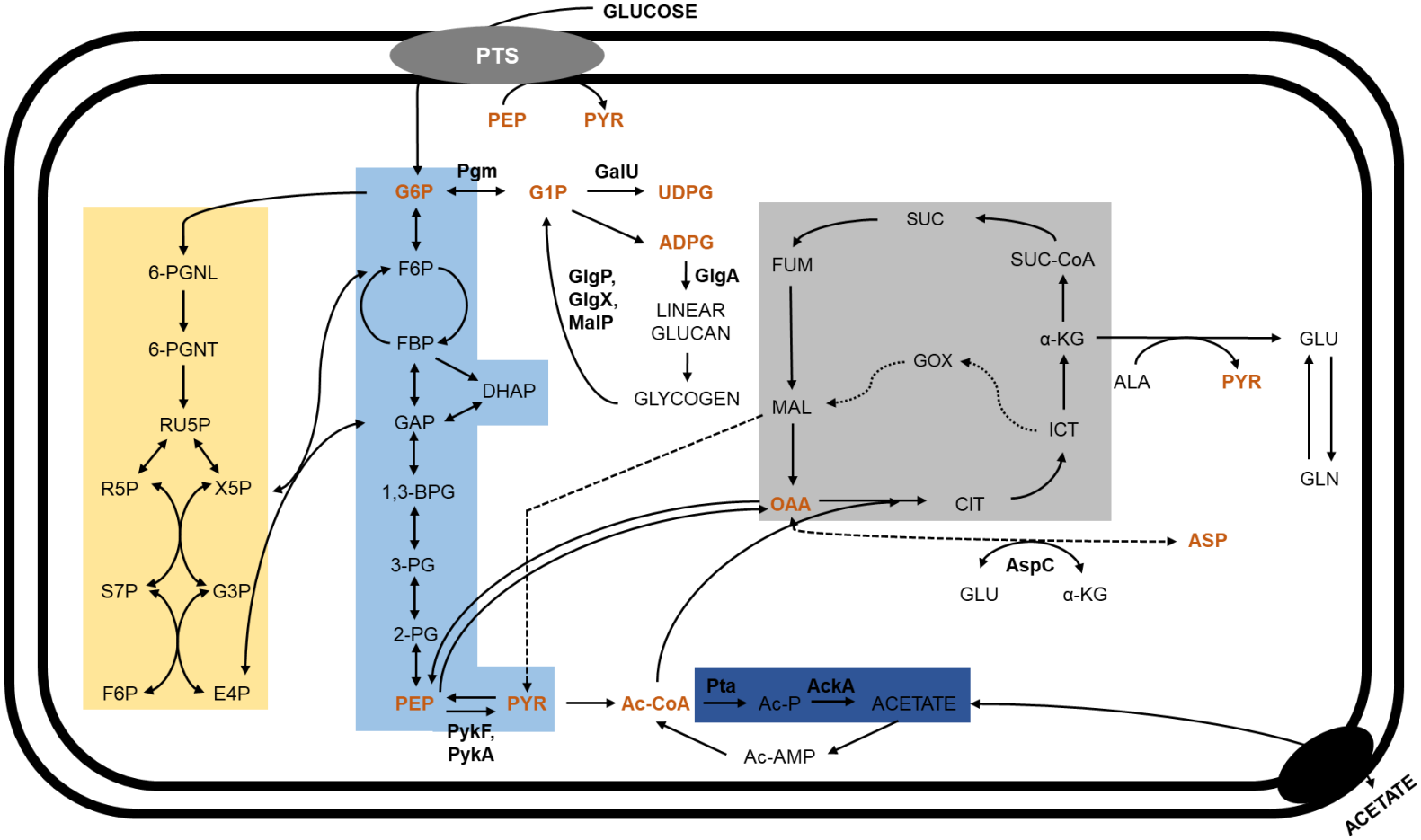

Figure 3.1. Central carbon metabolism and the roles fulfilled by key enzymes examined in this study. This cell is shown growing on glucose where rapid flux through glycolysis involves acetate excretion as part of the overflow pathway. The enzymes highlighted in this diagram (**bold**) include **Pgm**, phosphoglucomutase; **GalU**, UTP: glucose 1-phosphate uridylyltransferase; **GlgA**, glycogen synthase; **MalP**, maltodextrin phosphorylase; **GlgP**, glycogen phosphorylase; **GlgX**, glycogen debranching enzyme**; PykF**, major pyruvate kinase isoform; **PykA**, minor pyruvate kinase isoform; **Pta**, phosphate acetyltransferase; **AckA**, acetate kinase; **AspC**, aspartate aminotransferase. Metabolites of interest (gold) include **PEP**, phosphoenolpyruvate; **PYR**, pyruvate; **G6P**, glucose 6-phosphate; **G1P**, glucose 1-phosphate; **UDPG**, uridine diphosphate glucose; **ADPG**, adenosine diphosphate glucose; **ASP**, aspartate; **OAA**, oxaloacetate; **Ac-CoA**, acetyl coenzyme A. The pentose phosphate pathway is tinted in orange, the citric acid cycle in grey, whilst glycolysis/gluconeogenesis and acetate overflow are emphasized in light and dark blue respectively (adapted from Kumar and Shimizu, 2010, Maciąg et al., 2012 and Westfall and Levin, 2018).

RESULTS

Production of mutant *E. coli* strains

Manipulations to bacterial genomes were orchestrated using single-gene insertion mutants available from the Keio collection[187,188] along with Flp-FRT recombination[231] to remove antibiotic resistance cassettes. A list of strains manufactured throughout the course of this study is supplied (Supplementary Table 1), along with primer sequences used for genotyping (Supplementary Table 2). More than 50 new bacterial strains were manufactured, including single deletion mutants derived from Keio strains (~15 strains) and new genetic variants created by phage transduction[232] (~43 strains). For the sake of brevity, PCR screens are provided only for those mutants used/analysed in this section (Supplementary Figs. 1-6) along with a list of amplicon sizes expected when screening wild type or mutant alleles (Supplementary Table 3). The physical distance (kb) between *glg* genes is very short[20]. The *glgX*, *glgA* and *glgP* gene loci are thus tightly linked, complicating genetic disruption by phage transduction[232]. Because of this, it was decided to create and analyse a Δ*glgA*/Δ*malP* double mutant instead.

Mutants accumulate varying amounts of glycogen

To semi-quantitatively compare polyglucan content in the different strains, overnight liquid cultures were spotted onto solid LB plates supplemented with glucose, incubated overnight and then stained with iodine vapour[233]. The intensity of mutant colony staining was examined relative to the wild type, which stained reddish-brown (Figure 3.2; Table 3.2). Those mutants showing a glycogen-deficient phenotype stain lighter than the wild type; a glycogen-excess phenotype manifests as colonies that stain darker than the wild type[233], whilst glycogen-less colonies appear yellow upon exposure to iodine vapor[10,51].

Consistent with previous observations, the Δ*malP*/Δ*glgP*/Δ*glgX* triple mutant displayed a glycogen-excess phenotype when grown on solid LB supplemented with glucose, and stained markedly darker than the wild type[186] (Figure 3.2). Quadruple mutants lacking *galU*, *relA*, *aspC* or *minC* appeared to accumulate wild type glycogen levels (Figure 3.2). As expected, mutating *glgA* or *pgm* caused a glycogen-less phenotype[51,57]. The quintuple mutant (Δ*pykF*/Δ*pykA*/Δ*malP*/Δ*glgP*/Δ*glgX*) appeared to accumulate more glycogen than the triple mutant and stained darker black than its parental strain. Colonies of the other quadruple mutants (with a deletion to *sulA*, *opgH*, *pykF*, *pykA*, *diaA*, *hupA* or *hupB*) were all comparable to the triple mutant.

Figure 3.2. Staining of bacterial colonies to assess glycogen accumulation. Overnight cultures of the indicated strains were spotted onto LB plates supplemented with 1% w/v glucose and incubated for 15 hours, before being exposed to iodine vapours for polyglucan staining.

Pathways involved in glycogen and UDPG biosynthesis differentially impact the size and DNA defects of Δ*malP* and triple mutant cells

Bacteria were stained for lipids and DNA using the fluorescent dyes FM4-64 and DAPI, respectively. Protein was visualised using FITC, which enters cells without discrimination (unlike the viability dye employed under Chapter 2) and is known to covalently bind all intracellular protein[209]. Consequently, the entire cell interior is stained and occasionally seems to gather into punctate polar foci, likely representing polypeptide aggregates (Figs. 3.4, 3.5, 3.7; Table 3.2).

Deleting *glgA* in a Δ*malP* mutant background appeared to completely restore cell size to normal, but bacteria showed altered nucleoid staining patterns, evidenced by normal-sized cells containing poorly separated DNA or elongated stretches of relaxed genetic material (Fig. 3.3). Disrupting UDPG metabolism or utilization (i.e. quadruple mutants with a lesion in *pgm*, *galU* or *opgH*) impacted cell morphology to varying degrees (Fig. 3.3). Triple mutant cells with a mutated *pgm* allele formed small, rounded cells that vary morphologically and showed defects with DNA partitioning. A lesion in *galU* seemed to partially suppress the cell size defects of the triple mutant, as bacteria showed less heterogeneity in size and formed fewer filaments. Mutant Δ*galU*/Δ*malP*/Δ*glgP*/Δ*glgX* cells appeared to take on a more rounded

appearance, and still displayed chromosome partitioning hindrances (Fig. 3.3). Elimination of *opgH* in the triple mutant appeared to fully suppress its size defects, though nuclear staining still revealed some aberrant DNA partitioning occurring in mutant bacteria.

Amino acid metabolism affects cell size of the triple mutant

Reducing the ability of the triple mutant to form ppGpp by disrupting *relA* seemed to partially suppress the growth defects of the triple mutant (Fig. 3.4). However, cell shapes appeared highly heterogenous as some bacteria were thinned and others widened. Altered shapes of Δ*relA*/Δ*malP*/Δ*glgP*/Δ*glgX* mutant cells apparently accommodated genetic material that showed equally dramatic morphological heterogeneity. A partial suppression to the size defects of the triple mutant was evident when its ability to metabolise aspartate was affected through mutation of *aspC*. Fewer elongated bacteria were formed by Δ*aspC*/Δ*malP*/Δ*glgP*/Δ*glgX* mutant cells, but they still exhibited difficulties with DNA segregation (Fig. 3.4).

Disruptions to Pyk genes reveal putative links between glycolysis and cell size control

Deleting either (or both) genes encoding the two isoforms of Pyk in *E. coli* appeared to restore cell size of the triple mutant to normal (Fig. 3.5; Table 3.2). Both the quadruple and quintuple mutants of glycolysis with a lesion in *pykF* (i.e. Δ*pykF*/Δ*malP*/Δ*glgP*/Δ*glgX* and Δ*pykF*/Δ*pykA*/Δ*malP*/Δ*glgP*/Δ*glgX*) formed cells that were similar in size to the wild type. However, such mutant bacteria seemed to contain less DNA than wild type cells (Fig. 3.5). Wild type bacteria contained nucleoids that appeared as four fluorescent masses, whereas the quadruple and quintuple Δ*pykF* mutant strains mostly appeared with only two DNA masses. Hindrances with chromosome partitioning were still apparent in these two strains as cells occasionally contained unsegregated clumps of genetic material or elongated masses of DNA (Fig. 3.5). Curiously, Δ*pykA*/Δ*malP*/Δ*glgP*/Δ*glgX* mutant bacteria appeared rod-shaped but seemingly smaller than wild type cells. These diminutive mutants did not show signs of nuclear segregation defects but seemed to contain substantially less DNA than wild type cells as most of these mutant bacteria contained only two small nucleoid masses (Fig. 3.5).

Table 3.2. Phenotypic observations of wild type and mutant *E. coli* strains. Glycogen accumulation was assessed by exposing bacterial colonies to iodine vapor (Fig. 3.2). Interpretations of glycogen contents were made relative to the wild type which was considered to accumulate 'normal' glycogen amounts. Suppressions to size and DNA portioning defects of MalP deficient mutants is noted based on objective interpretation of at least four confocal images (~200 cells) per strain. Primary findings regarding cell morphology, nuclear and protein staining patterns are summarized.

Strain	Glycogen accumulation	Suppression of size defects	Cell morphology (FM4-64)	Nuclear staining pattern (DAPI)	Protein foci (FITC)
BW25113 (Wild type)	Normal	-	Normal, rod-shaped	Well separated nucleoids that appear either as two or four masses	-
ΔmalP/ΔglgP/ΔglgX(kan)	Glycogen excess	-	Elongated and filamentous cells; substantial heterogeneity in length	Normal sized cells contain separated nucleoids that appear as two or four masses; elongated cells and filaments show significant partitioning defects as DNA is found along the length of the cell	Yes
ΔglgA/ΔmalP(kan)	Glycogen-less	Complete	Normal, rod-shaped	Nucleoids not as well separated as in the wild type; DNA occasionally observed as relaxed stretches, but cells mostly contain DNA seen as either two or four masses	-
Δpgm/ΔmalP/ΔglgP/ΔglgX(kan)	Glycogen-less	Partial	Rounded, small cells; some heterogeneity in shape	Nucleoids appearing as two or four masses in some cells, but partitioning appears largely variable; elongated DNA masses and irregularly spaced nucleoids	-
ΔgalU/ΔmalP/ΔglgP/ΔglgX(kan)	Normal	Partial	Slightly rounded cells that appear smaller; does not appear to form as many elongated and filamentous cells as triple mutant; heterogenous cell populations still present	Comparable to the triple mutant	-
ΔopgH/ΔmalP/ΔglgP/ΔglgX(kan)	Glycogen excess	Complete	Normal, rod-shaped, but somewhat rounded and smaller than the wild type	Well separated nucleoids that appear mainly as two but sometimes four masses	-
ΔrelA/ΔmalP/ΔglgP/ΔglgX(kan)	Normal	Partial	Filamentation still present (but reduced) along with increased heterogeneity in cell shape; some cells appear thinned, others engorged	Some cells contain separated nucleoids appearing as two or four masses; others contain unsegregated DNA masses or haphazardly distributed nucleoids	Yes
ΔaspC/ΔmalP/ΔglgP/ΔglgX(kan)	Normal	Partial	Phenotype is less severe than triple mutant, but occasional filaments still formed	Nucleoids appear well separated and either as two or four masses; elongated and filamentous cells show less severe partitioning defects than the triple mutant	-

Strain	**Glycogen accumulation**	**Suppression of size/DNA partitioning defects**	**Cell morphology (FM4-64)**	**Nuclear staining pattern (DAPI)**	**Protein foci (FITC)**
ΔpykF/ΔmalP/ΔglgP/ΔglgX(kan)	Glycogen excess	Complete	Normal, rod-shaped	Chromosomes not well separated, and most cells appear to contain two and occasionally four nucleoid masses apart from unsegregated clumps or relaxed stretches of DNA	Yes
ΔpykA/ΔmalP/ΔglgP/ΔglgX(kan)	Glycogen excess	Complete	Small, rod-shaped	Chromosomes appear well separated, but most cells appear to contain two and occasionally four nucleoid masses	-
ΔpykF/ΔpykA/ΔmalP/ΔglgP/ΔglgX(kan)	Glycogen excess	Complete	Normal, rod-shaped	Chromosomes appear well separated, but most cells appear to contain two and occasionally four nucleoid masses along with some visible partitioning defects	Yes
ΔminC/ΔmalP/ΔglgP/ΔglgX(kan)	Normal	No	Significant filamentation along with polar septation and minicell production	Filaments may contain separated nucleoids, stretches of DNA or unsegregated masses; minicells are devoid of DNA	-
ΔsulA/ΔmalP/ΔglgP/ΔglgX(kan)	Glycogen excess	Complete	Normal, rod-shaped	Well separated nucleoids that appear either as two or four masses; Nucleoids occasionally aberrantly positioned	-
ΔdiaA/ΔmalP/ΔglgP/ΔglgX(kan)	Glycogen excess	Partial	Phenotype is less severe than triple mutant, but occasional filaments still formed	Partitioning defects less severe than triple mutant but still apparent in both normal and filamentous cells	Yes
ΔhupA/ΔmalP/ΔglgP/ΔglgX(kan)	Glycogen excess	Partial	Mostly rod-shaped, normal sized cells with occasional filaments that form multiple cell walls	Well separated nucleoids that appear either as two or four masses; partitioning defects significantly less severe than triple mutant and stretches of relaxed DNA almost absent in filaments	Yes
ΔhupB/ΔmalP/ΔglgP/ΔglgX(kan)	Glycogen excess	Partial	Mostly rod-shaped, normal sized cells with occasional filaments that form multiple cell walls	Well separated nucleoids that appear either as two or four masses; partitioning defects significantly less severe than triple mutant and stretches of relaxed DNA almost absent in filaments	Yes

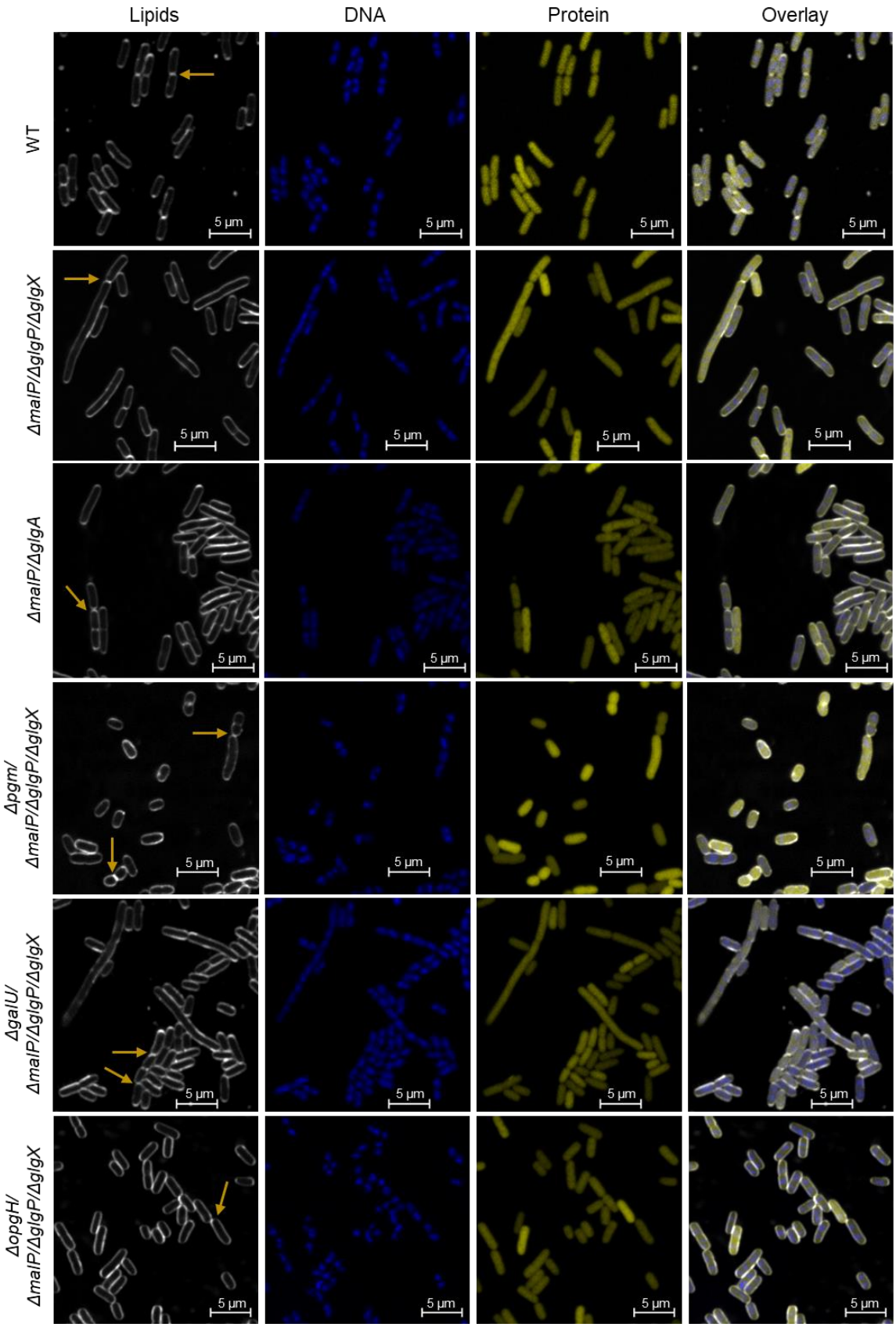

Figure 3.3. Confocal micrographs of exponentially growing bacteria including those impaired in glycogen and UDPG biosynthesis. Double mutant *E. coli* cells with lesions in both *malP* and *glgA* are shown alongside the wild type, triple mutant and quadruple mutant bacteria with deletions to *pgm*, *galU* or *opgH*. Lipids, DNA and proteins are stained white, blue and yellow, respectively. Yellow arrows point to septation sites.

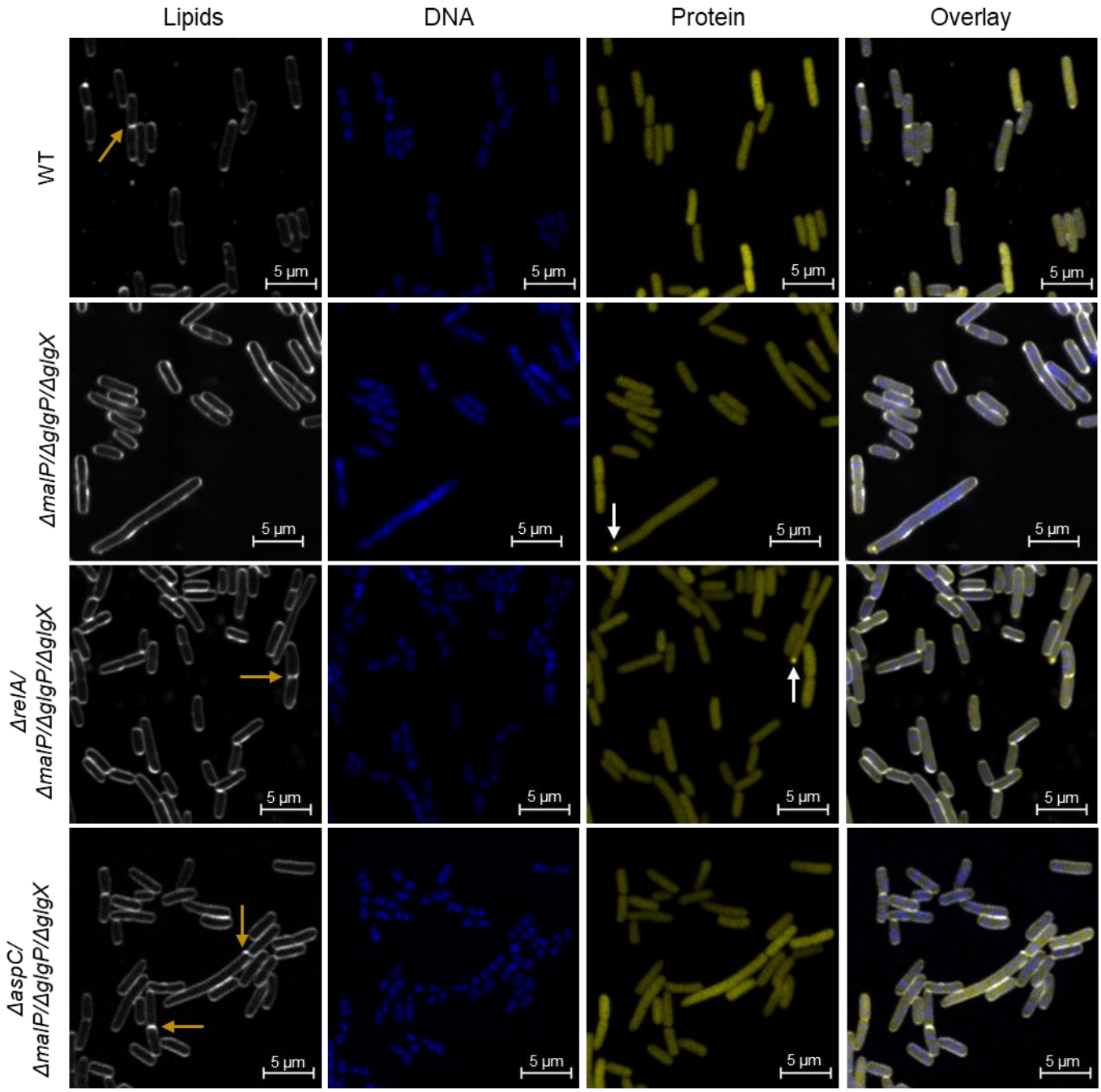

Figure 3.4. Confocal images of cell membranes, DNA and protein content of exponentially growing bacteria. Quadruple mutants with deletions to *relA* or *aspC* are shown alongside the wild type and triple mutant strains. Lipids are shown in white, genetic content in blue and protein in yellow. Yellow arrows demarcate sites of septation. White arrow point to punctate foci that are likely protein aggregates.

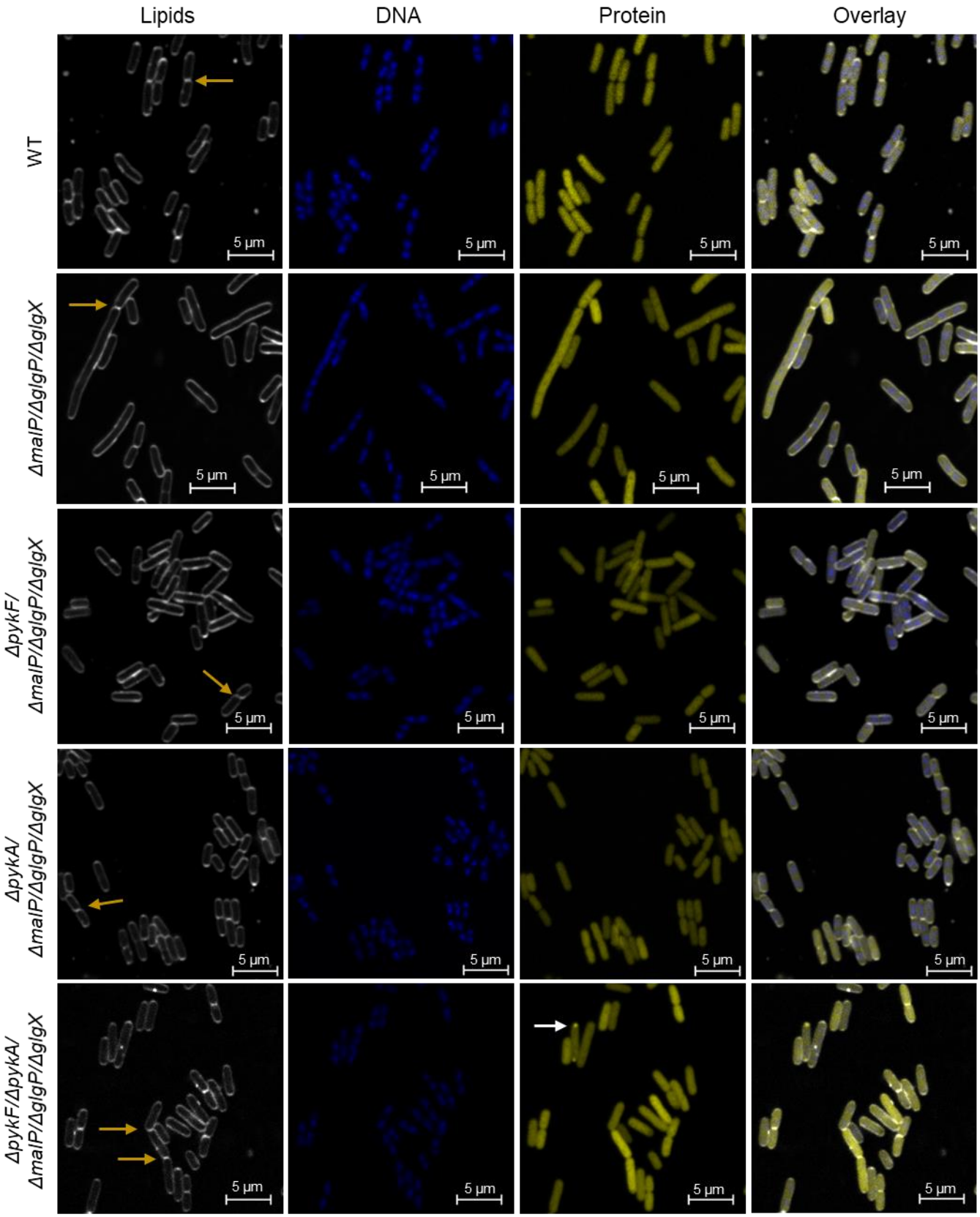

Figure 3.5. Micrographs of exponentially growing wild type and mutant bacteria. A link between glycolysis and the triple mutant's size defects examined by disrupting *pykF* and/or *pykA* in the triple mutant background. Cell membranes, DNA and protein are displayed in white, blue and yellow, respectively. Yellow arrows point to division sites and white ones to protein aggregates.

An SOS-mediated division block likely underlies filamentation in the triple mutant

The impact of the Min system on the triple mutant's phenotypic changes was investigated by deleting *minC*, the gene encoding the main effector of this system[148]. Quadruple Δ*minC*/Δ*malP*/Δ*glgP*/Δ*glgX* mutant cells showed enhanced difficulties with regulating their sizes and partitioning genetic material (Fig. 3.6). Most bacteria grew into elongated filaments with multiple nucleoids distributed along the length of the cell or with genetic material appearing as unsegregated clumps or relaxed stretches of DNA (Fig. 3.6). Round minicells, clearly devoid of DNA, were observed pinching off from nucleated mother cells. Mutating *sulA* in the triple mutant appeared to completely restore its phenotype to wild type (Fig. 3.6). Not only did quadruple Δ*sulA*/Δ*malP*/Δ*glgP*/Δ*glgX* mutant bacteria appear morphologically identical to the wild type, but DNA staining patterns also appeared largely invariable, though aberrant partitioning of genetic material was still occasionally observed.

Defective DNA replication seemingly triggers division inhibition in triple mutant cells

Delaying replication initiation by deleting *diaA*, *hupA* or *hupB* in the triple mutant partially suppressed its size and nucleoid distribution hindrances (Fig. 3.7; Table 3.2). Morphologically, Δ*diaA*/Δ*malP*/Δ*glgP*/Δ*glgX* cells did not appear to form as many long cells as the triple mutant (Fig. 3.7) and showed less severe difficulties with correctly portioning genetic material. Nucleoids seemed to be more compact than the sometimes expanded or in other cases unsegregated clumps of genetic material apparent in triple mutant cells (Fig. 3.7).

It should be noted that filaments were rarely observed that contained two (or more) complete septal invaginations at the same time (e.g. triple mutant, Δ*pykF*/Δ*pykA* quintuple mutant, Δ*galU* quadruple mutant). It is thus perplexing to observe more than two complete cell walls occasionally forming in elongated Δ*hupA*/Δ*malP*/Δ*glgP*/Δ*glgX* or Δ*hupB*/Δ*malP*/Δ*glgP*/Δ*glgX* bacteria (Fig. 3.7). Introducing a lesion either in *hupA* or *hupB* appears to furthermore largely ameliorate the DNA portioning defects of triple mutant cells as quadruple mutants contained nucleoids visualised as distinct, well separated masses (Fig. 3.7).

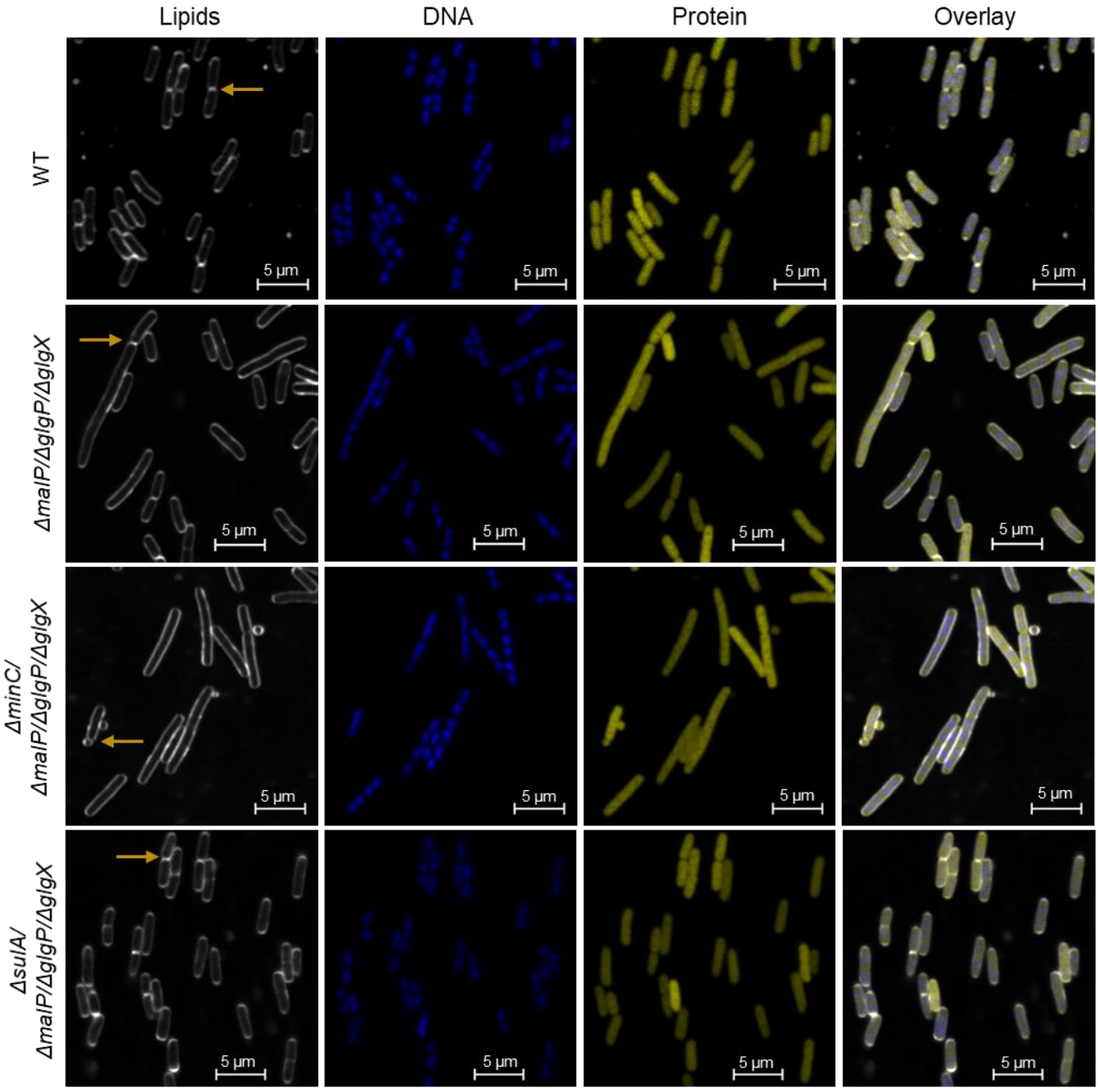

Figure 3.6. Confocal pictures of exponentially growing bacteria. The impact of the division inhibitors MinC and SulA on the triple mutant's size defects was examined by deleting *minC* or *sulA* in the triple mutant background, shown here along with the wild type during exponential growth. The cell envelope is shown in white, DNA in blue and protein in yellow. Yellow arrows point to sites of septation.

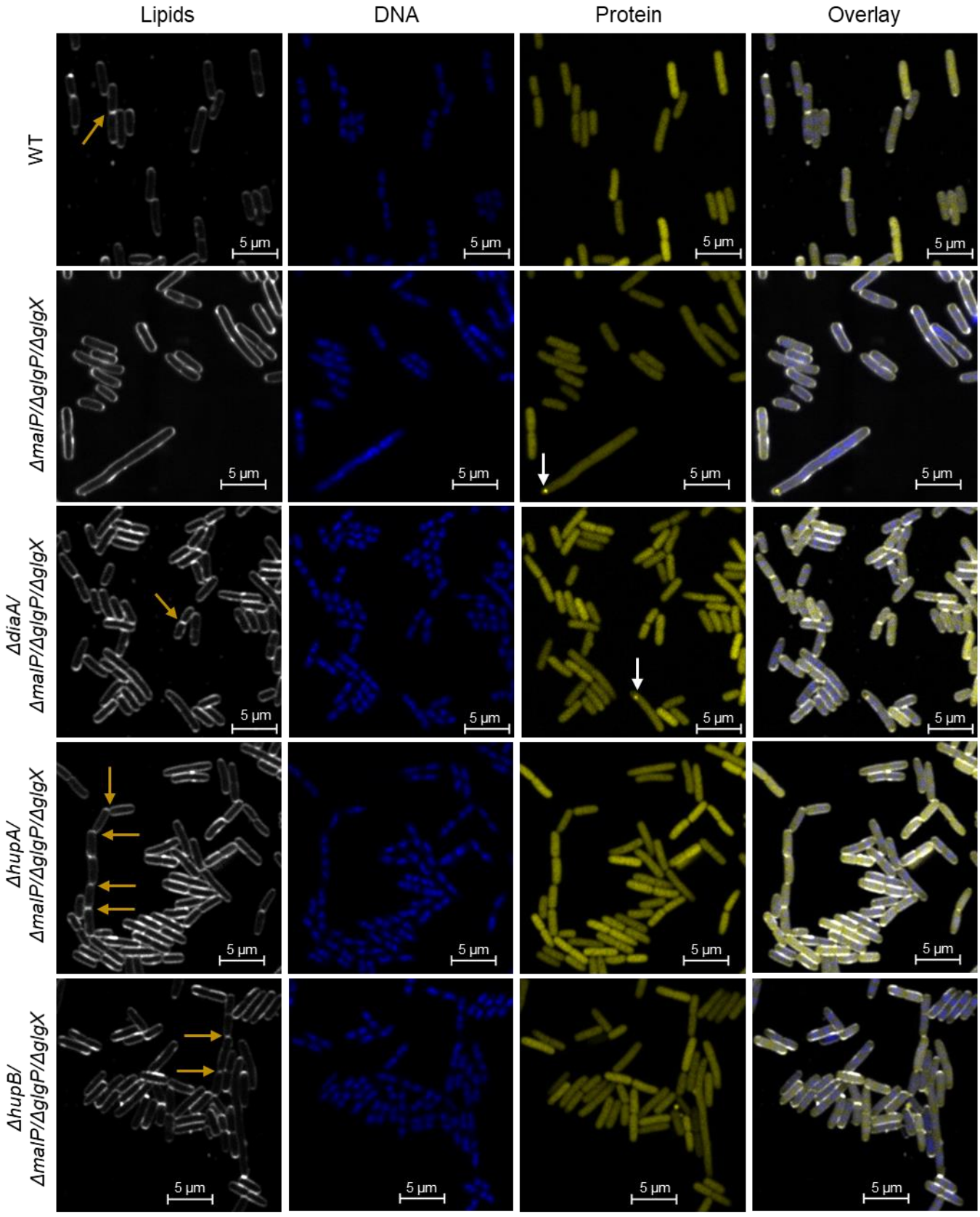

Figure 3.7. Confocal pictures of exponentially growing *E. coli*. A role for DNA replication in the triple mutant's size defects was investigated by deleting *diaA*, *hupA* or *hupB* in that mutant background. Cell membranes are shown in white, while DNA and proteins are stained blue and yellow, respectively. Yellow arrows demarcate septal invaginations and white ones point to protein aggregates.

DISCUSSION

To uncover the nature of the phenotypic changes observed in *E. coli* mutants of glycogen breakdown (Chapter 2), fourteen out of a total of 41 mutants, generated by phage transduction (Supplementary Figs. 1-6; Table S1) and lacking various non-essential proteins (Table 3.1) alongside either MalP action (such as the Δ*glgA*/Δ*malP* double mutant) or the activities of MalP, GlgP and GlgX (the quadruple and quintuple mutants) were screened for their phenotypes (Table 3.2). This provided a preliminary screen that identified genetic components affecting cell size in the triple mutant. A full-scale analysis can be performed that will involve integrating selected mutant alleles into the single (Δ*malP*, Δ*glgP* and Δ*glgX*) and double mutant (Δ*glgP*/Δ*glgX*, Δ*malP*/Δ*glgP* and Δ*malP*/Δ*glgX*) backgrounds, alongside more detailed analysis of all of these strains.

It was not possible to produce a quadruple mutant with a deletion to *glgA* within the timeframe so, instead, a double mutant strain was produced by introducing a mutated *glgA* allele into a Δ*malP* single mutant. As the Δ*malP* mutants showed a similar phenotype in terms of cell size to the Δ*malP*/Δ*glgP*/Δ*glgX* triple mutant strain (Chapter 2), it is reasonable to assume that an alteration in cell size here will be replicated in the triple mutant. A complete suppression of the Δ*malP* single mutant's size defects is observed upon mutating *glgA* (Fig. 3.3) and is most likely due to the inability of this strain to form glycogen[28,51,57] (Fig. 3.2). The glycogen screening assay used in this chapter provides only a semi-quantitative measure of glycogen content and significant polyglucan accumulation has been noted in the case of some glycogen-less *E. coli* mutants[10,51], so this should be confirmed by quantitating this polyglucan. Small amounts of glycogen could in theory be formed by the Δ*glgA*/Δ*malP* mutant on LB agar[28], providing a possible explanation as to why chromosome partitioning still appears abnormal in this strain.

Another glycogen-less mutant[51,57] examined here is the Δ*pgm* quadruple mutant (Fig. 3.2), though the sizes and shapes of these bacteria vary as dramatically as nuclear morphologies (Fig. 3.3). Pgm fulfils several roles in the cell, balancing G6P and G1P levels and thereby influencing UDPG levels[167], glycogen metabolism[51,57], sugar transport[179], cell cycle progression[115] and carbon fluxes in CCM[71,77] (Fig. 3.1). It is likely that a combination of these contribute to the reduced sizes and rounded shapes of these mutants. The cell unit of an elongated quadruple Δ*pgm* mutant appears smaller than that of the triple mutant and the nucleoids of putative daughter cells are well-separated as opposed to the unsegregated masses typically observed in triple mutant filaments. This begs the question how birth size and the duration of individual cell cycle periods (especially C + D) differ between these strains[104].

Deleting *galU* in the triple mutant background only partially restored its size and DNA partitioning to levels observed in the wild type strain and substantial heterogeneity in size was still evident (Fig. 3.3). Cells appeared somewhat rounded, likely due to the importance of UDPG in forming components of the cell envelope and thus affecting cell shape. Mutant Δ*galU*/Δ*malP*/Δ*glgP*/Δ*glgX* cells appeared to accumulate wild type levels of glycogen whilst Δ*galU*

single mutants reportedly display a glycogen-deficient phenotype[51,57]. GalU has been cited as a potential source of ADPG, since eliminating GlgC activity alone still leads to substantial glycogen synthesis upon ectopic expression of GlgA in a Δ*glgC* mutant[10,51], though concrete evidence to support this claim is still lacking.

A complete suppression of the deleterious size and nucleoid distribution defects of the triple mutant is observed when *opgH* is abolished in this background (Fig. 3.3) – despite quadruple mutant cells accumulating excessive amounts of glycogen (Fig. 3.2). Disrupting the activity of this division inhibitor results in more frequent division events in an Δ*opgH* single mutant as free cytosolic FtsZ pools increase in its absence[93] (See Chapter 1 Section 7.2). It may be argued that more frequent division events in the triple mutant background results in the restoration of size in quadruple mutant cells to normal. However, bacteria appeared marginally smaller and seemed to contain less DNA than wild type cells, so it is unlikely that septation alone is affected in these mutants.

No differences in cell sizes and growth rates have been reported previously for Δ*pykA* and Δ*pykF* single mutants relative to the wild type when grown in LB broth[107]. However, a Δ*pykF*/Δ*pykA* double mutant has been shown to double significantly faster than its wild type parent when cultured in minimal media containing glucose[223]. Intriguingly, quadruple mutants with a lesion in *pykA* formed small, rod-shaped cells that seem to contain very little DNA; mutating *pykF* either on its own or alongside *pykA* in the triple mutant resulted in quadruple and quintuple mutant strains that formed normal, rod-shaped cells with clear DNA partitioning defects (Fig. 3.5; Table 3.2).

PykF provides the primary Pyk activity which generates pyruvate via glycolysis when cells are grown on glucose, so less efficient flux through glycolysis is likely to affect cell size (by impacting acetyl-CoA pools and thus fatty acid availability), initiation of DNA replication (by disrupting the action of the PDH^{c}) and growth (by affecting sugar transport as a result of altered PEP/pyruvate levels). Reduced growth rates (data not shown) were noted both on solid media (LB agar) and in liquid culture (LB broth) for both the Δ*pykF* quadruple and quintuple mutants, compared to other strains examined under this section. This remains to be validated but if doubling times were increased, it would, in theory, permit the cell more time to repair damaged DNA/restart stalled replication forks as DNA replication rates would also be reduced[173]. Such an indirect suppression mechanism could explain why nucleoid partitioning appears defective in these strains, despite cell size appearing normal (Fig. 3.5).

Less clear is why disruption of the minor isoform of Pyk in the triple mutant has such a profound effect on size and DNA staining patterns without noticeably affecting growth rate (data not shown). Quadruple mutants with a mutated *pykA* gene were not only short, but also seemed to contain less DNA which is normally distributed in the cell (Fig. 3.5), indicating a more direct mechanism underlying the effect on cell size. The nucleotide diphosphate kinase action of PykA negatively regulates ATP levels under anaerobic conditions and it is tempting to speculate that

deleting *pykA* increases ATP levels in both the quadruple and quintuple mutant strains. Whilst it may be an artefact of the staining procedure, both quadruple (to a lesser extent) and quintuple mutant strains with a mutant *pykA* allele stained slightly darker than the triple mutant and elevated ATP levels could stimulate glycogen accumulation. It remains to be validated biochemically whether mutant cells contain more glycogen and or/ATP than the triple mutant.

PykA, but not PykF, has been shown to complex with other proteins[199] including chaperones involved in protein folding and DnaN (the sliding clamp of DNA polymerase III). The latter is worth noting as it would provide a direct link to one of the primary mechanisms that regulate replication initiation. DnaN, along with Hda (which is needed for ATP hydrolysis) carries out the regulatory inactivation of DnaA (RIDA – See Chapter 1 Section 6.1)[131,234]. It is interesting to speculate that PykA somehow affects RIDA and could be reducing its hydrolytic activity on ATP-DnaA during conditions of nutrient abundance (and elevated glycolytic flux/Pyk activity). In the absence of PykA (e.g. the quadruple mutant forming small cells with very little DNA), uninhibited RIDA could be lowering ATP-DnaA levels, thereby reducing replication rates and cell size.

Utilizing amino acids and oligopeptides in a growth medium like LB supports rapid growth of *E. coli* as these provide a source of both carbon and nitrogen[224,235]. Maximizing the availability of aspartate purportedly impacts UDPG levels (and thus OpgH activity) and the amount of DnaA per cell, so, given its importance, it is unsurprising that mutating *aspC* delays growth and reduces cell size and the number of origins of replication per cell relative to the wild type[178]. Deleting *aspC* in the triple mutant partially restored its size and chromosome partitioning defects to normal (Fig. 3.4) and this may be due to reduced replication rates and/or more frequent division events ameliorating problems with DNA replication and/or cell size. Disrupting genes whose protein products are responsible for amino acid biosynthesis or protein turnover (and thus reduced intracellular amino acid pools) has traditionally been associated with a glycogen excess phenotype, partly due to induction of the stringent response (See Chapter 1 Section 2.2.1). In this case, however, a lesion in *aspC* (Table 3.1) caused quadruple mutant cells to accumulate wild type glycogen levels (Fig. 3.2), so it is likely that AspC not only affects UDPG levels but also impacts ADPG availability (possibly by affecting carbon flux to the common precursor of both nucleotide sugars, namely G1P).

Some observations made in Chapter 2 point to induction of the SOS response (See Chapter 1 Section 6.3) influencing formation of filamentous *E. coli* cells in mutants with a disrupted *malP* allele. These include multinucleated filaments that remain metabolically active[236] and show no changes to viability during exponential growth despite having reduced culturability during this developmental phase[237,238]. Consistent with this idea, and the proposition that defective DNA replication is triggering a cell division block (Chapter 2), deleting *sulA* in the triple mutant background completely restored cell size to normal (Fig. 3.6). Nuclear staining patterns also appeared largely similar to that observed for the wild type strain, though aberrantly positioned nucleoids were occasionally observed in Δ*sulA*/Δ*malP*/Δ*glgP*/Δ*glgX* quadruple mutant cells (Fig. 3.6).

It is well known that disruptions to the Min system lead to a loss in spatial control of Z-ring placement, and aberrant division events at the poles give rise to minicells that are round and devoid of DNA, whilst a nucleated mother cell remains[239,148]. Such deviant division was apparent from confocal images of quadruple mutant cells with a lesion in *minC* (Fig. 3.6). Minicells, filled with protein, were formed alongside significant proportions of filaments with major chromosome partitioning problems, indicating that the growth defects of the triple mutant are exacerbated by deleting *minC*. This highlights the importance of the Min system in orchestrating division in filamentous cells[129], such as those formed by the triple mutant.

The observation that Δ*minC*/Δ*malP*/Δ*glgP*/Δ*glgX* mutant cells stained similar to the wild type for glycogen lends credence to the idea of co-aggregation between protein and glycogen proposed under Chapter 2. It was recently shown that *minC* mutants use minicells as a form of damage disposal[240]. Mutant *minC* cells treated with sublethal dosages of antibiotics sequester damaged proteins to cell poles, where these aggregates are eventually disposed of as minicells, before the nucleated mother divides and gives birth to two damage-free daughters. It is unlikely that the Min system affects glycogen metabolism. Instead, it is more likely that excess glycogen is passively sequestered to cell poles and discarded, along with proteins and other cellular constituents, as minicells. These glycogen-containing minicells would fail to grow on solid media as they lack genetic material and provides a plausible reason for Δ*minC* quadruple mutant cells accumulating less glycogen than the triple mutant on solid media (Fig. 3.2).

In support of the idea that delaying replication initiation in the triple mutant could alleviate its nuclear partitioning defects, a disruption to its *diaA* locus partly suppresses its size and DNA distribution hindrances (Fig. 3.7; Table 3.2). Mutant Δ*diaA*/Δ*malP*/Δ*glgP*/Δ*glgX* cells did not show normal chromosome staining patterns and unsegregated clumps or stretches of relaxed DNA were visible in these bacteria (Fig. 3.7) that still form substantial proportions of filaments. This likely reflects the non-essential role DiaA plays in replication initiation as an accessory protein to DnaA (Table 3.1).

Mutating *relA* causes single mutants to accumulate significantly less (~70%) glycogen on Kornberg media than wild type cells[51], highlighting RelA's importance in stimulating glycogen biosynthesis via ppGpp production in *E. coli* (See Chapter 1 Section 2.2.1). Deleting *relA* in the triple mutant reduced glycogen accumulation to such an extent in quadruple mutant cells that they stain similar to the wild type for glycogen (Fig. 3.2). Since SpoT may also produce ppGpp (albeit in response to different nutritional cues than RelA) and a Δ*relA*/Δ*spoT* double mutant (i.e. ppGpp^0 strain) is glycogen-less[241] it is reasonable that the ppGpp synthetase activity of SpoT is sufficient to stimulate glycogen accumulation in the absence of RelA (Fig. 3.2).

Greater heterogeneity in cell morphology (but less filamentation) was observed in quadruple Δ*relA*/Δ*malP*/Δ*glgP*/Δ*glgX* mutant bacteria compared to the triple mutant (Fig. 3.4) along with equally drastic heterogeneity in nuclear distribution patterns. Disrupting ppGpp balance in the cell has a

pleiotropic effect on cellular physiology by impacting processes such as cell division, DNA replication and cell size regulation[38,50]. Heterogeneity in cell size linked to disruptions in ppGpp homeostasis have been proposed to result from changes in ATP levels and/or gene expression patterns[242]. Since a partial suppression of the triple mutant's size control disturbances is observed in Δ*relA* quadruple mutant cells, it may be reasoned that reduced glycogen amounts and/or altered ppGpp levels (or some downstream process controlled by this alarmone) are suppressing the growth defects of the triple mutant.

Deleting either *hupA* or *hupB* in the triple mutant appears to significantly improve the DNA partitioning difficulties it undergoes (Fig. 3.7). Substantially fewer filaments were formed by both Δ*hupA*/Δ*malP*/Δ*glgP*/Δ*glgX* and Δ*hupB*/Δ*malP*/Δ*glgP*/Δ*glgX* strains and the filaments that form seem to divide into several 'normal' sized cells simultaneously. This was observed more frequently when *hupA* rather than *hupB* was deleted. The division dynamics of filamentous *E. coli* has been explored (See Chapter 1 Section 6.2.1) so the observation of these mutant filaments "breaking the rules" of cell division by constricting multiple times at once is intriguing for various reasons[129]. There are three possible explanations for this based on the involvement of HU heterodimers and HupA and HupB homodimers in replication initiation, transcription regulation and maintenance of nucleoid structure in *E. coli*[84,85,226].

Firstly, HupA is known to play a more dominant role than HupB in stimulating replication initiation by being directly recruited to *oriC* by DnaA during replication initiation. This creates a favourable environment at *oriC* by promoting strand opening, thereby assisting with the triggering of replication initiation[227]. HU heterodimers stimulate replication initiation to a lesser extent than HupA alone, so production of HupB could provide a means of sequestering HupA and reducing its stimulatory effect at *oriC*. It is well documented that DnaA alone is not the limiting factor that triggers replication initiation in *E. coli*[105,117,122] or *B. subtilis*[243], so identifying other initiator molecules that accumulate in a growth-dependent manner and trigger replication initiation in a size-dependent way, would answer important fundamental questions regarding replication initiation. HupA displays several of the hallmarks of such an initiator molecule - it accumulates in a nutrient and cell cycle dependent manner across various growth rates, and under steady-state growth, HupA amounts are proportional to cell size[244]; the stoichiometry between HupA and DNA increases with nutrient-imposed growth rate and the number of origins of replication per cell increases concomitant to the increase in HupA/DNA.

Secondly, although HU-DNA interactions are mostly sequence non-specific, HU heterodimers bind with a high affinity at anomalous DNA structures like gaps, nicks and Holliday junctions that are typically associated with DNA damage, repair and recombination[226]. Induction of SOS responsive genes involves degradation of the LexA repressor protein by ATP-bound RecA (See Chapter 1 Section 6.4) and it has been shown that HU may bind directly to DNA and displace LexA from its binding site, thereby inducing genes involved in the SOS response[84]. Since deleting *sulA* in

the triple Δ*malP*/Δ*glgP*/Δ*glgX* mutant restored its size and DNA partitioning defects to normal (Fig. 3.6), it could be that less efficient induction of SOS genes (including *sulA*) due to a deletion in either *hupA* or *hupB* indirectly suppresses the triple mutant's growth defects (Fig. 3.7). If less SulA were made it would be expected to increase free FtsZ pools and explain the formation of multiple Z-rings. This would not, however, explain how cells seemingly constrict multiple times simultaneously as removing the filament-inducing stress in elongated *E. coli* leads to sequential division (at one possible division site at a time) with interdivision times decreasing as cells become shorter[129].

Finally, it is interesting to note that nucleoids appeared more compact and regularly distributed in quadruple mutant cells with a lesion in *hupA* or *hupB*, relative to the triple mutant parent (Fig. 3.7). HU is known to affect chromosome architecture through DNA bending and by constraining supercoils[244]. Due to its impact on supercoiling[226] (both constraining negative supercoils and introducing negative supercoils into relaxed DNA in the presence of topoisomerase I) a lack of HU reduces the negative supercoiling state of the chromosome[84]. This is maintained by competing activities of DNA gyrase and topoisomerases while about half of the total supercoiling in *E. coli* is constrained by DNA binding to NAPs such as HU, so these interactions play important roles in transcription and DNA metabolism[226]. If MalP influenced the supercoiling state of the nucleoid it could explain why so many processes are seemingly affected by mutating *malP*. If the structure of the nucleoid in the triple Δ*malP*/Δ*glgP*/Δ*glgX* mutant were additively affected by limiting glycogen catabolism (by deleting *glgP* and *glgX* in the Δ*malP* mutant) it could explain why Flp-FRT recombination was unsuccessful in this strain (if the DNA molecule were underwound it would impair recombination). No problems with recombination were encountered with the Δ*malP* single mutant[186], so whether this is a completely coincidental observation, or perhaps points to a pleiotropic effect on regulating DNA structure in the triple mutant is currently unclear.

Taken together, it is clear from these observations that multiple pathways link cell physiology to DNA replication and cell size in *E. coli*. Diverse systems act in concert to facilitate a division block in mutants lacking MalP including the SOS response (via SulA) and OpgH which are both involved in delaying septation in the triple mutant. DNA replication and cell size seem to be more drastically altered when *pykA* is mutated in the triple mutant strain, than when either *pykF* or a combination of *pykA* and *pykF* is deleted in this strain. This could point to a novel role for PykA in DNA replication/cell size regulation. It is tempting to speculate what the underlying cause(s) are of defective DNA replication and apparent SOS induction in MalP deficient strains, as replication fork progression may be hindered when dNTP pools are depleted or when it encounters some form of DNA damage[191]. Whether MalP significantly impacts nucleotide levels or DNA metabolism/structure remains open for investigation.

MATERIALS & METHODS

Mutant strain construction and genotyping

Bacterial strains used for the generation of double, triple, quadruple and quintuple mutants are from the isogenic Keio collection[188] and were obtained from the *E. coli* genetic stock center (CGSC, Yale University). Mutant strains (Table S1) were generated by P1 phage transduction[232] and where necessary, kanamycin resistance cassettes were removed by Flp-mediated recombination using the pCP20 vector[231]. Mutant genotypes were confirmed by PCR, using allele-specific flanking primers (Table S2) and gDNA as a template. Primers were designed using the PrimerQuest tool from Integrated DNA Technologies (Coralville, USA) and obtained from Inqaba Biotech (Pretoria, South Africa). PCR reactions were performed using GoTaq DNA Polymerase (Promega, Madison, USA) according to the manufacturer's instructions.

Iodine staining

To semi-quantitively assess glycogen accumulation in the mutant strains, bacteria were cultured overnight from a single colony in LB broth and 10 µL was spotted on LB agar plates containing 1% w/v glucose. The plates were incubated for 15 hours at 37°C and then exposed to iodine vapors for 5 minutes before being imaged.

Sample preparation and confocal image acquisition

Bacteria were grown from a single colony, overnight in LB broth and then diluted 1:1000 into fresh LB. Cells were cultured until mid-exponential phase (OD_{600} ~ 0.2 – 0.6) at which point 1 mL of culture was harvested into a microfuge tube containing 40 µL $NaPO_4$ (pH 7.4) and 5 µL of 1 mg/mL FM™ 4-64FX (Thermo Fisher Scientific). Cells were stained for 4 minutes at room temperature and then fixed by the addition of 200 µL ice-cold fixative[211] [16% formaldehyde, 0.06% glutaraldehyde in 1X PBS (137 mM NaCl, 2.68 mM KCl, 10.1 mM Na_2HPO_4, 1.76 mM KH_2PO_4)]. Cells were incubated at room temperature for 15 minutes with slight agitation (100 RPM) and then placed on ice for another 30 minutes before being harvested by centrifugation (20 000 x g, 1 minute, 4°C) and washed three times with PBS-E.

Bacteria were resuspended in 0.1 M phosphate buffer (pH 9.0), and protein content stained with FITC at a final concentration of 5 µg/mL, overnight at 4°C. The next day, cells were collected by centrifugation, washed twice in PBS-E (1X PBS containing 1 mM EDTA) and resuspended in GTE before 20 µL of cells were airdried on an agarose pad (1% w/v in 1X PBS). A drop of Fluoroshield™ with 1.5 µg/mL DAPI (Sigma) was used to stain bacterial DNA and coverslips were placed over slides and kept at room temperature for at least 30 minutes before images were acquired.

Imaging occurred essentially as under Chapter 2 for confocal microscopy. Excitation and detection of FM 4-64FX and DAPI fluorescence were as described, whilst for this experiment a 488

nm laser was used to excite FITC, with FITC emission being detected in the ranges of 499 to 570 nm (λ_{em} = 535 nm) with a GaAsP detector.

ADDENDUM B

Table S1. Bacterial strains used and manufactured throughout the course of this study. More than 50 new mutant strains were created by deleting antibiotic resistance cassettes using Flp-FRT recombination and/or moving specific genetic elements between mutants using phage transduction.

Strain	Description	Reference
BW25113	*Δ(araD-araB)567 ΔlacZ4787(::rrnB-3) λ- rph-1 Δ(rhaD-rhaB)568 hsdR514*	187
ΔmalP(kan)	BW25113*ΔmalP::kan*	188
ΔglgP(kan)	BW25113*ΔglgP::kan*	188
ΔglgX(kan)	BW25113*ΔglgX::kan*	188
ΔmalPΔglgP(kan)	BW25113*ΔmalP::ΔglgP::kan*	186
ΔmalPΔglgX(kan)	BW25113*ΔmalP::ΔglgX::kan*	186
ΔglgPΔglgX(kan)	BW25113*ΔglgP::ΔglgX::kan*	186
ΔmalPΔglgPΔglgX(kan)	BW25113*ΔmalP::ΔglgP::ΔglgX::kan*	186
ΔglgA(kan)	BW25113*ΔglgA::kan*	188
ΔglgA	BW25113*ΔglgA*	This study
ΔglgAΔmalP(kan)	BW25113*ΔglgA::ΔmalP::kan*	This study
ΔglgAΔglgX(kan)	BW25113*ΔglgA::ΔglgX::kan*	This study
ΔglgAΔmalPΔglgX(kan)	BW25113*ΔglgA::ΔmalP::ΔglgX::kan*	This study
ΔopgH(kan)	BW25113*ΔopgH::kan*	188
ΔopgH	BW25113*ΔopgH*	This study
ΔopgHΔmalP(kan)	BW25113*ΔopgH::ΔmalP::kan*	This study
ΔopgHΔglgP(kan)	BW25113*ΔopgH::ΔglgP::kan*	This study
ΔopgHΔglgX(kan)	BW25113*ΔopgH::ΔglgX::kan*	This study
ΔopgHΔmalPΔglgP(kan)	BW25113*ΔopgH::ΔmalP::ΔglgP::kan*	This study
ΔopgHΔmalPΔglgX(kan)	BW25113*ΔopgH::ΔmalP::ΔglgX::kan*	This study
ΔopgHΔglgPΔglgX(kan)	BW25113*ΔopgH::ΔglgP::ΔglgX::kan*	This study
ΔopgHΔmalPΔglgPΔglgX(kan)	BW25113*ΔopgH::ΔmalP::ΔglgP::ΔglgX::kan*	This study
ΔgalU(kan)	BW25113*ΔgalU::kan*	188
ΔgalU	BW25113*ΔgalU*	This study
ΔgalUΔmalP(kan)	BW25113*ΔgalU::ΔmalP::kan*	This study
ΔgalUΔglgP(kan)	BW25113*ΔgalU::ΔglgP::kan*	This study
ΔgalUΔglgX(kan)	BW25113*ΔgalU::ΔglgX::kan*	This study
ΔgalUΔmalPΔglgP(kan)	BW25113*ΔgalU::ΔmalP::ΔglgP::kan*	This study
ΔgalUΔmalPΔglgX(kan)	BW25113*ΔgalU::ΔmalP::ΔglgX::kan*	This study
ΔgalUΔglgPΔglgX(kan)	BW25113*ΔgalU::ΔglgP::ΔglgX::kan*	This study
ΔgalUΔmalPΔglgPΔglgX(kan)	BW25113*ΔgalU::ΔmalP::ΔglgP::ΔglgX::kan*	This study
Δpgm(kan)	BW25113*Δpgm::kan*	188
Δpgm	BW25113*Δpgm*	This study
ΔpgmΔmalP(kan)	BW25113*Δpgm::ΔmalP::kan*	This study
ΔpgmΔglgP(kan)	BW25113*Δpgm::ΔglgP::kan*	This study
ΔpgmΔglgX(kan)	BW25113*Δpgm::ΔglgX::kan*	This study
ΔpgmΔmalPΔglgP(kan)	BW25113*Δpgm::ΔmalP::ΔglgP::kan*	This study
ΔpgmΔmalPΔglgX(kan)	BW25113*Δpgm::ΔmalP::ΔglgX::kan*	This study
ΔpgmΔglgPΔglgX(kan)	BW25113*Δpgm::ΔglgP::ΔglgX::kan*	This study
ΔpgmΔmalPΔglgPΔglgX(kan)	BW25113*Δpgm::ΔmalP::ΔglgP::ΔglgX::kan*	This study

Strain	Description	Reference
ΔrelA(kan)	BW25113*ΔrelA::kan*	[188]
ΔrelA	BW25113*ΔrelA*	This study
ΔrelAΔmalP(kan)	BW25113*ΔrelA::ΔmalP::kan*	This study
ΔrelAΔglgP(kan)	BW25113*ΔrelA::ΔglgP::kan*	This study
ΔrelAΔglgX(kan)	BW25113*ΔrelA::ΔglgX::kan*	This study
ΔrelAΔmalPΔglgP(kan)	BW25113*ΔrelA::ΔmalP::ΔglgP::kan*	This study
ΔrelAΔmalPΔglgX(kan)	BW25113*ΔrelA::ΔmalP::ΔglgX::kan*	This study
ΔrelAΔglgPΔglgX(kan)	BW25113*ΔrelA::ΔglgP::ΔglgX::kan*	This study
ΔrelAΔmalPΔglgPΔglgX(kan)	BW25113*ΔrelA::ΔmalP::ΔglgP::ΔglgX::kan*	This study
ΔaspC(kan)	BW25113*ΔaspC::kan*	[188]
ΔaspC	BW25113*ΔaspC*	This study
ΔaspCΔmalPΔglgPΔglgX(kan)	BW25113*ΔaspC::ΔmalP::ΔglgP::ΔglgX::kan*	This study
ΔminC(kan)	BW25113*ΔminC::kan*	[188]
ΔminC	BW25113*ΔminC*	This study
ΔminCΔmalPΔglgPΔglgX(kan)	BW25113*ΔminC::ΔmalP::ΔglgP::ΔglgX::kan*	This study
ΔglgX(kan)	BW25113*ΔglgX::kan*	[188]
ΔglgX	BW25113*ΔglgX*	This study
ΔamyA(kan)	BW25113*ΔamyA::kan*	[188]
ΔamyA	BW25113*ΔamyA*	This study
ΔamyAΔmalPΔglgPΔglgX(kan)	BW25113*ΔamyA::ΔmalP::ΔglgP::ΔglgX::kan*	This study
ΔpykA(kan)	BW25113*ΔpykA::kan*	[188]
ΔpykA	BW25113*ΔpykA*	This study
ΔpykAΔmalPΔglgPΔglgX(kan)	BW25113*ΔpykA::ΔmalP::ΔglgP::ΔglgX::kan*	This study
ΔpykF(kan)	BW25113*ΔpykF::kan*	[188]
ΔpykF	BW25113*ΔpykF*	This study
ΔpykFΔmalPΔglgPΔglgX(kan)	BW25113*ΔpykF::ΔmalP::ΔglgP::ΔglgX::kan*	This study
ΔpykFΔpykA(kan)	BW25113*ΔpykFΔpykA::kan*	This study
ΔpykFΔpykA(kan)	BW25113*ΔpykFΔpykA*	This study
ΔpykAΔpykFΔmalPΔglgPΔglgX(kan)	BW25113*ΔpykA::ΔpykF::ΔmalP::ΔglgP::ΔglgX::kan*	This study
ΔsulA(kan)	BW25113*ΔsulA::kan*	[188]
ΔsulA	BW25113*ΔsulA*	This study
ΔsulAΔmalPΔglgPΔglgX(kan)	BW25113*ΔsulA::ΔmalP::ΔglgP::ΔglgX::kan*	This study
ΔdiaA(kan)	BW25113*ΔdiaA::kan*	[188]
ΔdiaA	BW25113*ΔdiaA*	This study
ΔdiaAΔmalPΔglgPΔglgX(kan)	BW25113*ΔdiaA::ΔmalP::ΔglgP::ΔglgX::kan*	This study
ΔhupA(kan)	BW25113*ΔhupA::kan*	[188]
ΔhupA	BW25113*ΔhupA*	This study
ΔhupAΔmalPΔglgPΔglgX(kan)	BW25113*ΔhupA::ΔmalP::ΔglgP::ΔglgX::kan*	This study
ΔhupB(kan)	BW25113*ΔhupB::kan*	[188]
ΔhupB	BW25113*ΔhupB*	This study

Table S2. Primer sequences used for genotyping bacterial strains. Gene names are provided along with priming sequences used to screen bacteria by PCR. T_A, Annealing temperature.

Gene	Forward Primer	Reverse Primer	T_A	Primer reference
malP	5'AAGGTCAACATCGAGCCTGG3'	5'ATCCACCAGCATCGCTTTGA3'	54°C	[186]
glgX	5'GGCAGTAATGCAGGCAATGG3'	5'TGATGCAGTTAGACAGCGCA3'	54°C	[186]
glgP	5'TTGTGCAACGTCAGGCTATGG3'	5'TGGCAATAACCACCGCCAA3'	57°C	This study
glgA	5'TATTCCGGAAGGCATGGT3'	5'TCATGTTTATTGGCGACGAC3'	54°C	This study
amyA	5'ATCGGTGTTAAGTGCCTATG3'	5'CCGGGTAAGTTGACATTGAT3'	54°C	This study
aspC	5'GTTACCCTGATAGCGGACTTC3'	5'GTTGCGTTTGTCATCAGTCTC3'	54°C	This study
minC	5'GCGCTGGCGATGATTAATAG3'	5'CCTTTGCCCGAAGTAACAAC3'	54°C	This study
galU	5'CGCGGGCTAAATTTGCATTACC3'	5'GATGAGCAAGGTAAATCCCTCGAC3'	54°C	This study
opgH	5'GAGATAGTTGAAAGCACGGT3'	5'CACACCGGGATAATATTGGT3'	54°C	This study
pykA	5'CTCGACGTACCGGAAGATA3'	5'GTCCGCGACCAGAACAATACAC3'	54°C	This study
pykF	5'AGTTTCTCCCATCCTTCTCAAC3'	5'AGGATGCTTCCATCGGATTC3'	54°C	This study
pgm	5'GCGTTTACTTTGCGGCAGAT3'	5'GACGACCAGACTCCTGTTGG3'	54°C	This study
relA	5'ACTGGATCTGTTCTGCGGTATG3'	5'GACTTCCTTATCTTTCGGCTCTCC3'	55°C	This study
sulA	5'AAGCCCGAAGATACAACTCACC3'	5'TTGCGCCTCGTTATCATCCA3'	55°C	This study
diaA	5'TATTACAGACTGCCCGCTTGTG3'	5'CGAGCCGAAAGTTCAGCATTTG3'	55°C	This study
hupA	5'AACGCCTGATTTGTCGTACCTG3'	5'GCACATTATCGCCGCTGTCT3'	55°C	This study
hupB	5'TGATATAACTGCTGCGCGTTCG3'	5'ACTCCGCTGTAGATGACTGTGT3'	55°C	This study

Table S3. Amplicon sizes of mutant alleles screened by PCR. Length of each gene's ORF is provided, along with the approximate sizes of amplicons for each allelic variant.

		Allele-specific amplicon length (bp)		
Gene	**ORF length (bp)**	**Wild type**	**Insertion mutant**	**Deletion mutant**
malP	2 394	2 991	1 853	682
glgX	1 974	2 300	1 582	411
glgP	2 448	2 771	1 579	408
glgA	1 434	1 700	1 693	351
amyA	1 488	1 851	1 790	448
aspC	1 191	1 297	1 533	191
minC	696	793	1 524	182
galU	909	1 287	1 805	463
opgH	2 544	2 990	1 873	531
pykA	1 443	2 002	1 986	644
pykF	1 413	1 599	1 613	271
pgm	1 641	2 100	1 886	544
relA	2 235	3 035	2 227	885
sulA	510	1 238	2 155	813
diaA	591	1 031	1 867	525
hupA	273	643	1 797	455
hupB	273	753	1 907	565

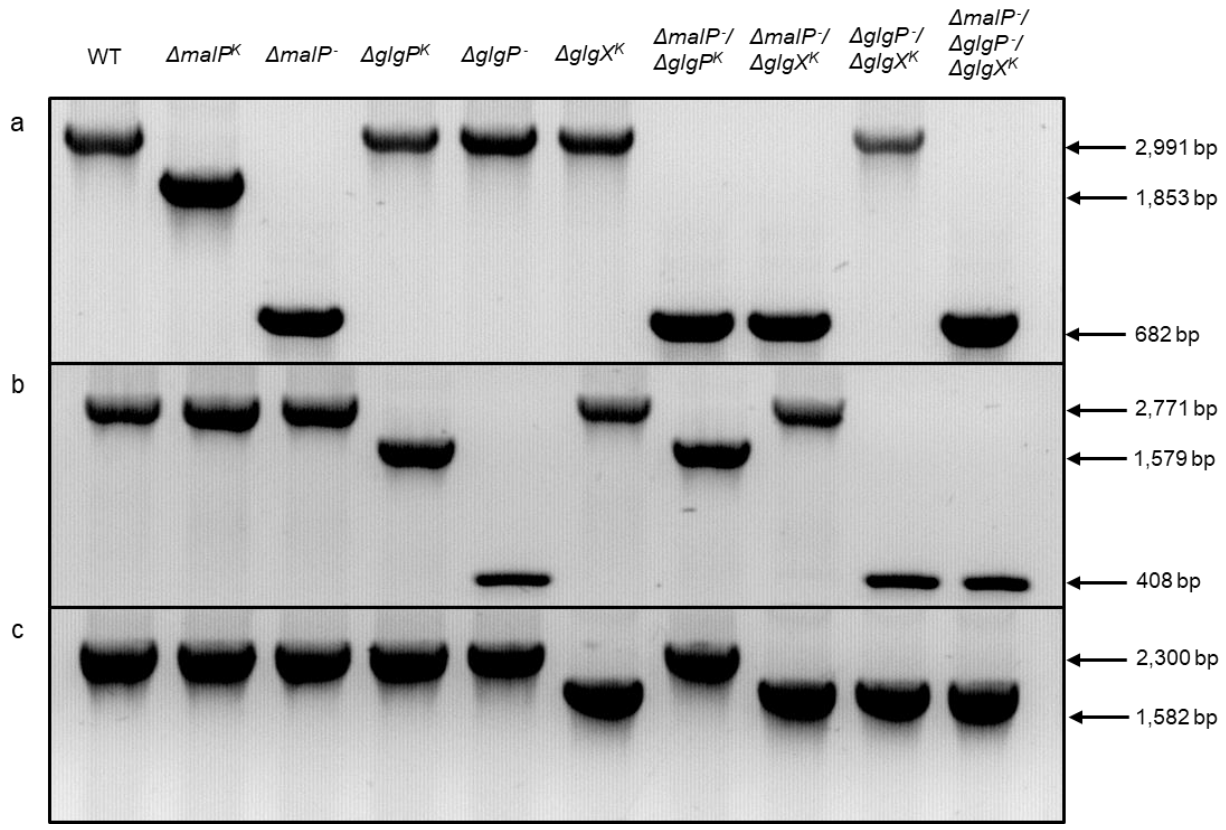

Figure S1. Genotyping bacterial strains by PCR. The wild type and several donor strains (mutants of glycogen breakdown) were screened using primers that specifically recognize regions flanking the (**a**) *malP*, (**b**) *glgP* or (**c**) *glgX* genes. Allele-specific amplicon sizes are indicated to the right with an arrow.

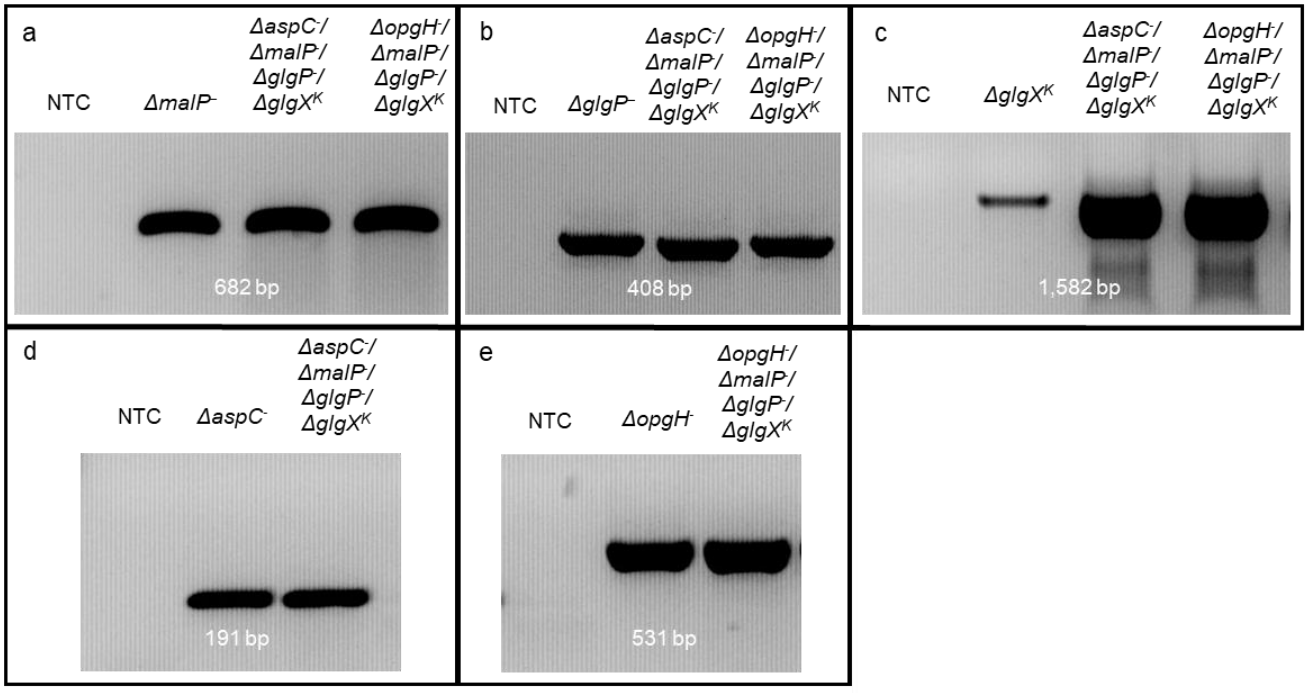

Figure S2. PCR analysis of mutant alleles of some quadruple mutants. Transfer of the triple mutant background was confirmed by screening for (**a**) *ΔmalP* (~682 bp), (**b**) *ΔglgP* (~408 bp) and (**c**) *ΔglgX(kan)* (~1 582 bp). Presence of a deletion in either the *aspC* or *opgH* locus was ascertained by screening putative quadruple mutants for (**d**) *ΔaspC* (~191 bp) or (**e**) *ΔopgH* (~531 bp) respectively.

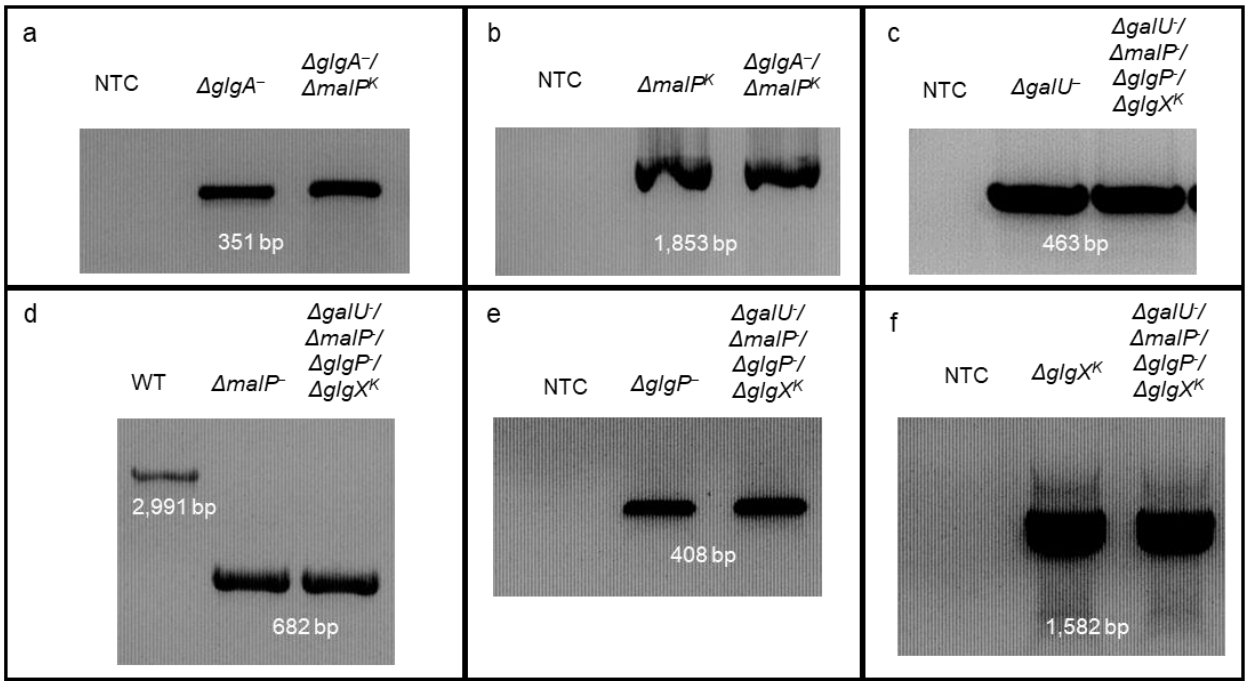

Figure S3. PCR screening of mutants. Presence of an insertion at *malP* in the *ΔglgA⁻/ΔmalP^K* double mutant was confirmed by screening for (**a**) *ΔglgA* (~351 bp) and (**b**) *ΔmalP(kan)* (~1 853 bp). Confirmation of the *ΔgalU⁻/ΔmalP⁻/ΔglgP⁻/ΔglgX^K* quadruple mutant was carried out by screening for (**c**) *ΔgalU* (~463 bp), (**d**) *ΔmalP* (~682 bp), (**e**) *ΔglgP* (~408 bp) and (**f**) *ΔglgX(kan)* (~1 582 bp).

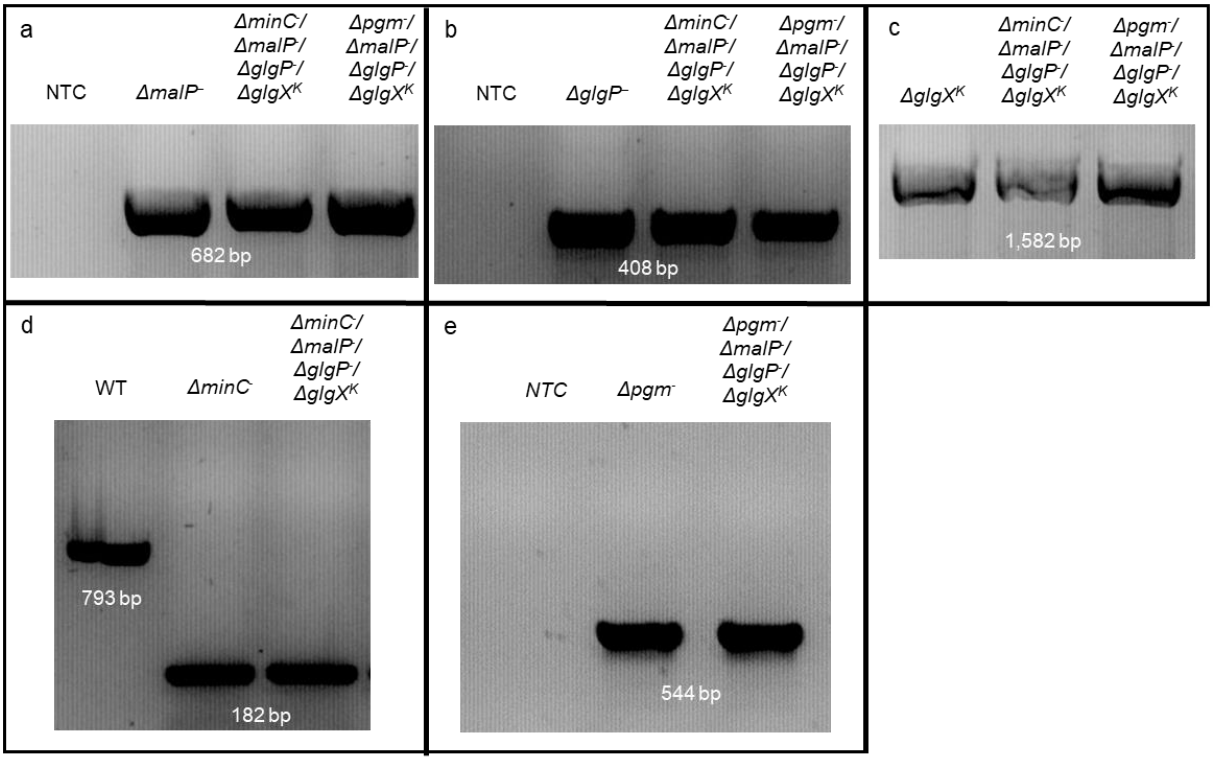

Figure S4. Genotyping mutant alleles of quadruple mutants by PCR. Transfer of the triple mutant background into mutants with a deletion at either the *minC* or *pgm* locus was confirmed by screening for (**a**) *ΔmalP* (~682 bp), (**b**) *ΔglgP* (~408 bp) and (**c**) *ΔglgX(kan)* (~1 582 bp) mutant alleles along with those for (**d**) *ΔminC* (~182 bp) or (**e**) *Δpgm* (~544 bp).

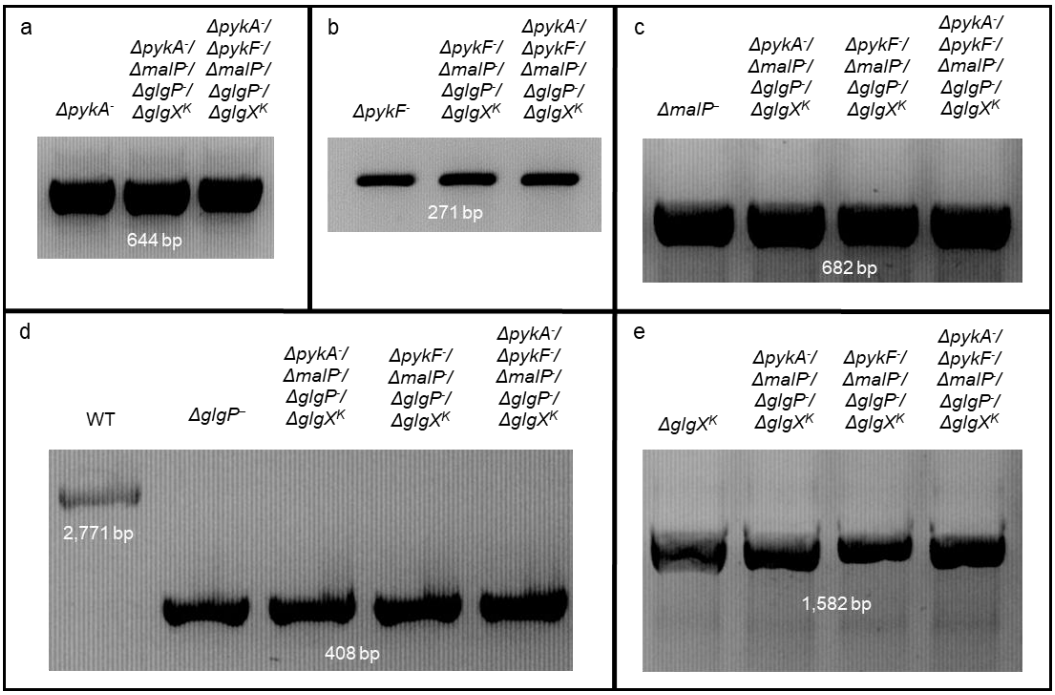

Figure S5. Genotyping mutant alleles of quadruple and quintuple mutants. Disruptions to *pykA* or *pykF* loci were confirmed by screening *ΔpykA⁻/ΔmalP⁻/ΔglgP⁻/ΔglgX^K*, *ΔpykF⁻/ΔmalP⁻/ΔglgP⁻/ΔglgX^K* and *ΔpykA⁻/ΔpykF⁻/ΔmalP⁻/ΔglgP⁻/ΔglgX^K* for (**a**) *ΔpykA* (~644 bp) and/or (**b**) *ΔpykF* (~271 bp). Successful integration of the triple mutant's disruptions into these backgrounds was determined by amplifying (**c**) *ΔmalP* (~682 bp), (**d**) *ΔglgP* (~408 bp) and (**e**) *ΔglgX(kan)* (~1 582 bp) in each of the mutant strains.

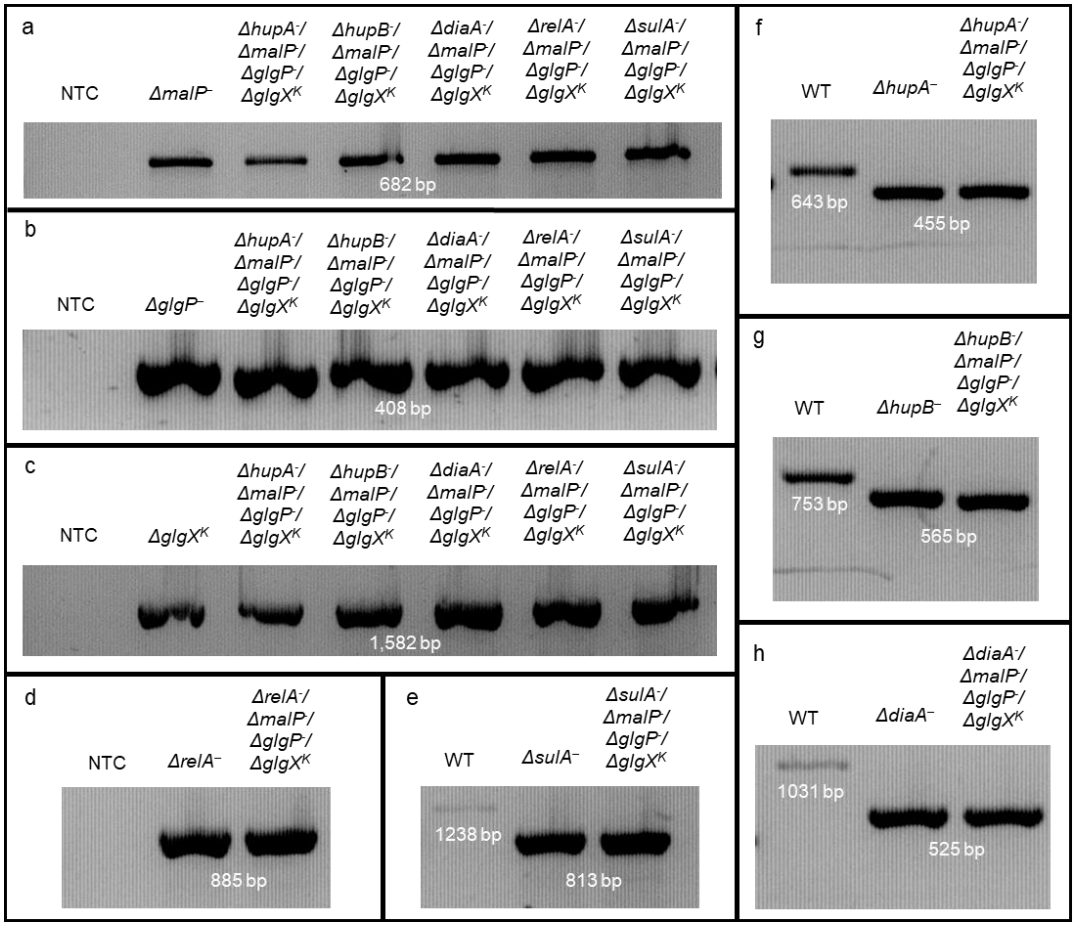

Figure S6. Screening of several quadruple mutants manufactured in this study. Transfer of the triple mutant's (**a**) *ΔmalP* (~682 bp), (**b**) *ΔglgP* (~408 bp) and (**c**) *ΔglgX(kan)* (~1 582 bp) alleles into *ΔhupA⁻/ΔmalP⁻/ΔglgP⁻/ΔglgX^K*, *ΔhupB⁻/ΔmalP⁻/ΔglgP⁻/ΔglgX^K* , *ΔdiaA⁻/ΔmalP⁻/ΔglgP⁻/ΔglgX^K* , *ΔrelA⁻/ΔmalP⁻/ΔglgP⁻/ΔglgX^K* and *ΔsulA⁻/ΔmalP⁻/ΔglgP⁻/ΔglgX^K* was confirmed by PCR. Screening of the respective quadruple mutant was performed by genotyping for (**d**) *ΔrelA* (~885 bp), (**e**) *ΔsulA* (~813 bp) (**f**) *ΔhupA* (~455 bp), (**g**) *ΔhupB* (~565 bp) (**h**) *ΔdiaA* (~525 bp).

4. Chapter 4 – General discussion

Some of the main observations made under Chapter 2 regarding the absence of MalP activity suggest that mutant bacteria are unable to efficiently integrate nutritional cues from CCM with growth rate and cell size, as mutant *malP* bacteria showed no changes to doubling time despite forming longer cells and showing significant heterogeneity in size, relative to the wild type. The time it takes a cell to replicate its genome and divide (C + D period), along with its size at birth, are the main determinants of individual size and overall growth rate in *E. coli*[104]. MalP deficient strains never formed cells that were smaller than the wild type (Chapter 2), so birth size is likely increased in these mutants. It was clear from confocal imagery and flow cytometry analysis that DNA replication is defective, which would undoubtedly alter the length of C + D. It would be worthwhile to confirm these assumptions in the future, but they place MalP, either directly or indirectly, within two spheres of size control – one relating to a larger signal transduction pathway affecting size and growth in response environmental stimuli (e.g. nutrients, osmolarity) and the other involved in coordinating DNA replication and cell division in response to the environment. These putative roles are not necessarily mutually exclusive.

The supercoiling state of DNA is an important factor that influences gene expression levels, DNA replication rates and recombination and repair mechanisms and is itself affected by transcription rates, DNA replication, the activity of topoisomerases and DNA gyrase and DNA being bound (constrained) by molecules like NAPs[226,244–246]. DNA supercoiling is sensitive to changes in environmental conditions like medium osmolarity, oxygen levels, temperature and nutrient abundance[246]. Supporting the idea that nutrient-dependent changes in DNA supercoiling may impact replication rates, it was shown that ppGpp accumulation affects the supercoiling status at *oriC*, by downregulating active transcription, thereby indirectly repressing DNA replication by creating a less favourable environment for DnaA to bind during stringent growth arrest[192].

Since deleting *malP* has a pleiotropic effect on diverse cellular processes it is tempting to argue a role for MalP in regulating cellular physiology by indirectly impacting ppGpp levels possibly through influencing adenylate pools, as disrupting ppGpp homeostasis would undoubtedly affect DNA replication, cell size and division[38]. Since ppGpp is known to be the main inhibitor of *dnaA* transcription[247] impaired ppGpp synthesis could explain why DnaA protein levels were elevated during stationary phase in the MalP deficient strains examined under Chapter 2. However, a more direct interaction between MalP and HU[199] or TopA[199] (encoding topoisomerase I) may somehow affect the architecture/superhelicity of the nucleoid. As MalP has been shown to interact with at least two members[199] of the PDH^{c} it becomes tempting to speculate that these enzymes are part of metabolic microcompartments (metabolons[63,248]) localised at specific sites within the cell to facilitate the channelling of metabolites (e.g. pyruvate) which could affect DNA replication rates. It would thus be practical to explore metabolic pathways (e.g. glycolysis and ppGpp biosynthesis) in these mutants

using flux analysis and to assess the localization of certain enzymes (like PykA and MalP) or protein complexes (PDH^c) in mutant strains using GFP analysis.

Whilst a role for glycogen/maltodextrin turnover has been discussed within the context of CCM, less clear is the exact role of sugar metabolism within the context of stressful situations like heat or osmotic shock. The survival rates of *E. coli* that accumulate glycogen are enhanced over mutants unable to synthesize this polymer when exposed to heat shock[12]. In eukaryotes, glycogen turnover not only provides carbon for energy, but also for osmolyte production so its catabolism allows the cell to better adapt to situations like hyperosmotic stress[249]. *E. coli* are known to accumulate osmoprotectants[250], like trehalose (formed from G6P and UDPG) in response to osmotic shock – a condition known to stimulate UDPG biosynthesis. This nucleotide sugar may be integrated into the cell envelope to help endure the trauma but could, in theory[93], stimulate OpgH's inhibitory action on cell division, delaying septation so the cell can address the stressful stimulus in a timely and coordinated manner.

Cell size, C + D period and DnaA levels are altered in response to medium osmolarity in *E. coli*[98]. The hydrophobic forces that chiefly affect the stability and structure of the DNA double helix and putatively impact the actions of DNA repair enzymes (like RecA) and polymerases are affected by the water content of the cell[251]. The question thus arises whether sugar metabolism (MalP activity specifically) plays a larger role in osmoregulation which, in turn, affects DNA metabolism and cell size? This would explain why suppressions to size defects are observed upon deleting *opgH* (increased UDPG and OpgH activity during osmotic stress) or *sulA* (problems with osmoregulation could lead to defects with DNA metabolism/structure which would induce the SOS response), and partial reversions upon deleting *hupA* or *hupB* (HU affects DNA metabolism/structure, and regulates expression of genes involved in osmoregulation and maltodextrin metabolism). Medium osmolarity has been shown to affect induction of *mal* genes[252] so, taken together, osmoregulation may be a lucrative pathway to explore within the context of glycogen/maltodextrin metabolism, DNA metabolism and cell size.

Overall, this thesis has examined why mutants affected in glycogen turnover accumulate longer cells than wild type *E. coli* cells. It has also produced a wide number of mutant strains that will help in elucidating the underlying mechanisms leading to this phenotype in future research projects. Although it is unclear if these mechanisms are universal in influencing cell size in all bacteria, it is possible that this understanding will help in the development of new drugs that can impair their growth. Gaining insight into the intricate affiliation between glycogen and protein metabolism and coaggregation of these macromolecules could provide invaluable insight into bacterial aging and the problematic multidrug tolerant persister state associated, at least in part, with protein aggregate turnover.

5. References

1. Adeva-Andany, M. M., González-Lucán, M., Donapetry-García, C., Fernández-Fernández, C. & Ameneiros-Rodríguez, E. Glycogen metabolism in humans. *BBA Clin.* **5**, 85–100 (2016).

2. Wilson, W. A. *et al.* Regulation of glycogen metabolism in yeast and bacteria. *FEMS Microbiol. Rev.* **34**, 952–85 (2010).

3. Ballicora, M. A., Iglesias, A. A. & Preiss, J. ADP-glucose pyrophosphorylase, a regulatory enzyme for bacterial glycogen synthesis. *Microbiol. Mol. Biol. Rev.* **67**, 213–25 (2003).

4. Park, K.-H. Roles of Enzymes in Glycogen Metabolism and Degradation in *Escherichia coli*. *J. Appl. Glycosci.* **62**, 37–45 (2015).

5. Cedergren, B. & Holme, T. On the glycogen in Escherichia coli B electron microscopy of ultrathin sections of cells. *J. Ultrastruct. Res.* **3**, 70–3 (1959).

6. Ovecka, M. *et al.* A sensitive method for confocal fluorescence microscopic visualization of starch granules in iodine stained samples. *Plant Signal. Behav.* **7**, 1146–1150 (2012).

7. Boehm, A. *et al.* Genetic Manipulation of Glycogen Allocation Affects Replicative Lifespan in *E. coli*. *PLoS Genet.* **12**, 1–17 (2016).

8. Makinoshima, H. *et al.* Growth phase-coupled alterations in cell structure and function of *Escherichia coli*. *J. Bacteriol.* **185**, 1338–45 (2003).

9. Morán-Zorzano, M. T. *et al.* Occurrence of more than one important source of ADPglucose linked to glycogen biosynthesis in *Escherichia coli* and *Salmonella enterica*. *FEBS Lett.* **581**, 4423–4429 (2007).

10. Eydallin, G. *et al.* An *Escherichia coli* mutant producing a truncated inactive form of GlgC synthesizes glycogen: Further evidences for the occurrence of various important sources of ADPglucose in enterobacteria. *FEBS Lett.* **581**, 4417–4422 (2007).

11. Alonso-Casajús, N. *et al.* Glycogen phosphorylase, the product of the *glgP* gene, catalyzes glycogen breakdown by removing glucose units from the nonreducing ends in *Escherichia coli*. *J. Bacteriol.* **188**, 5266–5272 (2006).

12. Bruhn-Olszewska, B. *et al.* Physiologically distinct subpopulations formed in *Escherichia coli* cultures in response to heat shock. *Microbiol. Res.* **209**, 33–42 (2018).

13. Hecker, M., Schroeter, A., Triider, K. & Maeh, F. Role of *relA* mutation in the survival of amino acid-starved *Escherichia coli*. *Arch. Microbiol.* **143**, 400–401 (1986).

14. Romeo, T., Black, J. & Preiss, J. Genetic regulation of glycogen biosynthesis in *Escherichia coli*: In vivo effects of the catabolite repression and stringent response systems in *glg* gene expression. *Curr. Microbiol.* **21**, 131–137 (1990).

15. Strange, R. E. Bacterial “Glycogen” and Survival. *Nature* **220**, 606–607 (1968).

16. Preiss, J. Bacterial Glycogen Synthesis and its Regulation. *Annu. Rev. Microbiol.* **38**, 419–458 (1984).

17. Eydallin, G. *et al.* Genome-wide screening of genes whose enhanced expression affects glycogen accumulation in *Escherichia coli*. *DNA Res.* **17**, 61–71 (2010).

18. Jones, S. A. *et al.* Glycogen and maltose utilization by *Escherichia coli* O157:H7 in the mouse intestine. *Infect. Immun.* **76**, 2531–2540 (2008).

19. Morin, M., Delphine Ropers, Eugenio Cinquemani, J.-C. P., Enjalbert, B. & Cocaign-Bousqueta, M. The Csr System Regulates *Escherichia coli* Fitness by Controlling Glycogen Accumulation and Energy Levels. *MBio* **8**, 1–14 (2017).

20. Montero, M. *et al. Escherichia coli* glycogen genes are organized in a single *glgBXCAP* transcriptional unit possessing an alternative suboperonic promoter within *glgC* that directs *glgAP* expression. *Biochem. J.* **433**, 107–117 (2011).

21. Traxler, M. F. *et al.* Discretely calibrated regulatory loops controlled by ppGpp partition gene induction across the ‘feast to famine’ gradient in *Escherichia coli*. *Mol. Microbiol.* **79**, 830–45 (2011).

22. Davidson, A. L., Dassa, E., Orelle, C. & Chen, J. Structure, Function, and Evolution of Bacterial ATP-Binding Cassette Systems. *Microbiol. Mol. Biol. Rev.* **72**, 317–364 (2008).

23. Kotrba, P., Inui, M. & Yukawa, H. Bacterial phosphotransferase system (PTS) in carbohydrate uptake and control of carbon metabolism. *J. Biosci. Bioeng.* **92**, 502–17 (2001).

24. Joshi, J. G. & Handler, P. Phosphoglucomutase. I. Purification and properties of phosphoglucomutase from *Escherichia coli*. *J. Biol. Chem.* **239**, 2741–51 (1964).

25. Hill, M. A., Kaufmann, K., Otero, J. & Preiss, J. Biosynthesis of bacterial glycogen. Mutagenesis of a catalytic site residue of ADP-glucose pyrophosphorylase from *Escherichia coli*. *J. Biol. Chem.* **266**, 12455–60 (1991).

26. Kumar, A., Larsen, C. E. & Preiss, J. Biosynthesis of bacterial glycogen. Primary structure of *Escherichia coli* ADP-glucose:alpha-1,4-glucan, 4-glucosyltransferase as deduced from the nucleotide sequence of the *glgA* gene. *J. Biol. Chem.* **261**, 16256–9 (1986).

27. Preiss, J. Bacterial Glycogen Inclusions: Enzymology and Regulation of Synthesis. in *Inclusions in Prokaryotes* 71–108 (Springer-Verlag, 2006). doi:10.1007/3-540-33774-1_4

28. Park, J. T. *et al.* Role of maltose enzymes in glycogen synthesis by *Escherichia coli*. *J. Bacteriol.* **193**, 2517–2526 (2011).

29. Boyer, C. & Preiss, J. Biosynthesis of bacterial glycogen. Purification and properties of the *Escherichia coli* B α-1,4-glucan:α-1,4-glucan 6-glycosyltransferase. *Biochemistry* **16**, 3693–3699 (1977).

30. Dauvillée, D. *et al.* Role of the *Escherichia coli glgX* gene in glycogen metabolism. *J. Bacteriol.* **187**, 1465–73 (2005).

31. Preiss, J. Glycogen: Biosynthesis and Regulation. *EcoSal Plus* **3**, 1–26 (2009).

32. Guan, H., Li, P., Imparl-Radosevich, J., Preiss, J. & Keeling, P. Comparing the Properties of *Escherichia coli* Branching Enzyme and Maize Branching Enzyme. *Arch. Biochem. Biophys.* **342**, 92–98 (1997).

33. Kawaguchi, K., Fox, J., Holmes, E., Boyer, C. & Preiss, J. De Novo synthesis of *Escherichia coli* glycogen is due to primer associated with glycogen synthase and activation by branching enzyme. *Arch. Biochem. Biophys.* **190**, 385–397 (1978).

34. Holme, T., Palmstierna, H., Aurivillius, B., Eliasson, N. A. & Thorell, B. Changes in Glycogen and Nitrogen-containing Compounds in *Escherichia coli* B during Growth in Deficient Media. II. Phosphorus and Sulphur Starvation. *Acta Chem. Scand.* **10**, 1553–1556 (1956).

35. Dietzler, D. N., Leckie, M. P. & Lais, C. J. Rates of glycogen synthesis and the cellular levels of ATP and FDP during exponential growth and the nitrogen-limited stationary phase of *Escherichia coli* W4597 (K). *Arch. Biochem. Biophys.* **156**, 684–693 (1973).

36. Romeo, T. & Preiss, J. Genetic regulation of glycogen biosynthesis in *Escherichia coli*: in vitro effects of cyclic AMP and guanosine 5'-diphosphate 3'-diphosphate and analysis of in vivo transcripts. *J. Bacteriol.* **171**, 2773–2782 (1989).

37. Maaløe, O. & Kjeldgaard, N. O. Control of macromolecular synthesis; a study of DNA, RNA, and protein synthesis in bacteria. 1–284 (1966).

38. Traxler, M. F. *et al.* The global, ppGpp-mediated stringent response to amino acid starvation in *Escherichia coli*. *Mol. Microbiol.* **68**, 1128–1148 (2008).

39. Cashel, M. & Gallant, J. Two Compounds implicated in the Function of the *RC* Gene of *Escherichia coli*. *Nature* **221**, 838–841 (1969).

40. Gentry, D. R. & Cashel, M. Mutational analysis of the *Escherichia coli spoT* gene identifies distinct but overlapping regions involved in ppGpp synthesis and degradation. *Mol. Microbiol.* **19**, 1373–84 (1996).

41. Magnusson, L. U., Farewell, A. & Nyström, T. ppGpp: a global regulator in *Escherichia coli*. *Trends Microbiol.* **13**, 236–242 (2005).

42. Xiao, H. *et al.* Residual guanosine 3',5'-bispyrophosphate synthetic activity of *relA* null mutants can be eliminated by *spoT* null mutations. *J. Biol. Chem.* **266**, 5980–90 (1991).

43. Vinella, D., Albrecht, C., Cashel, M. & D'Ari, R. Iron limitation induces SpoT-dependent accumulation of ppGpp in *Escherichia coli*. *Mol. Microbiol.* **56**, 958–970 (2005).

44. Battesti, A. & Bouveret, E. Acyl carrier protein/SpoT interaction, the switch linking SpoT-dependent stress response to fatty acid metabolism. *Mol. Microbiol.* **62**, 1048–1063 (2006).

45. Artsimovitch, I. *et al.* Structural basis for transcription regulation by alarmone ppGpp. *Cell* **117**, 299–310 (2004).

46. Paul, B. J., Ross, W., Gaal, T. & Gourse, R. L. rRNA Transcription in *Escherichia coli*. *Annu. Rev. Genet.* **38**, 749–770 (2004).

47. Barker, M. M., Gaal, T., Josaitis, C. A. & Gourse, R. L. Mechanism of regulation of transcription initiation by ppGpp. I. Effects of ppGpp on transcription initiation in vivo and in vitro. *J. Mol. Biol.* **305**, 673–688 (2001).

48. Barker, M. M., Gaal, T. & Gourse, R. L. Mechanism of regulation of transcription initiation by ppGpp. II. Models for positive control based on properties of RNAP mutants and competition for RNAP. *J. Mol. Biol.* **305**, 689–702 (2001).

49. Taguchi, M., Izui, K. & Katsuki, H. Augmentation of glycogen synthesis under stringent control in *Escherichia coli*. *J. Biochem.* **88**, 379–87 (1980).

50. Ferullo, D. J. & Lovett, S. T. The stringent response and cell cycle arrest in *Escherichia coli*. *PLoS Genet.* **4**, 21–23 (2008).

51. Montero, M. *et al.* Escherichia coli glycogen metabolism is controlled by the PhoP-PhoQ regulatory system at submillimolar environmental Mg2+ concentrations, and is highly interconnected with a wide variety of cellular processes. *Biochem. J.* **424**, 129–141 (2009).

52. Leckie, M. P., Tieber, V. L., Porter, S. E., Roth, W. G. & Dietzler, D. N. Independence of cyclic AMP and *relA* gene stimulation of glycogen synthesis in intact *Escherichia coli* cells. *J. Bacteriol.* **161**, 133–40 (1985).

53. Leckie, M. P., Ng, R. H., Porter, S. E., Compton, D. R. & Dietzler, D. N. Regulation of bacterial glycogen synthesis. Stimulation of glycogen synthesis by endogenous and exogenous cyclic adenosine 3':5'-monophosphate in *Escherichia coli* and the requirement for a functional *CRP* gene. *J. Biol. Chem.* **6**, 3813–3824 (1983).

54. Gosset, G., Zhang, Z., Nayyar, S., Cuevas, W. A. & Saier, M. H. Transcriptome analysis of Crp-dependent catabolite control of gene expression in *Escherichia coli*. *J. Bacteriol.* **186**, 3516–24 (2004).

55. Zheng, D. Identification of the CRP regulon using in vitro and in vivo transcriptional profiling. *Nucleic Acids Res.* **32**, 5874–5893 (2004).

56. Hengge-Aronis, R. & Fischer, D. Identification and molecular analysis of *glgS*, a novel growth-phase-regulated and RpoS-dependent gene involved in glycogen synthesis in *Escherichia coli*. *Mol. Microbiol.* **6**, 1877–1886 (1992).

57. Eydallin, G. *et al.* Genome-wide screening of genes affecting glycogen metabolism in *Escherichia coli* K-12. *FEBS Lett.* **581**, 2947–2953 (2007).

58. Monsieurs, P. *et al.* Comparison of the PhoPQ regulon in *Escherichia coli* and *Salmonella typhimurium*. *J. Mol. Evol.* **60**, 462–474 (2005).

59. Minagawa, S. *et al.* Identification and molecular characterization of the Mg2+ stimulon of *Escherichia coli*. *J. Bacteriol.* **185**, 3696–702 (2003).

60. Yamamoto, K., Ogasawara, H., Fujita, N., Utsumi, R. & Ishihama, A. Novel mode of transcription regulation of divergently overlapping promoters by PhoP, the regulator of two-component system sensing external magnesium availability. *Mol. Microbiol.* **45**, 423–438 (2002).

61. Moreno-Bruna, B. *et al.* Adenosine diphosphate sugar pyrophosphatase prevents glycogen biosynthesis in *Escherichia coli*. *Proc. Natl. Acad. Sci. U. S. A.* **98**, 8128–32 (2001).

62. Morán-Zorzano, M. T. *et al. Escherichia coli* AspP activity is enhanced by macromolecular crowding and by both glucose-1,6-bisphosphate and nucleotide-sugars. *FEBS Lett.* **581**, 1035–1040 (2007).

63. Morán-Zorzano, M. T. *et al.* Cytoplasmic *Escherichia coli* ADP sugar pyrophosphatase binds to cell membranes in response to extracellular signals as the cell population density increases. *FEMS Microbiol. Lett.* **288**, 25–32 (2008).

64. Edwards, A. N. *et al.* Circuitry linking the Csr and stringent response global regulatory systems. *Mol. Microbiol.* **80**, 1561–1580 (2011).

65. Romeo, T., Gong, M., Mu Ya Liu & Brun-Zinkernagel, A. M. Identification and molecular characterization of *csrA*, a pleiotropic gene from *Escherichia coli* that affects glycogen biosynthesis, gluconeogenesis, cell size, and surface properties. *J. Bacteriol.* **175**, 4744–4755 (1993).

66. Sabnis, N. A., Yang, H. & Romeo, T. Pleiotropic regulation of central carbohydrate metabolism in *Escherichia coli* via the gene *csrA*. *J. Biol. Chem.* **270**, 29096–104 (1995).

67. Morin, M. *et al.* The post-transcriptional regulatory system CSR controls the balance of metabolic pools in upper glycolysis of *Escherichia coli*. *Mol. Microbiol.* **100**, 686–700 (2016).

68. Yang, H., Liu, M. Y. & Romeo, T. Coordinate genetic regulation of glycogen catabolism and biosynthesis in *Escherichia coli* via the csrA gene product. *J. Bacteriol.* **178**, 1012–1017 (1996).

69. Baker, C. S., Morozov, I., Suzuki, K., Romeo, T. & Babitzke, P. CsrA regulates glycogen biosynthesis by preventing translation of *glgC* in *Escherichia coli*. *Mol. Microbiol.* **44**, 1599–610 (2002).

70. Bren, A. *et al.* Glucose becomes one of the worst carbon sources for *E.coli* on poor nitrogen sources due to suboptimal levels of cAMP. *Sci. Rep.* **6**, 2–11 (2016).

71. Boos, W. & Shuman, H. Maltose/Maltodextrin System of *Escherichia coli*: Transport, Metabolism, and Regulation. *Microbiol. Mol. Biol. Rev.* **62**, 204–229 (1998).

72. Seok, Y.-J., Koo, B.-M., Sondej, M. & Peterkofsky, A. Regulation of *E. coli* Glycogen Phosphorylase Activity by HPr. *J. Mol. Microbiol. Biotechnol* **3**, 385–393 (2001).

73. Yamamotoya, T. *et al.* Glycogen is the primary source of glucose during the lag phase of *E. coli* proliferation. *Biochim. Biophys. Acta - Proteins Proteomics* **1824**, 1442–1448 (2012).

74. Wang, L. & Wise, M. J. Glycogen with short average chain length enhances bacterial durability. *Naturwissenschaften* **98**, 719–729 (2011).

75. Dippel, R. & Boos, W. The Maltodextrin System of *Escherichia coli*: Metabolism and Transport. *J. Bacteriol.* **187**, 8322–8331 (2005).

76. Schwartz, M. Phenotypic expression and genetic localization of mutations affecting maltose metabolism in *Escherichia coli* K 12. *Ann. Inst. Pasteur (Paris).* **112**, 673–98 (1967).

77. Dippel, R., Bergmiller, T. & Bo, A. The Maltodextrin System of *Escherichia coli*: Glycogen-Derived Endogenous Induction and Osmoregulation. *J. Bacteriol.* **187**, 8332–8339 (2005).

78. Weiss, S. C., Skerra, A. & Schiefner, A. Structural Basis for the Interconversion of Maltodextrins by MalQ, the Amylomaltase of *Escherichia coli*. *J. Biol. Chem.* **290**, 21352–64 (2015).

79. Palmer, T. N., Ryman, B. E. & Whelan, W. J. The Action Pattern of Amylomaltase from *Escherichia coli*. *Eur. J. Biochem.* **69**, 105–115 (1976).

80. Chapon, C. Role of the catabolite activator protein in the maltose regulon of *Escherichia coli*. *J. Bacteriol.* **150**, 722–9 (1982).

81. Lin, E. C. C. & Lynch, A. S. *Regulation of Gene Expression in Escherichia coli*. (Springer US, 1996). doi:10.1007/978-1-4684-8601-8

82. Kuhlmann, N. *et al.* Transcription of *malP* is subject to phosphotransferase system-dependent regulation in *Corynebacterium glutamicum*. *Microbiol. (United Kingdom)* **161**, 1830–1843 (2015).

83. Constantinidou, C. *et al.* A reassessment of the FNR regulon and transcriptomic analysis of the effects of nitrate, nitrite, NarXL, and NarQP as *Escherichia coli* K12 adapts from aerobic to anaerobic growth. *J. Biol. Chem.* **281**, 4802–4815 (2006).

84. Oberto, J., Nabti, S., Jooste, V., Mignot, H. & Rouviere-Yaniv, J. The HU regulon is composed of genes responding to anaerobiosis, acid stress, high osmolarity and SOS induction. *PLoS One* **4**, (2009).

85. Bahloul, A., Boubrik, F. & Rouviere-Yaniv, J. Roles of *Escherichia coli* histone-like protein HU in DNA replication: HU-beta suppresses the thermosensitivity of *dnaA46ts*. *Biochimie* **83**, 219–29 (2001).

86. Williams, A. B. & Foster, P. L. The *Escherichia coli* histone-like protein HU has a role in stationary phase adaptive mutation. *Genetics* **177**, 723–735 (2007).

87. Schinzel, R. & Nidetzky, B. Bacterial α-glucan phosphorylases. *FEMS Microbiol. Lett.* **171**, 73–79 (1999).

88. Chapon, C. Expression of *malT*, the regulator gene of the maltose region in *Escherichia coli*, is limited both at transcription and translation. *EMBO J.* **1**, 369–374 (1982).

89. Ribbons, D. W. & Dawes, E. A. Environmental and growth conditions affecting the endogenous metabolism of bacteria. *Ann. N. Y. Acad. Sci.* **102**, 564–586 (2006).

90. Wilkinson, J. F. Carbon and Energy Storage in Bacteria. *J. Gen. Microbiol.* **32**, 171–176 (1963).

91. Weissborn, A. C., Liu, Q., Rumley, M. K. & Kennedy, E. P. UTP: alpha-D-glucose-1-phosphate uridylyltransferase of *Escherichia coli*: isolation and DNA sequence of the *galU* gene and purification of the enzyme. *J. Bacteriol.* **176**, 2611–2618 (1994).

92. Shapiro, J. A. Chromosomal location of the gene determining uridine diphoglucose formation in *Escherichia coli* K-12. *J. Bacteriol.* **92**, 518–20 (1966).

93. Hill, N. S., Buske, P. J., Shi, Y. & Levin, P. A. A Moonlighting Enzyme Links *Escherichia coli* Cell Size with Central Metabolism. *PLoS Genet.* **9**, (2013).

94. Genevaux, P., Bauda, P., DuBow, M. S. & Oudega, B. Identification of Tn10 insertions in the *rfaG*, *rfaP*, and *galU* genes involved in lipopolysaccharide core biosynthesis that affect *Escherichia coli* adhesion. *Arch. Microbiol.* **172**, 1–8 (1999).

95. Silljé, H. H. W. *et al.* Function of trehalose and glycogen in cell cycle progression and cell viability in *Saccharomyces cerevisiae*. *J. Bacteriol.* **181**, 396–400 (1999).

96. Planutis, K. S., Planutiene, M. V., Lazareva, A. V., Sel'kov, E. E. & Evtodienko, Y. V. Polyglucose content in the cell and the rate of glucose consumption during synchronous growth of *Escherichia coli*. *Biochem. Biophys. Res. Commun.* **109**, 583–587 (1982).

97. Mueller, E. A. & Levin, P. A. Environmental pH impacts division assembly and cell size in Escherichia coli. *bioRxiv* (2019). doi:10.1101/747808

98. Dai, X. & Zhu, M. High Osmolarity Modulates Bacterial Cell Size through Reducing Initiation Volume in *Escherichia coli*. *mSphere* **3**, (2018).

99. Schaechter, M., Maaløe, O. & Kjeldgaard, N. O. Dependency on Medium and Temperature of Cell Size and Chemical Composition during Balanced Growth of *Salmonella typhimurium*. *J. Gen. Microbiol.* **19**, 592–606 (1958).

100. Helmstetter, C. E. & Cooper, S. DNA Synthesis during the Division Cycle of Rapidly Growing *Escherichia coli* B/r. *J. Mol. Biol.* **31**, 507–518 (1968).

101. Donachie, W. D. Relationship between Cell Size and Time of Initiation of DNA Replication. *Nature* **219**, 1077–1079 (1968).

102. Campos, M. *et al.* A constant size extension drives bacterial cell size homeostasis. *Cell* **159**, 1433–1446 (2014).

103. Taheri-Araghi, S. *et al.* Cell-size control and homeostasis in bacteria. *Curr. Biol.* **25**, 385–391 (2015).

104. Si, F. *et al.* Invariance of Initiation Mass and Predictability of Cell Size in *Escherichia coli*. *Curr. Biol.* **27**, 1278–1287 (2017).

105. Si, F. *et al.* Mechanistic Origin of Cell-Size Control and Homeostasis in Bacteria. *Curr. Biol.* **29**, 1760-1770.e7 (2019).

106. Vadia, S. *et al.* Fatty Acid Availability Sets Cell Envelope Capacity and Dictates Microbial Cell Size. *Curr. Biol.* **27**, 1757-1767.e5 (2017).

107. Westfall, C. S. & Levin, P. A. Comprehensive analysis of central carbon metabolism illuminates connections between nutrient availability, growth rate, and cell morphology in *Escherichia coli*. *PLOS Genet.* **14**, e1007205 (2018).

108. Marshall, W. F. *et al.* What determines cell size? *BMC Biol.* **10**, 101 (2012).

109. Pierucci, O. Dimensions of *Escherichia coli* at various growth rates: model for envelope growth. *J. Bacteriol.* **135**, 559–574 (1978).

110. Sargent, M. G. Control of cell length in *Bacillus subtilis*. *J. Bacteriol.* **123**, 7–19 (1975).

111. Cooper, S. & Helmstetter, C. E. Chromosome replication and the division cycle of *Escherichia coli* B/r. *J. Mol. Biol.* **31**, 519–540 (1968).

112. Fuller, R. S., Funnell, B. E. & Kornberg, A. The DnaA protein complex with the *E. coli* chromosomal replication origin (*oriC*) and other DNA sites. *Cell* **38**, 889–900 (1984).

113. Løbner-Olesen, A., Skarstad, K., Hansen, F. G., von Meyenburg, K. & Boye, E. The DnaA protein determines the initiation mass of *Escherichia coli* K-12. *Cell* **57**, 881–889 (1989).

114. Ozaki, S. & Katayama, T. DnaA structure, function, and dynamics in the initiation at the chromosomal origin. *Plasmid* **62**, 71–82 (2009).

115. Hill, N. S., Kadoya, R., Chattoraj, D. K. & Levin, P. A. Cell size and the initiation of DNA replication in bacteria. *PLoS Genet.* **8**, 14–16 (2012).

116. Hirota, Y., Ryter, A. & Jacob, F. Thermosensitive Mutants of *E. coli* Affected in the Processes of DNA Synthesis and Cellular Division. *Cold Spring Harb. Symp. Quant. Biol.* **33**, 677–693 (1968).

117. Flåtten, I., Fossum-Raunehaug, S., Taipale, R., Martinsen, S. & Skarstad, K. The DnaA Protein Is Not the Limiting Factor for Initiation of Replication in *Escherichia coli*. *PLoS Genet.* **11**, 1–22 (2015).

118. Hajduk, I. V., Rodrigues, C. D. A. & Harry, E. J. Connecting the dots of the bacterial cell cycle: Coordinating chromosome replication and segregation with cell division. *Semin. Cell Dev. Biol.* **53**, 2–9 (2016).

119. Wu, L. J., Franks, A. H. & Wake, R. G. Replication through the terminus region of the *Bacillus subtilis* chromosome is not essential for the formation of a division septum that partitions the DNA. *J. Bacteriol.* **177**, 5711–5715 (1995).

120. Dewachter, L., Verstraeten, N., Fauvart, M. & Michiels, J. An integrative view of cell cycle control in *Escherichia coli*. *FEMS Microbiol. Rev.* **42**, 116–136 (2018).

121. Morcinek-Orłowska, J., Galińska, J. & Glinkowska, M. K. When size matters - coordination of growth and cell cycle in bacteria. *Acta Biochim. Pol.* **66**, 139–146 (2019).

122. Levin, P. A. & Taheri-Araghi, S. One is Nothing without the Other: Theoretical and Empirical Analysis of Cell Growth and Cell Cycle Progression. *J. Mol. Biol.* **431**, 2061–2067 (2019).

123. Wang, P. *et al.* Robust growth of *Escherichia coli*. *Curr. Biol.* **20**, 1099–103 (2010).

124. Campos, M. *et al.* Genomewide phenotypic analysis of growth, cell morphogenesis, and cell cycle events in *Escherichia coli*. *Mol. Syst. Biol.* **14**, e7573 (2018).

125. Wallden, M., Fange, D., Lundius, E. G., Baltekin, Ö. & Elf, J. The Synchronization of Replication and Division Cycles in Individual *E. coli* Cells. *Cell* **166**, 729–739 (2016).

126. Basan, M. *et al.* Inflating bacterial cells by increased protein synthesis. *Mol. Syst. Biol.* **11**, 836–836 (2015).

127. Osella, M., Nugent, E. & Cosentino Lagomarsino, M. Concerted control of *Escherichia coli* cell division. *Proc. Natl. Acad. Sci. U. S. A.* **111**, 3431–5 (2014).

128. Micali, G., Grilli, J., Marchi, J., Osella, M. & Lagomarsino, M. C. Dissecting the control mechanisms for DNA replication and cell division in *E. coli*. *bioRxiv* 308155 (2018). doi:10.1101/308155

129. Wehrens, M. *et al.* Size Laws and Division Ring Dynamics in Filamentous *Escherichia coli* cells. *Curr. Biol.* **28**, 972-979.e5 (2018).

130. Begg, K. J. & Donachie, W. D. Division planes alternate in spherical cells of *Escherichia coli*. *J. Bacteriol.* **180**, 2564–2567 (1998).

131. Rotman, E., Bratcher, P. & Kuzminov, A. Reduced lipopolysaccharide phosphorylation in *Escherichia coli* lowers the elevated *ori/ter* ratio in seqA mutants. *Mol. Microbiol.* **72**, 1273–1292 (2009).

132. Kato, J. & Katayama, T. Hda, a novel DnaA-related protein, regulates the replication cycle in *Escherichia coli*. *EMBO J.* **20**, 4253–62 (2001).

133. Norris, V. Phospholipid flip-out controls the cell cycle of *Escherichia coli*. *J. Theor. Biol.* **139**, 117–128 (1989).

134. Atlung, T., Clausen, E. S. & Hansen, F. G. Autoregulation of the *dnaA* gene of *Escherichia coli* K12. *MGG Mol. Gen. Genet.* **200**, 442–450 (1985).

135. Ishida, T. *et al.* DiaA, a novel DnaA-binding protein, ensures the timely initiation of *Escherichia coli* chromosome replication. *J. Biol. Chem.* **279**, 45546–45555 (2004).

136. Kitagawa, R., Ozaki, T., Moriya, S. & Ogawa, T. Negative control of replication initiation by a novel chromosomal locus exhibiting exceptional affinity for *Escherichia coli* DnaA protein. *Genes Dev.* **12**, 3032–3043 (1998).

137. Waldminghaus, T. & Skarstad, K. The *Escherichia coli* SeqA protein. *Plasmid* **61**, 141–150 (2009).

138. Dai, K. & Lutkenhaus, J. The proper ratio of FtsZ to FtsA is required for cell division to occur in *Escherichia coli*. *J. Bacteriol.* **174**, 6145–6151 (1992).

139. De Boer, P. A. J., Crossley, R. E. & Rothfield, L. I. Roles of MinC and MinD in the site-specific septation block mediated by the MinCDE system of *Escherichia coli*. *J. Bacteriol.* **174**, 63–70 (1992).

140. Bi, E. & Lutkenhaus, J. Cell division inhibitors SulA and MinCD prevent formation of the FtsZ ring. *J. Bacteriol.* **175**, 1118–1125 (1993).

141. Pichoff, S. & Lutkenhaus, J. Unique and overlapping roles for ZipA and FtsA in septal ring assembly in *Escherichia coli*. *EMBO J.* **21**, 685–693 (2002).

142. Aarsman, M. E. G. *et al.* Maturation of the *Escherichia coli* divisome occurs in two steps. *Mol. Microbiol.* **55**, 1631–1645 (2005).

143. Osawa, M., Anderson, D. E. & Erickson, H. P. Reconstitution of contractile FtsZ rings in liposomes. *Science* **320**, 792–794 (2008).

144. Mingorance, J., Rivas, G., Vélez, M., Gómez-Puertas, P. & Vicente, M. Strong FtsZ is with the force: Mechanisms to constrict bacteria. *Trends Microbiol.* **18**, 348–356 (2010).

145. Bisson-Filho, A. W. *et al.* Treadmilling by FtsZ filaments drives peptidoglycan synthesis and bacterial cell division. *Science* **355**, 739–743 (2017).

146. Coltharp, C., Buss, J., Plumer, T. M. & Xiao, J. Defining the rate-limiting processes of bacterial cytokinesis. *Proc. Natl. Acad. Sci.* **113**, E1044–E1053 (2016).

147. Pinho, M. G., Kjos, M. & Veening, J.-W. How to get (a)round: mechanisms controlling growth and division of coccoid bacteria. *Nat. Rev. Microbiol.* **11**, 601–614 (2013).

148. de Boer, P. A., Crossley, R. E. & Rothfield, L. I. A division inhibitor and a topological specificity factor coded for by the minicell locus determine proper placement of the division septum in *E. coli*. *Cell* **56**, 641–9 (1989).

149. Lutkenhaus, J., Pichoff, S. & Du, S. Bacterial cytokinesis: From Z ring to divisome. *Cytoskeleton* **69**, 778–790 (2012).

150. Mulder, E. & Woldringh, C. L. Actively replicating nucleoids influence positioning of division sites in *Escherichia coli* filaments forming cells lacking DNA. *J. Bacteriol.* **171**, 4303–4314 (1989).

151. Wu, L. J. & Errington, J. Coordination of cell division and chromosome segregation by a nucleoid occlusion protein in *Bacillus subtilis*. *Cell* **117**, 915–925 (2004).

152. Bernhardt, T. G. & de Boer, P. A. J. SlmA, a nucleoid-associated, FtsZ binding protein required for blocking septal ring assembly over chromosomes in *E. coli*. *Mol. Cell* **18**, 555–64 (2005).

153. Wu, L. J. & Errington, J. Nucleoid occlusion and bacterial cell division. *Nat. Rev. Microbiol.* **10**, 8–12 (2012).

154. Wainwright, M., Canham, L. T., Al-Wajeeh, K. & Reeves, C. L. Morphological changes (including filamentation) in *Escherichia coli* grown under starvation conditions on silicon wafers and other surfaces. *Lett. Appl. Microbiol.* **29**, 224–227 (1999).

155. Simmons, L. A., Foti, J. J., Cohen, S. E. & Walker, G. C. The SOS Regulatory Network. *EcoSal Plus* **2008**, (2008).

156. Janion, C., Sikora nee Wójcik, A., Nowosielska, A. & Grzesiuk, E. Induction of the SOS response in starved *Escherichia coli*. *Environ. Mol. Mutagen.* **40**, 129–133 (2002).

157. Miller, C. *et al.* SOS response induction by beta-lactams and bacterial defense against antibiotic lethality. *Science* **305**, 1629–31 (2004).

158. Cohen, S. S. & Barner, H. D. Studies on unbalanced growth in *Escherichia coli*. *Proc. Natl. Acad. Sci. U. S. A.* **40**, 885–93 (1954).

159. Little, J. W. & Mount, D. W. The SOS regulatory system of *Escherichia coli*. *Cell* **29**, 11–22 (1982).

160. Witkin, E. M. Ultraviolet mutagenesis and inducible DNA repair in *Escherichia coli*. *Bacteriol. Rev.* **40**, 869–907 (1976).

161. Huisman, O., D'Ari, R. & Gottesman, S. Cell-division control in *Escherichia coli*: Specific induction of the SOS function SfiA protein is sufficient to block septation. *Proc. Natl. Acad. Sci. U. S. A.* **81**, 4490–4494 (1984).

162. Torres-Barceló, C., Kojadinovic, M., Moxon, R. & MacLean, R. C. The SOS response increases bacterial fitness, but not evolvability, under a sublethal dose of antibiotic. *Proc. R. Soc. B Biol. Sci.* **282**, 20150885 (2015).

163. Erill, I., Campoy, S. & Barbé, J. Aeons of distress: an evolutionary perspective on the bacterial SOS response. *FEMS Microbiol. Rev.* **31**, 637–656 (2007).

164. Cambridge, J., Blinkova, A., Magnan, D., Bates, D. & Walker, J. R. A replication-inhibited unsegregated nucleoid at mid-cell blocks Z-ring formation and cell division independently of SOS and the SlmA nucleoid occlusion protein in *Escherichia coli*. *J. Bacteriol.* **196**, 36–49 (2014).

165. Weart, R. B. *et al.* A metabolic sensor governing cell size in bacteria. *Cell* **130**, 335–47 (2007).

166. Westfall, C. S. & Levin, P. A. Bacterial Cell Size: Multifactorial and Multifaceted. *Annu. Rev. Microbiol.* **71**, 499–517 (2017).

167. Chien, A.-C., Hill, N. S. & Levin, P. A. Cell Size Control in Bacteria. *Curr. Biol.* **22**, R340–R349 (2012).

168. Rajagopal, S., Eis, N., Bhattacharya, M. & Nickerson, K. W. Membrane-derived oligosaccharides (MDOs) are essential for sodium dodecyl sulfate resistance in *Escherichia coli*. *FEMS Microbiol. Lett.* **223**, 25–31 (2003).

169. Monahan, L. G., Hajduk, I. V., Blaber, S. P., Charles, I. G. & Harry, E. J. Coordinating bacterial cell division with nutrient availability: A role for glycolysis. *MBio* **5**, 1–13 (2014).

170. Sauer, U. & Eikmanns, B. J. The PEP-pyruvate-oxaloacetate node as the switch point for carbon flux distribution in bacteria. *FEMS Microbiol. Rev.* **29**, 765–794 (2005).

171. Tymecka-Mulik, J. *et al.* Suppression of the *Escherichia coli dnaA46* mutation by changes in the activities of the pyruvate-acetate node links DNA replication regulation to central carbon metabolism. *PLoS One* **12**, 1–24 (2017).

172. Maciag, M., Nowicki, D., Janniere, L., Szalewska-Pałasz, A. & Wegrzyn, G. Genetic response to metabolic fluctuations: Correlation between central carbon metabolism and DNA replication in *Escherichia coli*. *Microb. Cell Fact.* **10**, 1–11 (2011).

173. Maciąg, M., Nowicki, D., Szalewska-Pałasz, A. & Węgrzyn, G. Central carbon metabolism influences fidelity of DNA replication in *Escherichia coli*. *Mutat. Res. Mol. Mech. Mutagen.* **731**, 99–106 (2012).

174. Maciag-Dorszyńska, M., Ignatowska, M., Jannière, L., Wegrzyn, G. & Szalewska-Pałasz, A. Mutations in central carbon metabolism genes suppress defects in nucleoid position and cell division of replication mutants in *Escherichia coli*. *Gene* **503**, 31–35 (2012).

175. Jannière, L. *et al.* Genetic evidence for a link between glycolysis and DNA replication. *PLoS One* **2**, (2007).

176. Nouri, H. *et al.* Multiple links connect central carbon metabolism to DNA replication initiation and elongation in *Bacillus subtilis*. *DNA Res.* **25**, 641–653 (2018).

177. Pritchard, R. H., Meacock, P. A. & Orr, E. Diameter of cells of a thermosensitive *dnaA* mutant of *Escherichia coli* cultivated at intermediate temperatures. *J. Bacteriol.* **135**, 575 (1978).

178. Liu, F. *et al.* AspC-mediated aspartate metabolism coordinates the *Escherichia coli* cell cycle. *PLoS One* **9**, (2014).

179. Cunningham, D. S. *et al.* Pyruvate kinase-deficient *Escherichia coli* exhibits increased plasmid copy number and cyclic AMP levels. *J. Bacteriol.* **191**, 3041–3049 (2009).

180. Noirot-Gros, M.-F. *et al.* An expanded view of bacterial DNA replication. *Proc. Natl. Acad. Sci. U. S. A.* **99**, 8342–8347 (2002).

181. Laffan, J. J. & Firshein, W. Origin-specific DNA-binding membrane-associated protein may be involved in repression of initiation of DNA replication in *Bacillus subtilis*. *Proc. Natl. Acad. Sci. U. S. A.* **85**, 7452–7456 (1988).

182. Stein, A. & Firshein, W. Probable identification of a membrane-associated repressor of *Bacillus subtilis* DNA replication as the E2 subunit of the pyruvate dehydrogenase complex. *J. Bacteriol.* **182**, 2119–24 (2000).

183. Yao, Z., Davis, R. M., Kishony, R., Kahne, D. & Ruiz, N. Regulation of cell size in response to nutrient availability by fatty acid biosynthesis in *Escherichia coli*. *Proc. Natl. Acad. Sci. U. S. A.* **109**, E2561–E2568 (2012).

184. Zheng, H. *et al.* Interrogating the *Escherichia coli* cell cycle by cell dimension perturbations. *Proc. Natl. Acad. Sci. U. S. A.* **113**, 15000–15005 (2016).

185. Katayama, T., Kasho, K. & Kawakami, H. The DnaA cycle in *Escherichia coli*: Activation, function and inactivation of the initiator protein. *Front. Microbiol.* **8**, 1–15 (2017).

186. Strydom, L. *et al.* Analysis of genes involved in glycogen degradation in *Escherichia coli*. *FEMS Microbiol. Lett.* **364**, fnx016 (2017).

187. Datsenko, K. A. & Wanner, B. L. One-step inactivation of chromosomal genes in Escherichia coli K-12 using PCR products. *Proc. Natl. Acad. Sci. U. S. A.* **97**, 6640–6645 (2000).

188. Baba, T. *et al.* Construction of *Escherichia coli* K-12 in-frame, single-gene knockout mutants: The Keio collection. *Mol. Syst. Biol.* **2**, (2006).

189. Hansen, F. G. & von Meyenburg, K. Characterization of the *dnaA*, *gyrB* and other genes in the *dnaA* region of the *Escherichia coli* chromosome on specialized transducing phages lambda tna. *Mol. Gen. Genet.* **175**, 135–44 (1979).

190. Pedersen, I. B., Helgesen, E., Flatten, I., Fossum-Raunehaug, S. & Skarstad, K. SeqA structures behind *Escherichia coli* replication forks affect replication elongation and restart mechanisms. *Nucleic Acids Res.* **45**, 6471–6485 (2017).

191. Ikeda, M. *et al.* Quick replication fork stop by overproduction of *Escherichia coli* DinB produces non-proliferative cells with an aberrant chromosome. *Genes Genet. Syst.* **87**, 221–231 (2012).

192. Kraemer, J. A., Sanderlin, A. G. & Laub, M. T. The Stringent Response Inhibits DNA Replication Initiation in *E. coli* by Modulating Supercoiling of *oriC*. *MBio* **10**, 1–18 (2019).

193. Blaauwen, T. Den, Buddelmeijer, N., Aarsman, M. E. G., Hameete, C. M. & Nanninga, N. Timing of FtsZ assembly in *Escherichia coli*. *J. Bacteriol.* **181**, 5167–5175 (1999).

194. Grigorian, A. V, Lustig, R. B., Guzmán, E. C., Mahaffy, J. M. & Zyskind, J. W. *Escherichia coli* cells with increased levels of DnaA and deficient in recombinational repair have decreased viability. *J. Bacteriol.* **185**, 630–44 (2003).

195. Yu, J., Liu, Y., Yin, H. & Chang, Z. Regrowth-delay body as a bacterial subcellular structure marking multidrug-tolerant persisters. *Cell Discov.* **5**, (2019).

196. Coquel, A.-S. *et al.* Localization of Protein Aggregation in *Escherichia coli* Is Governed by Diffusion and Nucleoid Macromolecular Crowding Effect. *PLoS Comput. Biol.* **9**, e1003038 (2013).

197. Lindner, A. B., Madden, R., Demarez, A., Stewart, E. J. & Taddei, F. Asymmetric segregation of protein aggregates is associated with cellular aging and rejuvenation. *Proc. Natl. Acad. Sci. U. S. A.* **105**, 3076–3081 (2008).

198. Rolfe, M. D. *et al.* Lag phase is a distinct growth phase that prepares bacteria for exponential growth and involves transient metal accumulation. *J. Bacteriol.* **194**, 686–701 (2012).

199. Butland, G. *et al.* Interaction network containing conserved and essential protein complexes in *Escherichia coli*. *Nature* **433**, 531–537 (2005).

200. Clark, D. J. & Maaløe, O. DNA replication and the division cycle in *Escherichia coli*. *J. Mol. Biol.* **23**, 99–112 (1967).

201. Jensen, K. F. The *Escherichia coli* K-12 wild types W3110 and MG1655 have an *rph* frameshift mutation that leads to pyrimidine starvation due to low *pyrE* expression levels. *J. Bacteriol.* **175**, 3401–7 (1993).

202. Bradford, M. M. A rapid and sensitive method for the quantitation of microgram quantities of protein utilizing the principle of protein-dye binding. *Anal. Biochem.* **72**, 248–54 (1976).

203. Sambrook, J., Fritsch, E. F. & Maniatis, T. Molecular cloning: a laboratory manual. *Mol. cloning a Lab. manual.* (1989).

204. Skarstad, K., Boye, E. & Steen, H. B. Timing of initiation of chromosome replication in individual *Escherichia coli* cells. *EMBO J.* **5**, 1711–1717 (1986).

205. Flåtten, I., Morigen & Skarstad, K. DnaA protein interacts with RNA polymerase and partially protects it from the effect of rifampicin. *Mol. Microbiol.* **71**, 1018–1030 (2009).

206. Ferullo, D. J., Cooper, D. L., Moore, H. R. & Lovett, S. T. Cell cycle synchronization of *Escherichia coli* using the stringent response, with fluorescence labeling assays for DNA content and replication. *Methods* **48**, 8–13 (2009).

207. Wold, S., Skarstad, K., Steen, H. B., Stokke, T. & Boye, E. The initiation mass for DNA replication in *Escherichia coli* K-12 is dependent on growth rate. *EMBO J.* **13**, 2097–102 (1994).

208. Stokke, C., Flåtten, I. & Skarstad, K. An easy-to-use simulation program demonstrates variations in bacterial cell cycle parameters depending on medium and temperature. *PLoS One* **7**, (2012).

209. Boye, E., Steen, H. B. & Skarstad, K. Flow Cytometry of Bacteria: a Promising Tool in Experimental and Clinical Microbiology. *Microbiology* **129**, 973–980 (1983).

210. Morigen, Løbner-Olesen, A. & Skarstad, K. Titration of the *Escherichia coli* DnaA protein to excess *datA* sites causes destabilization of replication forks, delayed replication initiation and delayed cell division. *Mol. Microbiol.* **50**, 349–62 (2003).

211. Levin, P. A. Light microscopy techniques for bacterial cell biology. *Methods in Microbiology* **31**, 115–132 (2002).

212. Suvarna, S. K., Layton, C. & Bancroft, J. D. *Bancroft's Theory and Practice of Histological Techniques*. (Elsevier Ltd., 2019). doi:10.1016/C2015-0-00143-5

213. Buddelmeijer, N., Aarsman, M. E. G. & den Blaauwen, T. Immunolabeling of Proteins in Situ in *Escherichia coli* K12 Strains. *Bio-Protocols* **3**, 2–6 (2013).

214. Bradski, G. The OpenCV library. *Dr Dobb's J. Softw. Tools* **25**, 120–125 (2000).

215. van der Walt, S., Colbert, S. C. & Varoquaux, G. The NumPy Array: A Structure for Efficient Numerical Computation. *Comput. Sci. Eng.* **13**, 22–30 (2011).

216. McKinney, W. Data Structures for Statistical Computing in Python. in *Proceedings of the 9th Python in Science Conference (SCIPY 2010)* 51–56 (2010).

217. Hunter, J. D. Matplotlib: A 2D Graphics Environment. *Comput. Sci. Eng.* **9**, 90–95 (2007).

218. Waskom, M. *et al.* mwaskom/seaborn: v0.9.0 (July 2018). (2018). doi:10.5281/ZENODO.1313201

219. Carpenter, B. *et al. Stan* : A Probabilistic Programming Language. *J. Stat. Softw.* **76**, 1–32 (2017).

220. Kumar, R., Carroll, C., Hartikainen, A. & Martin, O. ArviZ a unified library for exploratory analysis of Bayesian models in Python Software. *PyMC* (2016). doi:10.21105/joss.01143

221. Lu, M. & Kleckner, N. Molecular cloning and characterization of the *pgm* gene encoding phosphoglucomutase of *Escherichia coli*. *J. Bacteriol.* **176**, 5847–51 (1994).

222. Kumar, R. & Shimizu, K. Metabolic regulation of *Escherichia coli* and its *gdhA*, *glnL*, *gltB*, D mutants under different carbon and nitrogen limitations in the continuous culture. *Microb. Cell Fact.* **9**, 1–17 (2010).

223. Ponce, E., Flores, N., Martinez, A., Valle, F. & Bolivar, F. Cloning of the two pyruvate kinase isoenzyme structural genes from *Escherichia coli*: The relative roles of these enzymes in pyruvate biosynthesis. *J. Bacteriol.* **177**, 5719–5722 (1995).

224. Zampieri, M., Hörl, M., Hotz, F., Müller, N. F. & Sauer, U. Regulatory mechanisms underlying coordination of amino acid and glucose catabolism in *Escherichia coli*. *Nat. Commun.* **10**, 1–13 (2019).

225. Rowlett, V. W. & Margolin, W. The bacterial Min system. *Curr. Biol.* **23**, R553–R556 (2013).

226. Stojkova, P., Spidlova, P. & Stulik, J. Nucleoid-associated protein HU: A lilliputian in gene regulation of bacterial virulence. *Front. Cell. Infect. Microbiol.* **9**, 1–7 (2019).

227. Chodavarapu, S., Felczak, M. M., Yaniv, J. R. & Kaguni, J. M. *Escherichia coli* DnaA interacts with HU in initiation at the *E. coli* replication origin. *Mol. Microbiol.* **67**, 781–792 (2008).

228. Lequette, Y., Lanfroy, E., Cogez, V., Bohin, J. P. & Lacroix, J. M. Biosynthesis of osmoregulated periplasmic glucans in *Escherichia coli*: The membrane-bound and the soluble periplasmic phosphoglycerol transferases are encoded by the same gene. *Microbiology* **154**, 476–483 (2008).

229. Rouvière-Yaniv, J., Gros, F. & Adhya, S. Characterization of a novel, low molecular weight DNA-binding protein from *Escherichia coli*. *Proc. Natl. Acad. Sci. U. S. A.* **72**, 3428–32 (1975).

230. Ryan, V. T., Grimwade, J. E., Nievera, C. J. & Leonard, A. C. IHF and HU stimulate assembly of pre-replication complexes at *Escherichia coli oriC* by two different mechanisms. *Mol. Microbiol.* **46**, 113–124 (2002).

231. Cherepanov, P. P. & Wackernagel, W. Gene disruption in *Escherichia coli*: TcR and KmR cassettes with the option of Flp-catalyzed excision of the antibiotic-resistance determinant. *Gene* **158**, 9–14 (1995).

232. Thomason, L. C., Costantino, N. & Court, D. L. *E. coli* Genome Manipulation by P1 Transduction. *Curr. Protoc. Mol. Biol.* 1.17.1-1.17.8 (2007). doi:10.1002/0471142727.mb0117s79

233. Govons, S., Vinopal, R., Ingraham, J. & Preiss, J. Isolation of mutants of *Escherichia coli* B altered in their ability to synthesize glycogen. *J. Bacteriol.* **97**, 970–972 (1969).

234. Riber, L. *et al.* Hda-mediated inactivation of the DnaA protein and *dnaA* gene autoregulation act in concert to ensure homeostatic maintenance of the *Escherichia coli* chromosome. *Genes Dev.* **20**, 2121–2134 (2006).

235. Sezonov, G., Joseleau-Petit, D. & D'Ari, R. *Escherichia coli* physiology in Luria-Bertani broth. *J. Bacteriol.* **189**, 8746–8749 (2007).

236. Walker, J. R. & Pardee, A. B. Conditional mutations involving septum formation in *Escherichia coli*. *J. Bacteriol.* **93**, 107–14 (1967).

237. Adler, H. I. & Hardigree, A. A. Analysis of a gene controlling cell division and sensitivity to radiation in *Escherichia coli*. *J. Bacteriol.* **87**, 720–6 (1964).

238. El-Hajj, Z. W. & Newman, E. B. How much territory can a single *E. coli* cell control? *Front. Microbiol.* **6**, 1–12 (2015).

239. Adler, H. I., Fisher, W. D., Cohen, A. & Hardigree, A. A. Miniature *Escherichia coli* cells deficient in DNA. *Proc. Natl. Acad. Sci. U. S. A.* **57**, 321–6 (1967).

240. Rang, C. U., Proenca, A., Buetz, C., Shi, C. & Chao, L. Minicells as a Damage Disposal Mechanism in *Escherichia coli*. *mSphere* **3**, (2018).

241. Montero, M. *et al.* Systematic Production of Inactivating and Non-Inactivating Suppressor Mutations at the *relA* Locus That Compensate the Detrimental Effects of Complete *spoT* Loss and Affect Glycogen Content in *Escherichia coli*. *PLoS One* **9**, (2014).

242. Ghosh, A. *et al.* Contact-dependent growth inhibition induces high levels of antibiotic-tolerant persister cells in clonal bacterial populations. *EMBO J.* **37**, (2018).

243. Murray, H. & Koh, A. Multiple Regulatory Systems Coordinate DNA Replication with Cell Growth in *Bacillus subtilis*. *PLoS Genet.* **10**, e1004731 (2014).

244. Abebe, A. H., Aranovich, A. & Fishov, I. HU content and dynamics in *Escherichia coli* during the cell cycle and at different growth rates. *FEMS Microbiol. Lett.* **364**, 1–8 (2017).

245. Mogil, L. S., Becker, N. A. & Maher, L. J. Supercoiling effects on short-range DNA looping in *E. coli*. *PLoS One* **11**, 14–19 (2016).

246. Lal, A. *et al.* Genome scale patterns of supercoiling in a bacterial chromosome. *Nat. Commun.* **7**, 1–8 (2016).

247. Hansen, F. G. & Atlung, T. The DnaA tale. *Front. Microbiol.* **9**, 1–19 (2018).

248. Shepherd, V. A. The Cytomatrix as a Cooperative System of Macromolecular and Water Networks. in *Current topics in developmental biology* **75**, 171–223 (2006).

249. Possik, E. & Pause, A. Glycogen: A must have storage to survive stressful emergencies. *Worm* **5**, e1156831 (2016).

250. Larsen, P. I., Sydnes, L. K., Landfald, B. & Strøm, A. R. Osmoregulation in *Escherichia coli* by accumulation of organic osmolytes: betaines, glutamic acid, and trehalose. *Arch. Microbiol.* **147**, 1–7 (1987).

251. Feng, B. *et al.* Hydrophobic catalysis and a potential biological role of DNA unstacking induced by environment effects. *Proc. Natl. Acad. Sci. U. S. A.* **116**, 17169–17174 (2019).

252. Bukau, B., Ehrmann, M. & Boos, W. Osmoregulation of the maltose regulon in *Escherichia coli*. *J. Bacteriol.* **166**, 884–891 (1986).